Ca^2+-dependent cytoplasmic and nuclear contraction in protozoa

有川, 幹彦

(Degree)
博士（理学）

(Date of Degree)
2003-03-31

(Date of Publication)
2008-11-12

(Resource Type)
doctoral thesis

(Report Number)
甲2767

(URL)
https://hdl.handle.net/20.500.14094/D1002767

博　士　論　文

Ca^{2+}-dependent Cytoplasmic and Nuclear Contraction in Protozoa

（原生動物の細胞質および核内に存在するCa^{2+}依存性収縮系の解析）

平成15年1月

神戸大学大学院自然科学研究科

有　川　幹　彦

INDEX

ACKNOWLEDGEMENTS 3

SUMMERY 4

INTRODUCTORY REVIEW 8

CHAPTER I 11
Reactivation of Ca^{2+}-dependent Cytoplasmic Contraction in Permeabilized Cell Models of the Heliozoon *Echinosphaerium akamae*

CHAPTER II 18
Ca^{2+}-dependent Cytoplasmic Contractility of the Heliozoon *Actinophrys sol*

CHAPTER III 26
Ca^{2+}-dependent In Vitro Contractility of the Contractile Tubules in the Heliozoon *Actinophrys sol*

CHAPTER IV 35
High-Resolution Scanning Electron Microscopy of Chromatin Bodies and Replication Bands of Isolated Macronuclei in the Hypotrichous Ciliate *Euplotes aediculatus*

CHAPTER V 42
Ca^{2+}-dependent Contractility of Isolated and Demembranated Macronuclei in the Hypotrichous Ciliate *Euplotes aediculatus*

CHAPTER VI 47
Ca^{2+}-dependent Nuclear Contraction in the Heliozoon *Actinophrys sol*

GENERAL DISCUSSION 56

REFERENCES 59

ACKNOWLEDGEMENTS

First of all, I wish to thank my supervisor Dr. Toshinobu Suzaki for his unfailing guidance and valuable discussions throughout the course of this work. I am further indebted to Dr. Kiyoshi Watanabe (Emeritus Professor of Fukuoka University of Education), Dr. Shigeko Takaichi (National Cardiovascular Center), Drs. Hiroshi Kawai and Mitsunobu Kamiya (Research Center for Inland Seas, Kobe University), and Dr. Naoaki Saito (Biosignal Research Center, Kobe University) for their generous help in electron microscopy. It is a pleasure to be able to thank students of the Laboratory of Cell Dynamics and the entire staff and students of the Graduate School of Science and Technology for their friendship, help, and discussion. The critical reading and excellent advice are gratefully acknowledged to Professor Dr. Yoshihiro Matsuda, Professor Dr. Teizo Tsuchiya and Professor Dr. Fumio Hayashi.

This work was partly supported by the Sasakawa Scientific Research Grant from The Japan Science Society, the Research Fellowship of the Japan Society for the Promotion of Science for Young Scientists, and the Travel Award from the Japan Society of Protozoology to participate in the 11th International Congress of Protozoology.

SUMMARY

CHAPTER I

Permeabilized cell models of the large heliozoon *Echinosphaerium akamae* were prepared by treatment with 100 mM EGTA or 1% Triton X-100. When > 10^{-6} M Ca^{2+} was added to the EGTA-permeabilized cells, axopodial cytoplasm became contracted and several swellings were formed along the axopodial length. Axonemal microtubules remained intact, while higher concentration of Ca^{2+} (> 10^{-4} M) induced microtubule disassembly and complete breakdown of the axopodia. In Triton-permeabilized cells, cytoplasmic contraction and relaxation of the cell body were induced repeatedly by successive addition and removal of Ca^{2+}. The contraction did not require ATP, and was not inhibited by cytochalasin B. Electron microscopy showed, in EGTA-permeabilized axopodia, contractile tubules became granulated by the addition of Ca^{2+}. From these observations, it is strongly suggested that Ca^{2+}-dependent granulation of the contractile tubules is responsible for the axopodial contraction. (Published in *Cell Motility and the Cytoskeleton.* 2002. 53: 267-272.)

CHAPTER II

A "contractile tubules structure (CTS)" has been described in the radiating axopodia and cytoplasm of the heliozoon *Actinophrys sol.* Permeabilized cell models with fully-extended axopodia were prepared with 100 mM EGTA. When Ca^{2+} was added to the permeabilized cells, cytoplasmic swellings formed along the length of axopodia in a concentration-dependent manner. Triton X-100 was also used to prepare cell models of heliozoa. In the Triton-extracted cell model, axopodia were detached, but the cell body remained as a mass of cytoplasm which showed repetitive contraction and relaxation in a Ca^{2+}-dependent manner with 10^{-8} M as its threshold level. A cell homogenate of *A. sol* was found to yield a precipitate following the addition of Ca^{2+}. Formation of the precipitate occurred within a few minutes after the addition of Ca^{2+}, and was dependent on the concentration of Ca^{2+}. Electron microscopy showed that the CTS-like filamentous structures were present in the cell homogenate, and that the precipitate obtained from the cell homogenate by adding Ca^{2+} was composed of granular aggregates morphologically similar to the transformed CTS observed after axopodial contraction. (Published in *European*

Journal of Protistology. 2002. 38: 365-372.)

CHAPTER III

Contraction of axopodia in actinophrid heliozoons (protozoa) is induced by a unique contractile structure, called "contractile tubules structure (CTS)". I have previously shown that the cell homogenate of the heliozoon *Actinophrys sol* yields a precipitate by the addition of Ca^{2+}, which was mainly composed of filamentous structures morphologically identical to the CTS. To further characterize the nature of the CTS in vitro, biochemical and physiological properties of the precipitate were examined. SDS-PAGE showed that the Ca^{2+}-induced precipitate was composed of many proteins, and that no proteins showed any detectable changes in electrophoretic mobility by the addition of Ca^{2+}. Addition of exogenous proteins such as bovine serum albumin to the cell homogenate resulted in co-sedimentation of the proteins with the precipitate, suggesting that the CTS has a high affinity to other proteins. Dis- and re-appearance of the precipitate were repeatedly induced by the alternate addition of EGTA and Ca^{2+}, and its protein composition kept unchanged even after repeated cycles of precipitate formation. The precipitate showed a Ca^{2+}-dependent contractility with 10 - 100 nM as its threshold level, and the contractility was not inhibited by colchicine or cytochalasin B. The precipitate was repeatedly contracted and relaxed by successive addition and removal of Ca^{2+}, indicating that the contraction of the precipitate was controlled by only Ca^{2+} without any other energy supply. From my findings by the characterization of the precipitate, I concluded that the Ca^{2+}-dependent formation and contraction of the precipitate are closely related to the unique contractile organelle "contractile tubules structure". (In preparation)

CHAPTER IV

I observed isolated and demembranated macronuclei of *Euplotes aediculatus* with a field-emission scanning electron microscope (JEOL JSM-6401F) to examine three-dimensional surface structures of chromatin bodies and the replication band. Freezing and thawing in 0.25 M sucrose followed by treatment with 1% acetic acid demembranated the isolated macronuclei. Each macronucleus was composed of a large number of granular chromatin bodies of various sizes (0.2 - 1.0 μm in diameter). Despite their size variation, each chromatin body was composed of small granules with uniform diameter of ca. 50 nm, with frequent filamentous bridge connections to neighboring chromatin bodies. On the

replication band, the chromatin bodies were disintegrated into their component 50 nm granules. In some areas, the surface was observed to be composed of smaller particles of ca. 10 nm in diameter. (Published in *European Journal of Protistology*. 2000. 36: 40-45.)

CHAPTER V

The hypotrichous ciliated protozoan *Euplotes aediculatus* possesses a characteristic C-shaped somatic nucleus (macronucleus) within the cytoplasm, which shows dynamic shape change during the cell cycle. It is shown that isolated macronuclei possess Ca^{2+}-dependent contractility. Macronuclei were isolated, stuck fast on the glass surface, and subjected to different concentrations of Ca^{2+} in a Ca^{2+}-EGTA buffer. The nuclei became expanded at $[Ca^{2+}] < 10^{-7}$ M, and they contracted on subsequent addition of higher concentrations of Ca^{2+}. Cycles of expansion and contraction of the nucleus could be repeated many times by alternate addition of EGTA and Ca^{2+}, indicating that the size of isolated nuclei can be regulated by $[Ca^{2+}]$ alone. The nuclear contraction was observed in all phases of the cell cycle, but contractility was less evident around replication bands in the S phase. In addition to the hypotrichous ciliate *Euplotes*, similar Ca^{2+}-dependent nuclear contractility was found to exist in other cell types, including protozoans of different taxa (a heliozoon *Actinophrys sol* and a peniculine ciliate *Paramecium bursaria*), and also mammalian culture cells (HeLa cells). My findings suggest a possibility that Ca^{2+}-dependent nuclear contractility may be shared among diverse eukaryotic organisms. (In press in *Cell Calcium*. 2003. 33.)

CHAPTER VI

Ca^{2+}-dependent contractility was found to exist in the nucleus of the heliozoon *Actinophrys sol*. Upon addition of Ca^{2+} ($[Ca^{2+}]_{free} = 2.0 \times 10^{-3}$ M), diameters of isolated nuclei became reduced from 16.5 ± 1.7 μm to 11.0 ± 1.3 μm. The threshold level of $[Ca^{2+}]_{free}$ for the nuclear contraction was 2.9×10^{-7} M. The nuclear contraction was not induced by Mg^{2+}, and was not inhibited by colchicine or cytochalasin B. Contracted nuclei became re-expanded when Ca^{2+} was removed by EGTA; thus cycles of contraction and expansion could be repeated many times by alternate addition of Ca^{2+} and EGTA. The Ca^{2+}-dependent nuclear contractility remained even after treatment with 2 M NaCl for 30 min, suggesting a possible involvement of the nucleoskeletal components in the nuclear contraction. In the expanded state, filamentous structures were observed to be spread in the

nucleus to form a network. After addition of Ca^{2+}, they became aggregated and constructed a mass of thicker filaments, followed by re-distribution of the filaments spread around inside of the nucleus when Ca^{2+} was removed. These results suggest that the nuclear contraction is induced by Ca^{2+}-dependent transformation of the filamentous structures in the nucleus. (In preparation)

INTRODUCTORY REVIEW

The main objective of my research is to elucidate the mechanism of axopodial contraction of the actinophryid heliozoa, which is commonly observed when heliozoons capture prey organisms. In 1973, Ockleford and Tucker discovered the phenomenon of axopodial contraction in *Actinophrys sol*, and described that it was accompanied by breakdown of the axonemal microtubules (Ockleford and Tucker, 1973). Degradation and reformation of microtubule-containing axopodia are also involved in many other important cell functions such as locomotion (Watters, 1968; Suzaki et al, 1980a), division (Suzaki et al., 1978), and fusion between adjacent cells (Shigenaka and Kaneda, 1979). During these processes, axopodia changes in length in accordance with the breakdown and reformation of the microtubules as a cytoskeletal element in axopodia, and its velocity is around 2.0 μm/sec (Suzaki and Shigenaka, 1982; Suzaki et al., 1992). In the case of axopodial contraction during food-uptake, its velocity is up to 2×10^3 μm/sec (Suzaki et al., 1980a; Ando and Shigenaka, 1989; Suzaki et al., 1992; 1994) and direct measurement of the force of rapid axopodial contraction in heliozoa showed that the motive force for axopodial contraction cannot be explained as an axopodial tension generated as a result of disassembly of the microtubules (Suzaki et al., 1992). Quantitative light microscopy showed that disassembly of the axonemal microtubules does not accompany the axopodial contraction but the microtubules are only severed into smaller fragments when contraction occurs (Suzaki et al., 1994).

Tilney and co-workers have reported the existence of a non-microtubular structure inside the cell body, and termed it as "excretion body" (Tilney and Porter, 1965; Tilney et al., 1966). Many investigators have observed a variety of filamentous structures, and described it as macrotubules, filaments, C-shaped tubules, wavy tubules, paracrystalline arrays, multivesicular bodies, and morulate bodies. Among these structures, macrotubules, C-shaped tubules, wavy tubules and paracrystalline arrays have been identified as structures derived from microtubules. Based on their morphological similarities, multivesicular bodies and morulate bodies have been suggested as artifacts derived from axonemal microtubules (Patterson and Hausmann, 1982). However, careful investigations on the ultrastructure of these structures revealed that they are not related to microtubules but are now identified as contracted states of the CTS in poorly-fixed specimens (Kinoshita et al., 2001). Shigenaka and Kaneda (1979) have first noted that the non-microtubular structures named X-bodies might be involved in the control of cytoplasmic contractility. By detailed electron microscopic observations, a bundle of conspicuous filamentous structures named "contractile tubules structure (CTS)" was found to be located along the whole length of the axonemal microtubules, and the CTS transforms from tubular to granular forms when axopodial contraction occurs (Suzaki et al., 1980a; Shigenaka et al., 1982; Ando and Shigenaka, 1989). The CTS has been distinguished from the axonemal microtubules by experimental evidences that the CTS is clearly stained unlike the axonemal microtubules by uranyl magnesium acetate (Shigenaka et al., 1982), and that transformation of the CTS was not induced by colchicine treatment (Kinoshita et al., 2001). Based on its unique appearance, the CTS has long been speculated to be responsible for

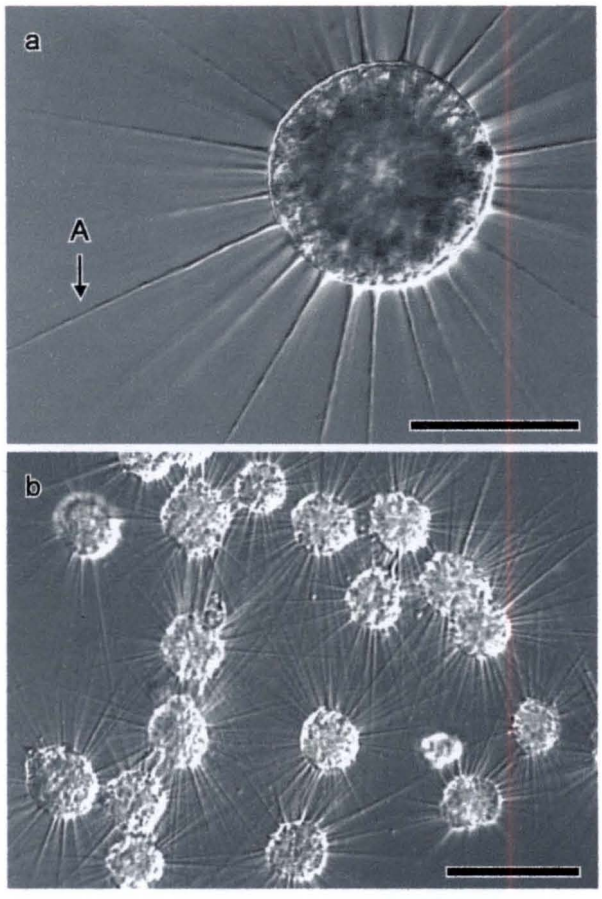

Fig. 1. Light micrographs of a living *Echinosphaerium akamae* (**a**) and *Actinophrys sol* cells (**b**) taken with Nomarski differential interference optics, showing many needle-like axopodia radiating from the spherical cell body. A, axopodium. Bars = 100 μm.

axopodial contraction, though no evidence has been presented to support this hypothesis (Matusoka et al., 1985; Ando and Shigenaka, 1989; Suzaki et al., 1994; Kinoshita et al., 2001). Is the CTS really a contractile organelle? To reply to this question, attempts were carried out in this study to prove that the CTS observed in actinophrid heliozoa is a motile structure in axopodia that is responsible for rapid axopodial contraction. First, in vitro reactivation of the cytoplasmic contraction in *Echinosphaerium akamae* (Fig. 1a) and *Actinophrys sol* (Fig. 1b) was carried out by using membrane-permeabilized cell models, and evidence was presented that the CTS contracts in a Ca^{2+}-dependent manner (Chapters I and II). Next, cell homogenate of *A. sol* was prepared that yields contractile precipitate by addition of Ca^{2+}. The precipitate was composed of CTS-like filaments, and the motile response of the precipitate to Ca^{2+} was similar to that of the permeabilized cell models. Based on these observations, a possible mechanism of formation and contraction of the precipitate was discussed in Chapter III.

It was incidentally found in *Echinosphaerium* that nuclei in the isolated cytoplasm contracted simultaneously with the cytoplasm. As well as cytoplasmic contraction, contraction of the isolated nuclei occurred in a Ca^{2+}-dependent manner, and was inhibited by neither colchicine nor cytochalasin B. These results indicate that a certain contractile system exists inside a nucleus, and its mechanism differs from those of the acto-myosin and the microtubular motilities. In an isolated macronucleus of *Tetrahymena* (ciliated protozoa), Wunderlich and Herlan have reported that the nuclear matrix, or a nucleoskeletal framework structure, showed reversible contraction which was induced by contraction of a peripheral layer of the nucleus (Wunderlich and Herlan, 1977; Wunderlich et al., 1978). Although a large number of investigations have been focused on fundamental structures and functions of the nuclear matrix in various kinds of cells, nuclear dynamics in contractility and its volume change have attracted less attention. In this study, nuclear contractility was observed in various types of cells including other species of protozoans (*Euplotes aediculatus* and *Paramecium bursaria)* and even in cultured mammalian cells (HeLa cells). To eliminate the possibility of involvement of the nuclear membrane in nuclear contraction, I attempted to develop a procedure of isolation and demembranation of the macronucleus in *E. aediculatus*. By using the procedure, in

Chapter IV, three-dimensional surface structures of the naked nuclear chromatin was observed by scanning electron microscopy. The isolated and demembranated macronucleus of *E. aediculatus* was found to show Ca^{2+}-dependent contractility (Chapter V). Furthermore, heliozoon *Actinophrys sol* also showed similar nuclear contraction (Chapter VI). Morphological and physiological characterization of the nuclear contractility was carried out, and possible mechanism of Ca^{2+}-dependent dynamics of the nuclear matrix is discussed.

CHAPTER I

Reactivation of Ca^{2+}-dependent Cytoplasmic Contraction in Permeabilized Cell Models of the Heliozoon *Echinosphaerium akamae*

INTRODUCTION

Rapid axopodial contraction of actinophrid heliozoa is a protozoan motile system that is not explained by either actomyosin or tubulin-based machineries (Suzaki et al., 1980a). The heliozoon cells have a large number of needle-like axopodia that radiate from their spherical cell bodies. When a prey protozoan becomes attached to an axopodium, the prey is trapped at the surface of the axopodium, and is conveyed toward the cell body by rapid shortening of the axopodium (Ockleford and Tucker, 1973; Suzaki et al., 1980a; Sakaguchi et al., 1998). Many investigations have been carried out at light and electron microscopic levels, but the mechanism of axopodial contraction is still poorly understood.

It has been shown that slow axopodial retraction is induced by Ca^{2+} in the presence of calcium ionophore A23187 (Schliwa, 1976; Matsuoka and Shigenaka, 1984). Calcium pyroantimonate cytochemistry and X-ray microanalysis has shown that the axopodial contraction is related to intracellular calcium release from either the cell cortex or vesicles surrounding the axonemal microtubules (Matsuoka and Shigenaka, 1984, 1985). Suzaki and co-workers measured the force of axopodial contraction and estimated it to be in the order of 10^{-9} N. The force of the axopodial retraction induced by treatment with colchicine was also estimated to be in the order of 10^{-11} N. They accordingly concluded that the motive force for axopodial contraction cannot be explained by an axopodial tension generated as a result of disassembly of the microtubules (Suzaki et al., 1992). The axopodium contains a bundle of microtubules as a cytoskeletal element (Tilney and Porter, 1965; Tilney et al., 1966; Ockleford, 1974). Contractile tubules (formerly called X-bodies) are also located inside the axopodium and run parallel to the microtubules throughout the axopodial length (Shigenaka and Kaneda, 1979; Suzaki et al., 1980a; Shigenaka et al., 1982). Electron microscopy has shown that the contractile tubules become granulated in contracted axopodia (Suzaki et al., 1980a; Ando and Shigenaka, 1989; Suzaki et al., 1994). From these observations, it has been postulated that the rapid axopodial contraction may be a consequence of the conformational change of the contractile tubules induced by Ca^{2+}. However, there is no direct evidence to support this hypothesis.

In the present study, I attempted to prepare cell models of the actinophrid heliozoon *Echinosphaerium akamae*, and observed responses of the models to Ca^{2+} at the light microscopic level. Furthermore, electron microscopy was carried out to examine the relationship between cytoplasmic contraction and the morphological change of the contractile tubules. From these observations, the possible mechanism of cytoplasmic contraction in the heliozoan axopodia is discussed.

MATERIALS AND METHODS

Organism and Culture

Living samples of the heliozoon *Echi-*

nosphaerium akamae (Shigenaka et al., 1980) were collected from a pond in the campus of Kobe University in Kobe City, Hyogo Prefecture, Japan, and maintained in 0.01% Knop solution (0.24 mM $Ca(NO_3)_2$, 0.14 mM KNO_3, 0.06 mM $MgSO_4$, and 0.1 mM KH_2PO_4) at 20 ± 1°C with *Chlorogonium elongatum* added as a food source. *C. elongatum* was cultured in a medium (0.1% sodium acetate, 0.1% polypepton, 0.2% tryptone, 0.2% yeast extract, and 0.01 mg/ml $CaCl_2$) under constant light conditions. Subculturing was carried out at intervals of about 2 weeks.

Preparation of Permeabilized Model of Axopodium

Two lines of Vaseline ledges were placed on a glass slide parallel to the longer edge of the slide, and a small drop of fresh culture medium was placed between the Vaseline ledges with several fibers of absorbent cotton as spacers (Ishida et al., 1996). After being washed with culture medium, cells were placed in the drop, covered with a coverslip, and left for about 10 min at room temperature so that the axopodia could recover from damages caused by pipetting. For permeabilizing the cell membrane, the cells were treated with ethylene glycol bis(β-aminoethylether)-N ,N ,N',N'-tetraacetic acid (EGTA) for 1 min at room temperature in a solution consisting of 100 mM EGTA, 5 mM $MgSO_4$, and 20 mM N-(2-Hydroxyethyl) piperazine-N'-2-ethanesulfonic acid (HEPES, pH 7.0). Test solutions were introduced into the narrow gap between the slide and the coverslip from one side using a Pasteur pipette. For replacement of the solution, the preparation was drained from the other side using a piece of filter paper. The cells were then washed with EGTA in a solution consisting of 5 mM EGTA, 5 mM $MgSO_4$, and 200 mM HEPES (pH 7.0). To examine cytoplasmic contraction of axopodia, a solution consisting of 5 mM EGTA, 5 mM $MgSO_4$, 4 mM $CaCl_2$, and 200 mM HEPES (pH 7.0) was added. The free concentration of Ca^{2+} in this solution was calculated to be 1.7×10^{-6} M by an iterative procedure according to Suzaki and Williamson (1986).

Preparation on Permeabilized Model of Cell Body

In order to examine the contractility of the cell body, an alternative procedure was developed to maintain a mass of cell body cytoplasm. Cells were washed with a fresh culture medium, placed on a hollow slide with a little amount of the culture medium, and quickly stirred up with a Pasteur pipette in a medium consisting of 100 mM ethylenediamine-N ,N ,N',N'-tetraacetic acid (EDTA) at room temperature. After 1 min, the cells were put on a glass slide prepared as mentioned above, covered with a coverslip, and pressed with a glass needle. By this procedure, most of the axopodia became detached, and cell bodies adhered to the glass surface. The cytoplasm was then treated with Triton X-100 in a solution consisting of 1% Triton X-100, 1 mM EGTA, and 5 mM HEPES (pH 7.0) for 1 min to permeabilize the cell membrane. Then, the isolated cytoplasm was washed in a solution consisting of 1 mM EGTA and 5 mM HEPES (pH 7.0). To induce contraction, the cytoplasm was treated with a solution consisting of 1 mM EGTA, 5 mM HEPES (pH 7.0), and various concentrations of $CaCl_2$.

Analysis of Light Microscopic Images

Light microscopic observations of the permeabilized models were carried out at room temperature under an Olympus DH-2 microscope equipped with Nomarski differential interference optics. Microscopic images were taken with a

video camera (Victor, KY-F30), recorded by either a video cassette recorder (Victor, BR-S822) or a digital recorder (Konica, MR-1500). Recorded images were processed by a personal computer (NEC, PC-9801 DA) for measuring areas of isolated cytoplasm using the image analyzing software NIH Image 1.61.

Measurement of the Area of Isolated Cytoplasm

A fractional area (A*) of the isolated cytoplasm was expressed as a value calculated as: $A^* = (A - A_{min}) / (A_{init} - A_{min})$, where A_{init} is the initial area of a cytoplasmic mass, A_{min} is the area of the cytoplasm at the completely contracted stage, and A is the area at a given time.

Transmission Electron Microscopy

Samples were prefixed with a fixative consisting of 3% glutaraldehyde, 0.01 mM $MgSO_4$, 1 mM sucrose, and 50 mM sodium cacodylate (pH 7.0) for 3 min at room temperature. They were then postfixed with buffered 1% OsO_4 for 30 min at room temperature. After being rinsed in 50 mM cacodylate buffer (pH 7.0), the fixed samples were dehydrated in a graded ethanol series, followed by embedding in Spurr's resin (Spurr, 1969). Ultrathin sections were stained with 3% aqueous uranyl acetate for 15 min and Reynolds' lead citrate stain (Reynolds, 1963) for 5 min at room temperature. Observations were made with a transmission electron microscope (JEOL JEM-1010).

RESULTS

Effect of Ca^{2+} on the permeabilized axopodia was examined and results are shown in Fig. I.1. The permeabilized axopodia were well preserved in the state of full extension even after treatment with 100 mM EGTA (Fig. I.1a). When Ca^{2+} was added at free $[Ca^{2+}] > 1 \times 10^{-6}$ M, several beadings appeared along the length of each axopodium as a result of contraction of the axopodial cytoplasm (arrowheads in Fig. I.1b). As a result of cytoplasmic accumulations, diameter of axopodia between cytoplasmic beads became markedly reduced. The contraction was not inhibited by cytochalasin B. The contracted cytoplasm recovered to its initial state when Ca^{2+} was removed by the addition of EGTA (data not shown). When surplus amount of Ca^{2+} was successively added at free $[Ca^{2+}] > 1 \times 10^{-4}$ M, the axopodia became collapsed and shortened toward the cell body as the result of disassembly of cytoskeletal microtubules (Fig. I.1c).

Ultrastructural observations were carried out by transmission electron microscopy to investigate whether morphological changes of contractile tubules or axonemal microtubules accompany Ca^{2+}-induced contraction of the permeabilized axopodia. As a result, contractile tubules (arrowheads) were found to transform from tubular to granular forms and accumulated in the axopodial beading (Fig. I.2b) by the addition of 1.7×10^{-6} M Ca^{2+}, while axonemal microtubules (asterisks in Fig. I.2) remained unchanged.

In the permeabilized cell body, cytoplasmic contraction was also induced by the addition of Ca^{2+} (Fig. I.3). Although most of the membranous structures had disappeared in the isolated cytoplasm after the treatment with Triton X-100, nuclei (marked "N" in Fig. I.3a) remained in the cytoplasmic mass. When Ca^{2+} was added at 1.9×10^{-5} M, both isolated cytoplasm and nuclei contracted (Fig. I.3b). Upon subsequent addition of EGTA, the contracted cytoplasm and nuclei expanded (Fig. I.3c). Contraction of the cell body was not inhibited by cytochalasin B.

Contraction and relaxation of the isolated cytoplasm were observed repeatedly by alternate addition of Ca^{2+} and EGTA. The approximate area

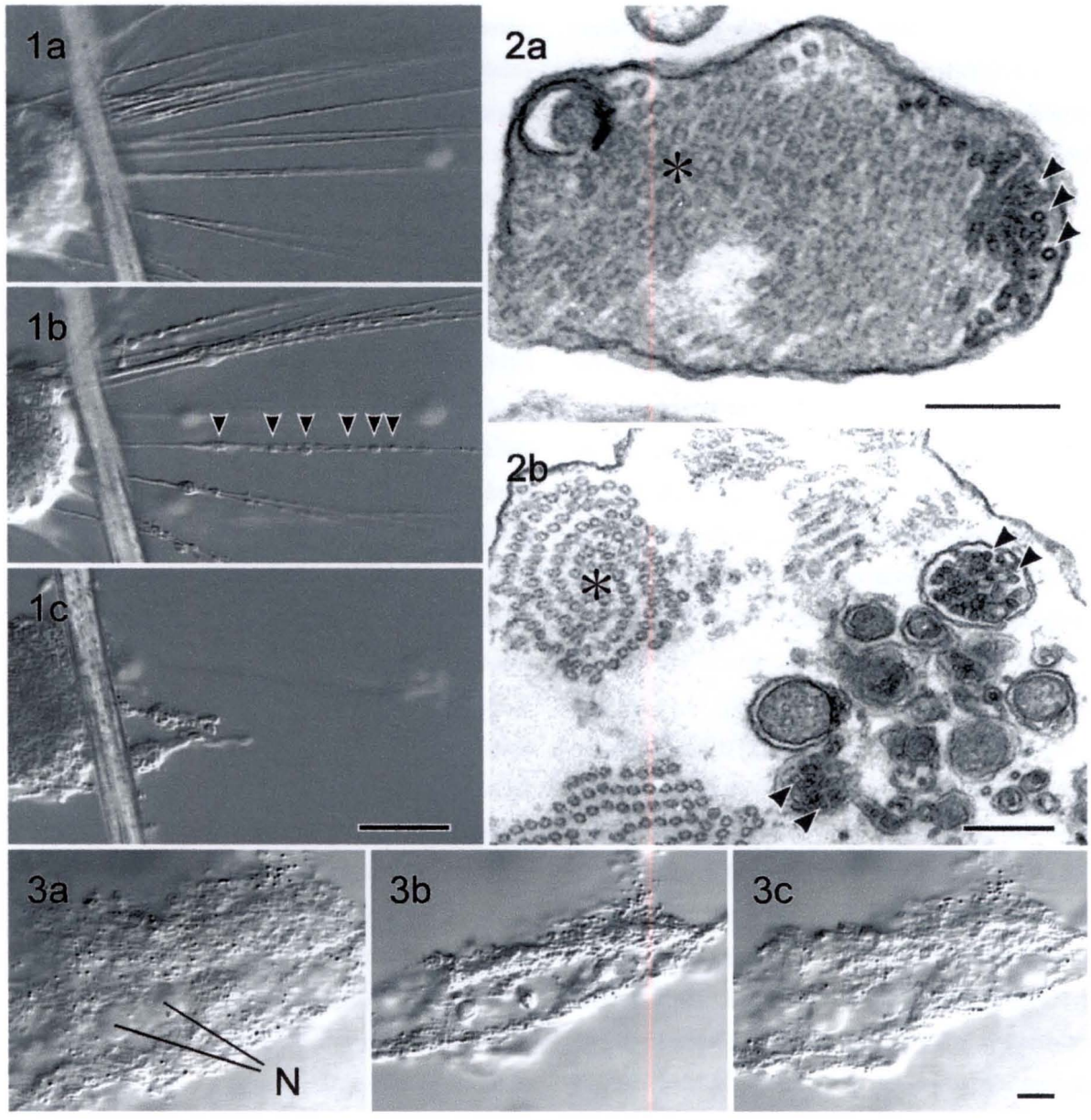

Fig. I.1. Light micrographs of the EGTA models of axopodia of *Echinosphaerium akamae*. **a:** EGTA-permeabilized axopodia after washing with 5 mM EGTA. The axopodia remained in a state of full extension. **b:** When Ca^{2+} (free $[Ca^{2+}] = 1.7 \times 10^{-6}$ M) was added, several swellings (arrowheads) appeared along the length of each axopodium as a result of cytoplasmic contraction. **c:** Addition of 1 mM Ca^{2+} caused complete collapse and shortening of the axopodia as a result of disassembly of the axonemal microtubules. Bar = 100 µm.

Fig. I.2. Electron micrographs of cross sections through the permeabilized axopodia of *Echinosphaerium akamae* before (**a**) and after (**b**) addition of Ca^{2+}. The addition of Ca^{2+} (1.9×10^{-6} M) induced a morphological change of the contractile tubules (arrowheads) from tubular to granular forms, without disassembly of the microtubules (asterisks). Bar = 200 nm.

Fig. I.3. Light micrographs of the Triton model of the cell body of *Echinosphaerium akamae*. **a:** A mass of cytoplasm and nuclei (N) after treatment with Triton X-100. **b:** After washing with EGTA, contraction of cytoplasm and nuclei occurred when Ca^{2+} (free $[Ca^{2+}] = 1.9 \times 10^{-5}$ M) was added. **c:** Relaxation of cytoplasm and nuclei was induced by the addition of EGTA. Bar = 10 µm.

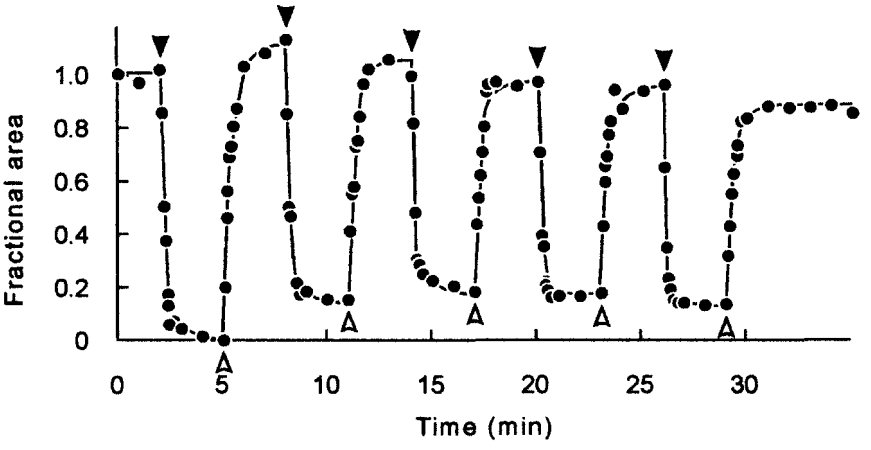

Fig. I.4. Successive contraction and relaxation of a mass of isolated cytoplasm. Fractional area (A*) of the isolated cytoplasm was expressed as a value between 0 and 1 using the equation: $A^* = (A - A_{min}) / (A_{init} - A_{min})$, where A_{init} is the initial area of a cytoplasmic mass, A_{min} is the area of the completely contracted cytoplasmic mass, and A is the area of the cytoplasm at a given time. Closed and open arrowheads indicate the moments when Ca^{2+} (1 mM) and EGTA (1 mM) were added, respectively.

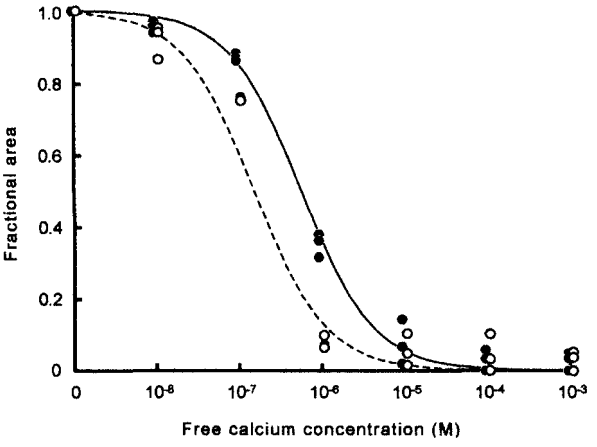

Fig. I.5. Relationship between the fractional area of a mass of isolated cytoplasm and free calcium concentration in the medium. The fractional area was determined as described in the legend for Fig. I.4. The threshold level of the free calcium concentration for cytoplasmic contraction was in the order of 10^{-7} M, and the maximal contraction was obtained at 0.1 mM. Closed circles, process of progressive contraction; Open circles, process of progressive relaxation.

of the isolated cytoplasm was continuously measured as shown in Fig. I.4. The contraction-relaxation cycle could be repeated many times (as many as 38 times in this study) by manipulating free Ca^{2+} concentration in the medium. The degree of contraction of the isolated cytoplasm was dependent on the free calcium concentration (Fig. I.5). When the free Ca^{2+} concentration was raised stepwise from 10^{-8} to 10^{-3} M, the isolated cytoplasm contracted in a sigmoidal manner as shown in Fig. I.5 (closed circles). The threshold level of free calcium concentration for the contraction of the cytoplasm was in the order of 10^{-7} M, and the maximal contraction was achieved at 0.1 mM. The km value estimated from the data presented in Fig. I.5 was 5.8×10^{-7} M. After complete contraction, free Ca^{2+} concentration was gradually lowered from 10^{-3} to 10^{-8} M. The km value obtained from the curve for the relaxation process (open circles) was 2.1×10^{-7} M.

DISCUSSION

In this study, permeabilized cell models of *E. akamae* were prepared to investigate the contractility of the cytoplasm and the axopodium. Axopodia are known to be sensitive to detergent; they become retracted immediately after living cells are treated with Triton X-100 (Suzaki et al., 1980b). It is, therefore, difficult to prepare cell models by Triton X-100 with their axopodia in the state of full extension. Alternatively, by using EGTA at high concentrations, permeabilized cell models were successfully prepared without artificial shortening of axopodia (Fig. I.1a). High concentration of EGTA was found to be effective for preservation of the axonemal microtubules (Suzaki et al., 1980b). Electron microscopy showed that although the original arrays of axonemal microtubules were slightly disordered, each microtubule in the perme-

abilized axopodia was well preserved both before and after Ca^{2+} addition (Fig. I.2).

At free Ca^{2+} concentrations between 1×10^{-6} and 1×10^{-4} M, cytoplasmic contraction of axopodia was observed without disassembly of the axonemal microtubules. After addition of Ca^{2+} to the permeabilized models, several swellings of axopodial cytoplasm were formed along the length of axopodia as a result of contraction of the axopodial cytoplasm. This phenomenon is similar to that usually observed in heliozoons during prey capture (Suzaki et al., 1980a). In living cells, electron microscopic observations showed that contractile tubules were transformed into granular forms inside the cytoplasmic swellings (Suzaki et al., 1980a; Ando and Shigenaka, 1989). Contractile tubules have tubular or lamellar profiles in cross section and a wavy appearance in longitudinal section. When cytoplasmic contraction occurred, they change their appearance to small granules or spherules, sometimes surrounded by membrane-like structures (Kinoshita et al., 2001). Similarly, in the permeabilized axopodia, contractile tubules were also found to change their appearance from tubular to granular forms when Ca^{2+}-dependent cytoplasmic contraction occurred. Furthermore, as shown in Fig. I.2b, microtubules in the permeabilized axopodia remained intact after addition of Ca^{2+} at 1.9×10^{-6} M. From these observations, it is strongly suggested that transformation of the contractile tubules and concomitant cytoplasmic contraction are caused by Ca^{2+}, not as the result of disassembly of the microtubules.

In this study, contraction and relaxation of permeabilized cell bodies were induced repeatedly by successive additions of Ca^{2+} and EGTA (Fig. I.4), which demonstrate that the cytoplasmic contraction occurs in a Ca^{2+}-dependent manner. Similar to the cytoplasmic contraction in axopodia, neither contraction nor relaxation of the cell body required ATP. The cytoplasmic contraction of the cell body was not inhibited by cytochalasin B. These results indicate that a certain Ca^{2+}-dependent contractile system exists in the cytoplasm of the heliozoa. Contraction of the cell body is probably based on the same molecular mechanism as that for the axopodial contraction, because both contractile phenomena share common characteristics for their reactivation in permeabilized cell models. The contractile tubules are not only localized inside the axopodia but also in the cell body, especially near the periphery of the nucleus where axonemal microtubules are terminated (Suzaki et al., 1980a). It is, therefore, probable that the cell body contraction is also mediated by the Ca^{2+}-dependent transformation of the contractile tubules.

A large number of investigations have been made on the Ca^{2+}-dependent contraction of the glycerinated stalk of vorticellid ciliates (Asai et al., 1978; Ochiai et al., 1979; Yokoyama and Asai, 1987) and Triton-extracted models of heterotrichous ciliates (Ishida and Shigenaka, 1988; Ishida et al., 1996). They showed that such contractions occur in an all-or-none fashion (Katoh and Kikuyama, 1997; Moriyama et al., 1998). The threshold level of free calcium concentration for the contraction is estimated to be in the order of 10^{-7} M, and degree of contraction and free calcium concentration show a sigmoidal relationship (Katoh and Naitoh, 1994; Ishida et al., 1996). In this study, the cell models showed contractility similar to those of spasmonemes and myonemes. They contracted in an ATP-independent and Ca^{2+}-dependent manner, and were not inhibited by cytochalasin B. In the heliozoa, however, the contractile organelle is morphologically different in appearance. The spasmoneme and the myoneme are composed of 2 - 3 nm and 3.5 - 10 nm filaments, respectively

(Huang and Pitelka, 1973; Yogosawa-Ohara and Shigenaka, 1985). However, contractile tubules have a diameter of about 22 nm, and a characteristic transformation occurs when they become contracted (Matsuoka et al., 1985). These differences suggest that the molecular mechanism of cytoplasmic contraction of heliozoa may be different from those for the spasmoneme of vorticellid ciliates and the myoneme of heterotrichous ciliates.

CHAPTER II

Ca^{2+}-dependent Cytoplasmic Contractility of the Heliozoon *Actinophrys sol*

INTRODUCTION

A number of protozoan cells are known to show characteristic cell movements which are controlled by intracellular calcium ions. They include coiling of the stalk in vorticellid ciliates (Amos, 1978; Asai et al., 1978; Ochiai et al., 1979; Yokoyama and Asai, 1987; Katoh and Kikuyama, 1997; Moriyama et al., 1998), twisting contraction of the cell body in heterotrichous ciliates (Huang and Pitelka, 1973; Yogosawa-Ohara and Shigenaka, 1985; Yogosawa-Ohara et al., 1985; Ishida and Shigenaka, 1988; Ishida et al., 1996) and contraction of the flagellar root fiber in algal cells (Salisbury et al., 1984; Salisbury, 1998). Ca^{2+}-dependent rapid axopodial contraction in heliozoa also belongs to this type of motility (Kinoshita et al., 2001). The heliozoon cells extend a large number of axopodia radiating from their spherical cell bodies, and they usually capture prey organisms by rapid axopodial contraction (Ockleford and Tucker, 1973; Suzaki et al., 1980a, Kinoshita et al., 2001). Ultrastructural studies showed a presumed contractile element (called the contractile tubules structure: CTS) inside the axopodia which transforms into a mass of small granules during axopodial contraction (Suzaki et al., 1980a; Ando and Shigenaka, 1989; Suzaki et al., 1994). Although granulation of the CTS has been considered to be responsible for axopodial contraction, its molecular mechanism has not been explained.

MATERIALS AND METHODS

Organism and Culture

The heliozoon *Actinophrys sol* was cultured monoxenically according to Sakaguchi and Suzaki (1999). Cells were collected by centrifugation and washed with artificial brackish water (47 mM NaCl, 1.1 mM KCl, 1.1 mM $CaCl_2$, 2.5 mM $MgCl_2$, 2.5 mM $MgSO_4$, and 1 mM Tris-HCl at pH 7.8) before they were used for experiments.

Preparation of Permeabilized Model of Axopodium

A. sol cells were washed and left for about 1 hour in a 1.5 ml test tube at room temperature until they settled to the bottom of the tube and formed cell colonies as a result of naturally-occurring membrane fusion. For perfusion experiments, cell colonies were placed between two lines of Vaseline ledges placed parallel to the longer edge of a glass slide. After being covered with a glass coverslip, cells were gently compressed with a glass needle from the top of the coverslip until cell colonies were firmly sandwiched between the glass surfaces. Individual cells were flushed away by a stream of artificial brackish water introduced from one side of the preparation, while excess solution was absorbed from the other side by touching a tip of a filter paper cut in a triangular shape. In contrast to individual cells, clustered cells in a colony remained in the same place because they were large enough to be held between the glass slide and the coverslip. Settled samples were permeabilized by treatment with 100 mM EGTA, and washed with a solution consisting of 5 mM EGTA and 100 mM HEPES, (pH 7.0). Then, a solution consisting of 5 mM

EGTA, 2.9 mM $CaCl_2$, and 100 mM HEPES at pH 7.0 was added to induce a cytoplasmic contraction in response to Ca^{2+}. The concentration of free calcium in this solution was calculated as 5.0×10^{-7} M by an iterative procedure according to Suzaki and Williamson (1986).

Preparation of Permeabilized Model of Cell Body

In order to examine contractility of the cell body cytoplasm, washed cells were placed on a hollow slide with a small amount of artificial brackish water, and a solution consisting of 0.1% Triton X-100, 3 mM EGTA, 1 mM $MgSO_4$, 5 mM $CaCl_2$, and 5 mM HEPES at pH 8.0 (free $[Ca^{2+}] = 2.0 \times 10^{-3}$ M) was added to permeabilize the cell membrane. The mixture was quickly stirred up with a glass needle, and cells were pipetted out and placed on a glass slide with Vaseline ledges, which had been coated with 0.1% poly-L-lysine. By this procedure, axopodia were all broken down into small pieces, but cytoplasm of the cell body remained as a globular mass of the same size. After being covered with a glass coverslip, the preparation was left for about 10 min at room temperature until the permeabilized cell body adhered to the surface of the glass slide. EGTA solution (3 mM EGTA, 1 mM $MgSO_4$, and 5 mM HEPES at pH 8.0) or Ca^{2+} solution (3 mM EGTA, 1 mM $MgSO_4$, 5 mM $CaCl_2$, and 5 mM HEPES at pH 8.0) was added to observe relaxation or contraction of the permeabilized cell body, respectively. To quantify Ca^{2+}-dependent contractility of the cytoplasm, washed cells in Ca^{2+}-depleted artificial brackish water were mixed with the same amount of a test solution consisting of 0.02% Triton X-100, 6 mM EGTA, 10 mM HEPES (pH 7.0) and various concentrations of $CaCl_2$. After vortexing for 5 seconds, the mixture was placed on a glass slide and covered with a glass coverslip. Microscopic images were recorded within a few minutes after addition of the test solution, and areas of the permeabilized cell bodies were measured from their images.

Preparation of Precipitate

Washed cells were collected by centrifugation at room temperature, and were suspended in a solution consisting of 3 mM EGTA and 5 mM HEPES (pH 7.0), followed by homogenization using a Potter homogenizer equipped with a Teflon pestle. After centrifugation at 7,700 × g for 5 min, the supernatant was collected and a small amount of 5 mM $CaCl_2$ was added to make the final free calcium concentration at 2.0×10^{-3} M. A precipitate appeared within 5 min, and was collected as a pellet by centrifugation at 200 × g for 5 min. The precipitate was placed on a slide glass with Vaseline ledges, and observed after being covered with a glass coverslip.

Microscopy

Light and electron microscopy of reactivation of the permeabilized models or the precipitate obtained from cell homogenate was carried out as described in Chapter I. Negative staining for electron microscopy was also carried out by a conventional method. Samples were put on a Formvar-coated grid mesh, drained, and treated with 1% uranyl acetate, drained again by attaching a piece of filter paper, and observed with a transmission electron microscope (Hitachi H-7100).

Spectroscopy

The supernatant of the cell homogenate was put into an acrylic microcuvette, and turbidity at 500 nm was monitored with a spectrophotometer (Shimadzu, UV-1200) to examine the effect of various concentrations of Ca^{2+} on the supernatant.

Sodium Dodecyl Sulfate (SDS)-Polyacrylamide Gel Electrophoresis

SDS-PAGE was carried out according to the method of Laemmli (1970) in slab gels containing 12% polyacrylamide at room temperature. After pre-fixation with 20% methanol and 7.5% acetic acid for 20 min, gels were stained by 0.15% Coomassie brilliant blue in 50% methanol and 10% acetic acid for 20 min, and then destained in 25% methanol and 7.5% acetic acid.

RESULTS

In this study, permeabilized cell models of *Actinophrys sol* were prepared to investigate the cytoplasmic contractility of the axopodium and the cell body. When *A. sol* (Fig. II.1a) was collected by centrifugation and left in a test tube for about one hour, cell colonies were formed as shown in Fig. II.1b. Axopodia of such fused cells appeared normal, and they remained in the state of full extension even after permeabilization with 100 mM EGTA (Fig. II.1c). By the addition of Ca^{2+} at 5.0×10^{-7} M, several beads of cytoplasm appeared along the length of each axopodium as a result of partial contraction of the axopodial cytoplasm (Fig. II.1d, arrowheads) without apparent breakdown of the cytoskeletal microtubules. The contracted cytoplasm recovered to its original state when Ca^{2+} was removed by the subsequent addition of EGTA (data not shown).

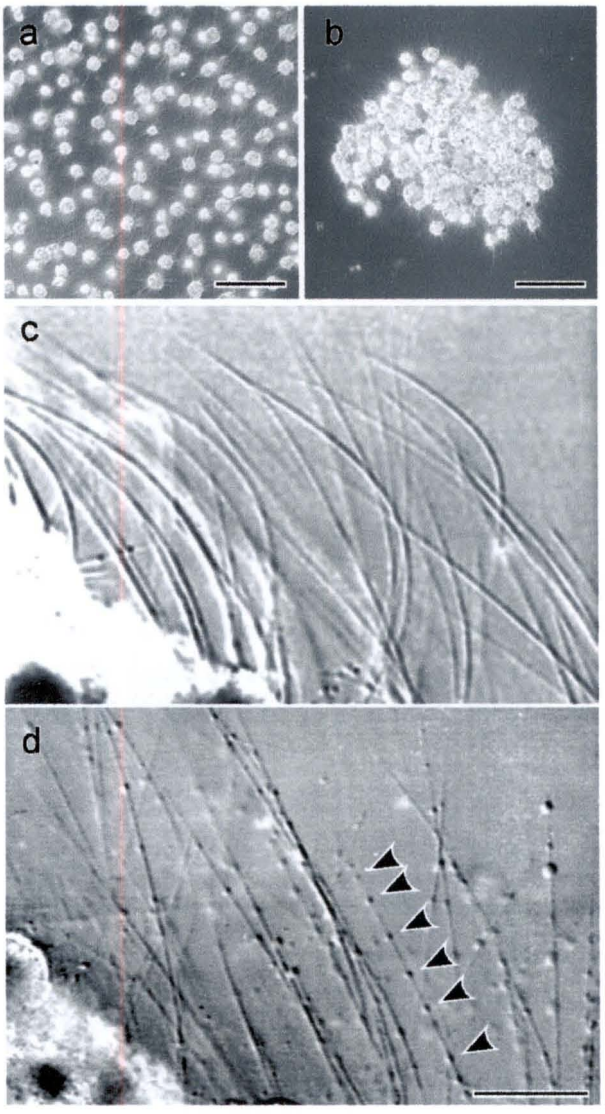

Fig. II.1. Light micrographs of *Actinophrys sol*. **a:** Living cells under culture conditions, showing that most of the cells are solitary. **b:** A cell colony formed by centrifugation. **c:** A magnified micrograph of a part of an EGTA-treated cell colony. Axopodia retained their fully extended state even after EGTA-permeabilization. **d:** The EGTA-treated cell colony (same specimen as **c**) after addition of Ca^{2+} at free $[Ca^{2+}] = 5.0 \times 10^{-7}$ M. Several swellings appeared (arrowheads) along the length of every axopodium as a result of cytoplasmic contraction. Bar = 200 μm (**a** and **b**) and 20 μm (**d**).

Cytoplasmic contractility of the cell body was also investigated in the detergent-permeabilized cell model. When Triton X-100 was added to the cell, the axopodia collapsed and were flushed away by the stream of solution, while cytoplasm of the cell body remained attached to the glass slide coated with poly-L-lysine. As shown in Fig. II.2, relaxation and subsequent contraction of the permeabilized cell body cytoplasm were observed under the light microscope. The cell model was first prepared in its contracted state with Ca^{2+} at free $[Ca^{2+}] = 2.0 \times 10^{-3}$ M (Fig. II.2a). It expanded by the addition of EGTA (Fig. II.2b), followed by re-contraction upon subsequent addition of Ca^{2+} (Fig. II.2c). Cytoplasmic contraction of permeabilized axopodia and cell bodies was not induced by

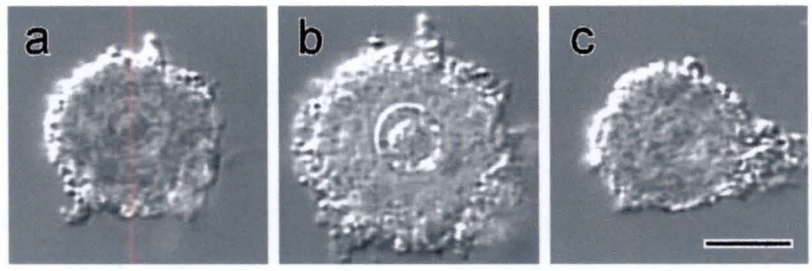

Fig. II.2. Light micrographs of the Triton-extracted model of the cell body. **a:** The mass of cytoplasm of the cell body retained its spherical shape after extraction with Triton X-100 at free [Ca^{2+}] = 2.0×10^{-3} M. **b:** Expansion of the cytoplasm occurred when EGTA was added. **c:** Subsequent addition of Ca^{2+} (free [Ca^{2+}] = 2.0×10^{-3} M) induced re-contraction of the cytoplasm. Bar = 20 μm.

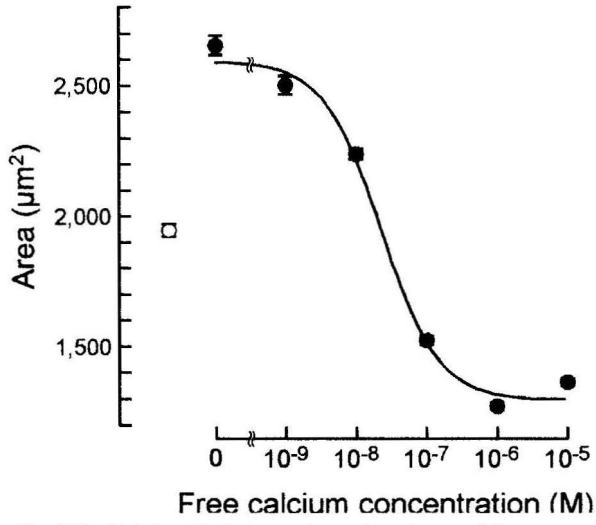

Fig. II.3. Relationship between the projected area of the permeabilized cell body and free calcium concentration. An open circle shows the approximate projected area of the cell body of living cells. At free Ca^{2+} concentrations of 10^{-8} M or below, cell models were expanded as compared with the living cells. On the contrary, at concentrations of 10^{-7} M or above, cell models were in the state of contraction. From the data, the Km value was estimated to be 2.4×10^{-8} M. Bars represent standard errors.

Mg^{2+} even at concentrations higher than that required for Ca^{2+}, and was not inhibited by cytochalasin B. The degree of contraction of the permeabilized cell body was dependent on free Ca^{2+} concentration (Fig. II.3). The approximate areas of the cell models were measured as a function of free Ca^{2+} concentration from 0 to 10^{-5} M. At free Ca^{2+} concentrations lower than 10^{-8} M, cell models were in the expanded state. At concentrations higher than 10^{-7} M, cell models were in the state of contraction. A relationship between the area of the cell model and the free Ca^{2+}concentrations fits fairly closely to a sigmoidal curve, with the Km value estimated as 2.4×10^{-8} M. An open circle in Fig. II.3 shows that the approximate area of the cell body of the living cell was about 1,900 - 2,000 μm^2.

I obtained a precipitate by addition of Ca^{2+} to the supernatant of the cell homogenate. To examine the effect of various concentrations of Ca^{2+}, the turbidity of the supernatant was continuously measured at 500 nm with a spectrophotometer. As shown in Fig. II.4, a significant increase of turbidity was induced by addition of Ca^{2+} at concentrations higher than 10^{-5} M, while no turbidity change was observed in Ca^{2+}-concentrations lower than 10^{-7} M. The precipitate disappeared when Ca^{2+} was removed by adding EGTA to the precipitate, and reappeared when Ca^{2+} concentration was increased $> 10^{-5}$ M. Such a cyclic formation of the precipitate was possible at least 3 times by repetitive addition and removal of Ca^{2+}. The relationship between free Ca^{2+} concentration and turbidity of the cell homogenate at 500 nm, shown at ten minutes in Fig. II.4, indicates that the formation of the precipitate depends on free Ca^{2+} concentration. Light and electron microscopy of the precipitate were carried out as shown in Fig. II.5. When observed by a light microscope, the precipitate was observed as packed particles or amorphous materials (Fig. II.5a). However, electron microscopy showed that a large number of granular aggregates were contained in the precipitate (Fig. II.5b). When the precipitate was compared with the contractile tubules in intact cells, it was morphologically similar to that in the

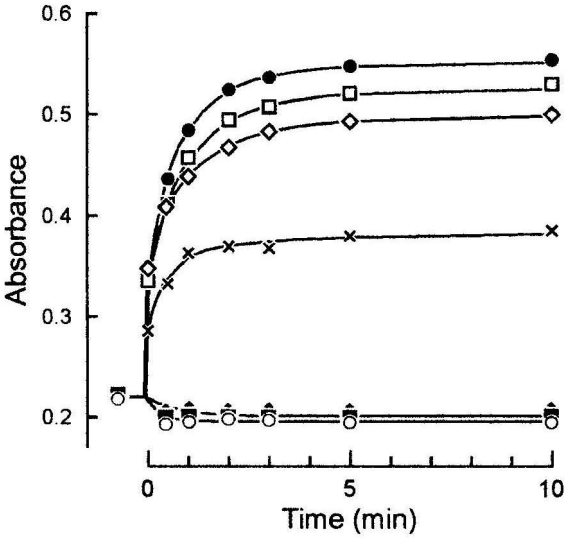

Fig. II.4. Turbidity (absorbance) changes of the cell homogenate measured at 500 nm. Measurements were carried out for 10 min after addition of various concentrations of Ca^{2+} to the supernatant of the cell homogenates. When Ca^{2+} was added at concentrations lower than 10^{-7} M, the turbidity became slightly decreased due to the effect of dilution. Addition of Ca^{2+} at concentrations of 10^{-6} M or above induced significant increase in turbidity within a few minutes. Different symbols (●, □, ◊, ×, ▲, ■, and ○) indicate different free Ca^{2+} concentrations (10^{-3}, 10^{-4}, 10^{-5}, 10^{-6}, 10^{-7}, 10^{-8}, and 10^{-9} M, respectively).

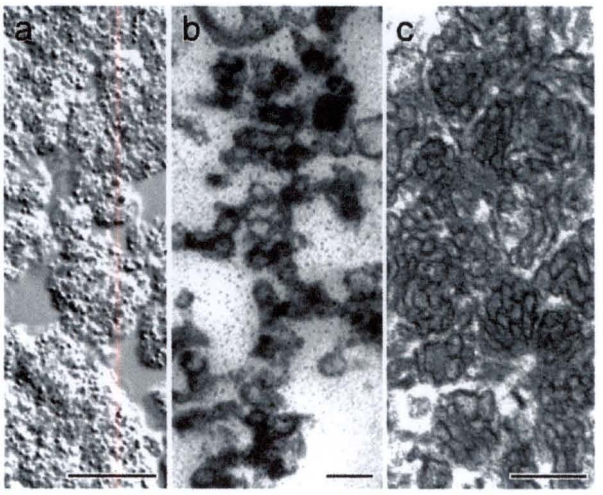

Fig. II.5. Microscopic observations of the precipitate and the contractile tubules. **a:** Light micrograph of the precipitate, which appeared when Ca^{2+} was added to the cell homogenate. The precipitate was composed of packed small granules. **b** and **c:** Electron micrographs of the precipitate and the contractile tubules. The precipitate was composed of aggregated granules or vesicles (**b**) which are morphologically similar to the granulated form of the contractile tubules in an intact cell (**c**). Bar = 20 μm (**a**) and 100 nm (**b** and **c**).

granulated state of the contractile tubules (Fig. II.5c).

As shown in Fig. II.6, negatively-stained cell homogenate of *A. sol* was found to be composed of filamentous structures with tubular and wavy appearance (Figs. II.6a and b). Diameter of these filamentous structures was about 20 nm. When Ca^{2+} (2 mM) was added to the cell homogenate, the filamentous structures changed their appearance from tubular to granular forms (Fig. II.6c).

SDS-PAGE analysis of a homogenate of the cytoplasm was carried out before and after some fractionation and precipitation with calcium. As shown in Fig. II.7, Coomassie brilliant-blue-stained gel electrophoresis showed that a precipitate obtained by addition of Ca^{2+} to a cell homogenate contained a large number of proteins, especially in low-molecular weight regions (Lane 3 in Fig. II.7). The overall gel profiles of the precipitate remained unchanged even after 3 cycles of formation and dissociation of the precipitates (data not shown).

DISCUSSION

In the large heliozoon *Echinosphaerium akamae*, cell motilities such as axopodial contraction and cytoplasmic streaming in axopodia can be easily observed under a light microscope (Shigenaka et al., 1974; Edds, 1975; Suzaki and Shigenaka, 1982). During food uptake, attached prey cells are carried toward the cell body surface by a rapid axopodial contraction (Suzaki et al., 1980a; Shigenaka et al., 1982). The driving force for the axopodial contraction is considered to be generated by transformation of CTS (Suzaki et al., 1994). Recently, I have shown that a Ca^{2+}-dependent contractility exists in a cytoplasm of a large heliozoan *Echinosphaerium akamae* (Arikawa and Suzaki, 2002). When Ca^{2+} was added to permeabilized cell models of axopodia, a mass of granulated CTS was observed in a contracted cyto-

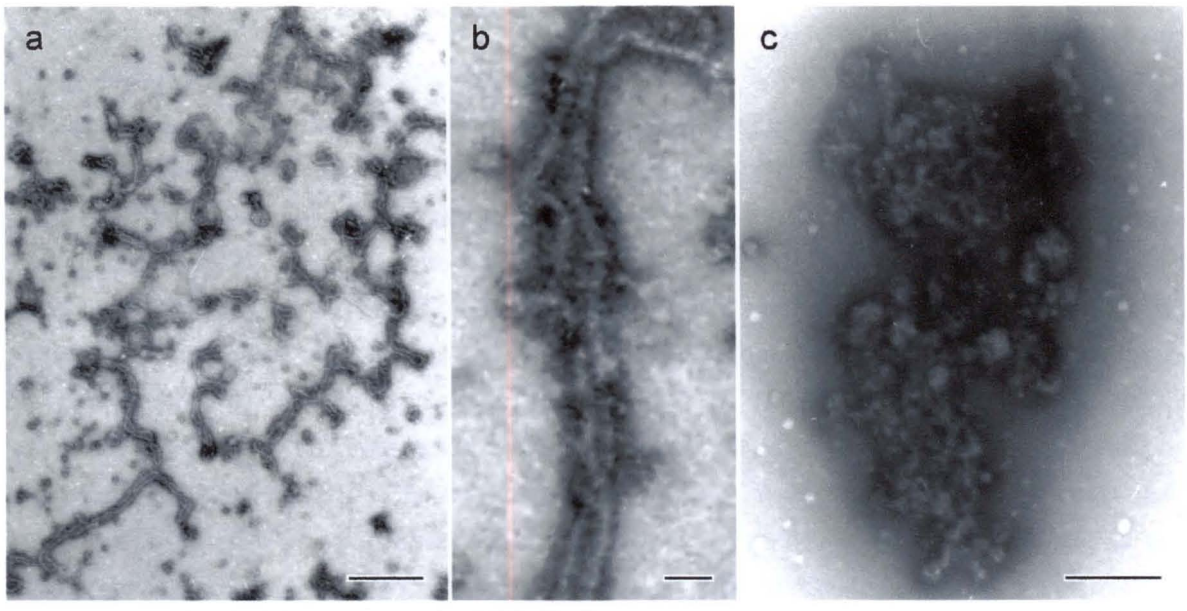

Fig. II.6. Negatively-stained electron micrographs of CTS -like filamentous structures in the cell homogenate. **a:** Filamentous structures in the cell homogenate that were prepared before addition of Ca^{2+}. They are dispersed in the suspension, and have many branches. Bar = 1 μm. **b:** An enlarged micrograph of the filamentous structures, showing that they have a tubular and wavy appearance. Bar = 100 nm. **c:** CTS-like structure after addition of Ca^{2+}. The filamentous structures transformed into a mass of aggregated granules. Bar = 1 μm.

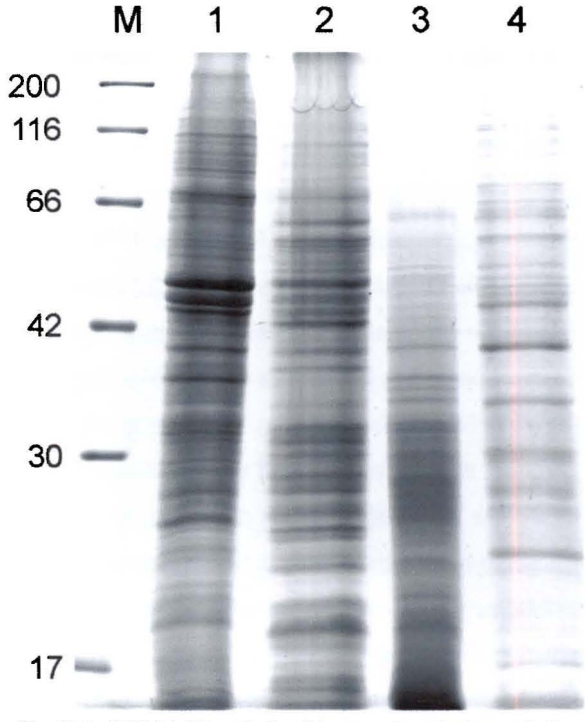

Fig. II.7. SDS-PAGE analysis of the cytoplasm before and after precipitation with calcium. Raw cell homogenate (Lane 1). This was centrifuged at 7,700 × g for 5 min and the gel of the supernatant is shown in Lane 2. After addition of Ca^{2+} at 2.0×10^{-3} M this was separated by centrifugation at 200 × g for 5 min into the precipitate (Lane 3) and supernatant (Lane 4). Note that a large number of proteins are still present in the Ca^{2+}-induced precipitate. The gel was stained with Coomassie brilliant blue, and molecular weight standards (M) are shown at the left of the gel, calculated in kD.

plasm, indicating that a Ca^{2+}-dependent transformation of the CTS results in a cytoplasmic contraction. *E. akamae* and *A. sol* are taxonomically classified into the same order, both having morphologically similar structures in axopodia. Although there are some differences such as number of nuclei and living conditions between *E. akamae* and *A. sol*, both are able to capture food organisms by rapid axopodial contraction which accompanies transformation of the contractile tubules in the axopodia. Therefore, it is natural to consider that the two species may share a common mechanism for the cytoplasmic contraction (Kinoshita et al., 2001).

In this study, Ca^{2+}-dependent reactivation of the cytoplasmic contraction of axopodia and the cell body was demonstrated in 'model' cells. The addition of Ca^{2+} to the permeabilized cells induced localized cytoplasmic contraction, resulting in the formation of several swellings or beads along the length of axopodia (Fig. II.1d). This phenomenon is similar to that usually observed during prey cap-

ture, which usually occurs when a food organism is trapped at the middle or proximal regions of the axopodia (Suzaki et al., 1980a). Electron microscopic observations showed that CTS was transformed into a granular form inside such cytoplasmic swellings both in living cells (Suzaki et al., 1980a; Shigenaka et al., 1982; Ando and Shigenaka, 1989) and also in the permeabilized cell model (Arikawa and Suzaki, 2002) of *Echinosphaerium*. In addition to these morphological observations, reactivation of cytoplasmic contraction in permeabilized axopodia serves as direct evidence for the presence of a Ca^{2+}-dependent contractile system in the heliozoon axopodia. Contraction and relaxation of permeabilized cell bodies were also induced by additions of Ca^{2+} and EGTA (Fig. II.2), indicating that the contractile system exists not only inside the axopodia but also in the cell body. The contraction of the cell body cytoplasm may also be attributed to the contractile tubules, because they are also present in the cell body, running parallel to the axonemal microtubules which terminate deep towards the center of the cell body (Suzaki et al., 1980a; Kinoshita et al., 2001).

A Ca^{2+}-induced precipitate was obtained from the cell homogenate of *A. sol* (Fig. II.4). Continuous spectrophotometric measurement of turbidity of the cell homogenate at 500 nm showed that the precipitate appears within a few minutes after addition of Ca^{2+} at concentrations higher than 10^{-6} M. It is evident from Fig. 4 that the formation of the precipitate depends on Ca^{2+} concentration. SDS-PAGE analysis showed that a large number of proteins are contained in the precipitate; many of those are also present in the supernatant (Fig. II.7, Lanes 3 and 4). When a small amount of bovine serum albumin (BSA) was added to the cell homogenate, it was also recovered in the Ca^{2+}-induced precipitate (data not shown). These results suggests that the Ca^{2+}-induced precipitate may be composed of not only Ca^{2+}-sensitive proteins but also other associated proteins which are not involved in the mechanism of the precipitate formation. In this study, formation and disappearance of the precipitate could be repeated many times by alternate addition of Ca^{2+} and EGTA, indicating that this phenomenon is regulated by only Ca^{2+} without any other energy supply. It is well known that some peritrich ciliates (Amos, 1975) and some flagellates (Salisbury et al., 1984) possess Ca^{2+}-dependent contractile organelles, a spasmoneme and a flagellar root, within their cytoplasm. Contraction of these organelles is mediated by Ca^{2+}-binding proteins (spasmin and centrin, respectively), whose molecular weights are about 20 kDa. As shown in Fig. II.7, SDS-PAGE pattern shows a protein band of about 20 kDa in the Ca^{2+}-induced precipitate. This result suggests that a spasmin- or centrin-like Ca^{2+}-binding protein may be present in *A. sol*, which is to be examined in the future. The precipitate was found to be composed of small granules morphologically similar to CTS (Fig. II.5b). In intact cells, CTS changes its appearance from wavy tubules to granules or spherules when axopodial contraction occurs (Kinoshita et al., 2001). Judging from its characteristic ultrastructure, the aggregated granules in the Ca^{2+}-induced precipitate are most likely the granulated forms of CTS. Elongated CTS-like filaments were found to be present in the cell homogenate. As shown in Fig. II.6, these filaments have a wavy tubular appearance (approximately 20 nm in diameter), which was morphologically similar to CTS in its elongated state (Kinoshita et al., 2001). They are morphologically distinct from microtubules, as they have branches, smaller in diameter, and wavy in appearance. Moreover, immunoelectron microscopy demonstrated that they were not labeled by a tubu-

lin antibody (data not shown). These results indicate that the filamentous structures shown in Fig. II.6 are CTS, not the axonemal or cytoplasmic microtubules. Furthermore, the filamentous structures changed their form to aggregated granules after adding of Ca^{2+}, indicates that isolated CTS possesses an ability of transformation in vitro in a Ca^{2+}-dependent manner. Ca^{2+}-dependent contractility of CTS is functionally similar to those of spasmonemes and myonemes (Huang and Pitelka, 1973; Ochiai et al., 1979; Ishida and Shigenaka, 1988). However, CTS in heliozoa is distinguished from the contractile filaments of these ciliates, since it is thicker in diameter and it shows a characteristic transformation from tubes to granules (Kinoshita et al., 2001; Arikawa and Suzaki, 2002).

Compared with other protozoan species, it has not been possible to culture heliozoons in axenic conditions so far. Due to this difficulty, biochemical approaches to understanding the mechanism of cytoplasmic contraction have been limited. Recently, however, a method of bacteria-free monoxenic culture of *A. sol* was established (Sakaguchi and Suzaki, 1999), which yielded a cell density up to 4,000 cells/ml that is > 100 times more efficient than conventional culture. Thus, *A. sol* can now be used for biochemical research, in which a large quantity of materials is usually required. In this study, I succeeded in partial isolation of cytoplasmic structures, which show a unique response to Ca^{2+} in forming precipitates and having an appearance similar to the contractile tubules. This indicates that the contractile tubules may have been isolated in vitro, but further purification and biochemical characterization are needed to identify proteins which are required for the cytoplasmic contraction in heliozoa.

CHAPTER III

Ca^{2+}-dependent In Vitro Contractility of the Contractile Tubules in the Heliozoon *Actinophrys sol*

INTRODUCTION

Heliozoons capture prey organisms by using a large number of cytoplasmic tentacles called axopodia that are radiating from the spherical cell body. After a prey is trapped on the surface of an axopodium, rapid contraction of the axopodial cytoplasm occurs to convey the prey towards the cell body surface where formation of a food vacuole takes place (Ockleford and Tucker, 1973; Suzaki et al, 1980a; Shigenaka et al., 1982). The axopodial contraction involves rapid breakdown of the cytoskeletal microtubules (Suzaki et al., 1994) and contraction of the "contractile tubules structure (CTS)" that is running in parallel to the microtubules (Suzaki et al., 1980a; Kinoshita et al., 2001). In Chapters I and II, I have shown with a detergent-extracted cell model that contraction of the demembranated axopodia that contain the CTS is a calcium-dependent phenomenon without requirement for other energy supply (Arikawa and Suzaki, 2002; Arikawa et al., 2002b). These characteristics resemble calcium-dependent contractile systems in other unicellular organisms such as vorticellid ciliate (Asai et al., 1978; Ochiai et al., 1979; Yokoyama and Asai, 1987; Katoh and Naitoh, 1994; Katoh and Kikuyama, 1997; Moriyama et al., 1998), heterotrichous ciliate (Ishida and Shigenaka, 1988; Ishida et al., 1996) and green algae (Salisbury and Floyd, 1978; Salisbury et al., 1984; Coling and Salisbury, 1992; Salisbury, 1998), in which conformational changes of the calcium-binding contractile proteins such as spasmin and centrin exert a motive force for contraction. In heliozoons, however, the mechanism of axopodial contraction is poorly understood, and the tubular appearance of the CTS is characteristic to this group of protozoa (Suzaki et al., 1980a; Matsuoka et al., 1985). The CTS transforms from a bundle of elongated tubules to a mass of small granules when axopodial contraction occurs (Suzaki et al., 1980a; Ando and Shigenaka, 1989; Suzaki et al., 1994; Kinoshita et al., 2001; Arikawa and Suzaki, 2002), and it is surmised that such a morphological change of the CTS may be responsible for the contractile mechanism (Matsuoka et al., 1985).

In the previous study, I have obtained a precipitate from a cell homogenate of the actinophrid heliozoon *A. sol*, which appeared in a Ca^{2+}-dependent manner (Arikawa et al., 2002b). In the cell homogenate, CTS-like structures were observed that changed their appearances from tubular filaments to small granules by the addition of Ca^{2+}. Judging from morphological and physiological similarities, I have concluded that the CTS was crudely isolated as a main component of the Ca^{2+}-induced precipitate (Arikawa et al., 2002b). Here, I succeeded in reactivating in vitro contraction of the precipitate in a Ca^{2+}-dependent manner. Biochemical characterization of the precipitate was carried out to understand properties and mechanism of contraction of the isolated CTS.

MATERIALS AND METHODS

Organisms and Culture

Actinophrys sol was monoxenically cultured as described in Chapter II. Cells were harvested

when the cell density reached 2,000 - 4,000 cells/ml in the culture medium. Prior to each experiment, cells were collected by centrifugation and were washed with fresh 10% artificial sea water.

Preparation of Precipitate

Ca^{2+}-induced precipitate was obtained from cell homogenate as described in Chapter II. When the precipitate was pressed strongly from the top of the coverslip, it adhered to the glass surface like a viscous paste. Contraction of the adhered precipitate was induced by introducing a solution consisting of 3 mM EGTA, 5 mM HEPES (pH 7.0), and various concentrations of $CaCl_2$ from a side of the preparation.

Protein assay

For the determination of protein concentrations, a bicinchoninic acid (BCA) assay procedure was used (Smith et al., 1985). For the BCA assay, reagents were added to a sample, and the mixture was incubated a few hours at room temperature. After the incubation, absorbance at 562 nm was recorded with a spectrophotometer (Shimadzu, UV-1200). Bovine serum albumin (BSA) was used as a standard.

Fractionation of Cell Homogenate

Cell homogenate was fractionated by sucrose density gradient ultracentrifugation. Two milliliters of a solution consisting of 2.0 M sucrose, 10 μM leupeptin, 0.2 mM phenylmethylsulfonyl fluoride (PMSF), 3 mM EGTA, and 5 mM HEPES (pH 7.0) were placed on the bottom of a centrifuge tube, and was gently overlaid with 1.5, 1.0, and 0.5 M sucrose in 5 mM HEPES buffer (2.0 ml each). Cell homogenate was centrifuged at 10,000 × g for 10 min, and the resulting supernatant (1.5 ml) was placed on top of the layered sucrose solutions, and subjected to ultracentrifugation (100,000 × g) for 20 hours at 4°C (Hitachi, CP70MX). After ultracentrifugation, 1.0 ml fractions were collected from the top of the tube downward and were stored on ice before using. These fractions were sampled for SDS-PAGE after trichloroacetic acid (TCA) precipitation, or for inducing precipitates by the addition of Ca^{2+}.

Microscopy

Reactivation of the adhered precipitate was observed as described in Chapters I and II.

Electrophoresis and Immunoblotting

Sodium dodecyl sulfate polyacrylamide gel electrophoresis (SDS-PAGE) was performed according to Laemmli (1970) as described in Chapter II. For immunoblotting analysis, proteins of Ca^{2+}-induced precipitate were separated by SDS-PAGE, and transferred to a PVDF-membrane (ATTO, Clear blot membrane-p) in a transfer buffer (192 mM glycine and 27 mM Tris). The membrane was incubated more than 30 min at room temperature in a washing buffer (0.05% Tween 20, 154 mM NaCl, and 10 mM Tris at pH 7.4) containing 1% dehydrated skim milk (DIFCO). After washed in the washing buffer, membranes were cut and incubated for 1 h at room temperature with 200-fold dilution of anti-α tubulin or anti-tubulin antibodies. The membranes were washed again with the washing buffer and then incubated for 1 h at room temperature with 500-fold horseradish peroxidase (HRP)-conjugated secondary antibodies. The membranes were gently washed again in the washing buffer before detection of HRP activity with Konica immunostaining kit HRP-1000.

RESULTS

Previously, I have reported that a clear su-

pernatant of the cell homogenate of *Actinophrys sol* yielded a precipitate by addition of Ca^{2+}. In this study, the Ca^{2+}-induced precipitate was further characterized to understand the relationship between precipitate formation and Ca^{2+}-dependent cytoplasmic contractility of the heliozoon. By adding Ca^{2+} to a supernatant of the cell homogenate prepared with 1% Triton X-100, a precipitate with a granular appearance was obtained (Fig. III.1). In addition to Triton X-100, other kinds of detergents were also found to be effective for preparing cell extract that formed a Ca^{2+}-dependent precipitate. As shown in Fig. III.2a, nonionic detergents (Triton X-100, Triton X-114, Nonidet P-40, Tween 20, and Tween 80) and anionic detergents (deoxycholic acid sodium salt (DASS) and sodium dodecyl sulfate (SDS)) were tested, and obtained precipitates were analyzed by SDS-PAGE. In case of anionic detergents, the supernatant of the cell homogenate became turbid by addition of Ca^{2+}, but only a trace amount of precipitate was obtained after centrifugation. On the other hand, all the nonionic detergents were found to yield cell homogenates that resulted in precipitate formation by addition of Ca^{2+}. SDS-PAGE showed that their band patterns are similar to each other with a lot of protein components in the precipitates. A zwitterionic detergent CHAPS was also effective in formation of a Ca^{2+}-induced precipitate, and the resulting SDS-PAGE pattern was also similar to those obtained with the nonionic detergents (data not shown). Immunoblot analysis was carried out to identify components of the Ca^{2+}-induced precipitate, and showed that both α- and β-tubulin were involved in the precipitate as one of the components (Fig. III.2b). As an approach to detect Ca^{2+}-binding proteins, samples were mixed with sample buffers with or without Ca^{2+}, and subjected to SDS-PAGE. The supernatant of the cell homogenate was found

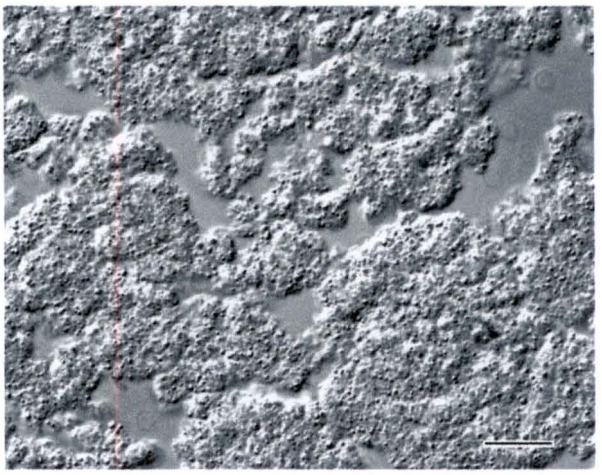

Fig. III.1. Light micrograph of a Ca^{2+}-induced precipitate of *Actinophrys sol*. The precipitate was obtained as a pellet by centrifugation after addition of Ca^{2+} to the supernatant of a cell homogenate. The precipitate was composed of small granules. Bar = 20 μm.

to contain a protein that changed its mobility on a gel by addition of Ca^{2+} (Fig. III.3). This protein has an apparent molecular weight of about 17 kDa in the absence of Ca^{2+}, which shifted to 15 kDa when Ca^{2+} was added to the sample buffer. The protein was not detected in the Ca^{2+}-induced precipitate but remained in the supernatant collected after the precipitate was formed by Ca^{2+}, indicating that the protein is not a component of the precipitate. As schematically shown in Fig. III.4, a Ca^{2+}-induced precipitate could easily be dissolved by addition of EGTA, and was reappeared by subsequent addition of Ca^{2+}. Furthermore, such cycles of dis- and reappearance of the precipitate could be repeated several times by alternate addition of EGTA and Ca^{2+}. By a spectrometric method using BCA reagents, protein concentration was determined during successive cycles of precipitate formation. About 46% of the proteins in the supernatant of the cell homogenate were recovered in the Ca^{2+}-induced precipitate. In each successive cycle of precipitate formation, certain loss of proteins occurred. In 2nd, 3rd, and 4th cycles, the precipitates were found to contain 78%, 81%, and 83% of the

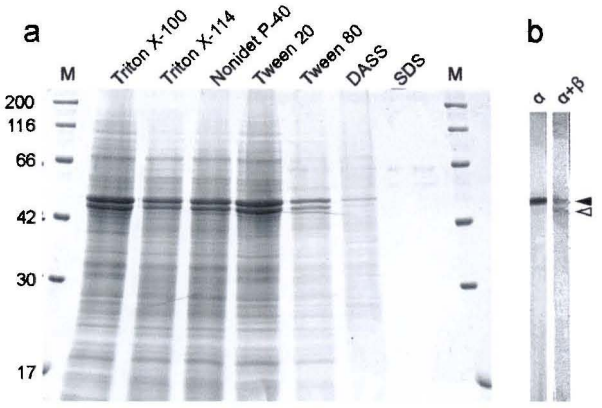

Fig. III.2. **a:** SDS-PAGE of Ca^{2+}-induced precipitates obtained from a cell homogenate of *Actinophrys sol* which were extracted with different kinds of detergents. Precipitates formed when Ca^{2+} was added to cell homogenates which were extracted with non-ionic detergents (Triton X-100, Triton X-114, Nonidet P-40, Tween 20, and Tween 80), while only small amounts of precipitates were obtained with anionic detergents (DASS and SDS). Molecular weights of the marker proteins (M) are shown at the left side of the gel. **b:** Immunoblotting analysis for the presence of α- and β-tubulin in the Ca^{2+}-inducled precipitate. Positive reactions against α-tubulin (α) and tubulin (α+β) antibodies were observed, indicating that the two dominant protein bands contain α- and β-tubulins. Black and white arrowheads point positions of α- and β-tubulin, respectively.

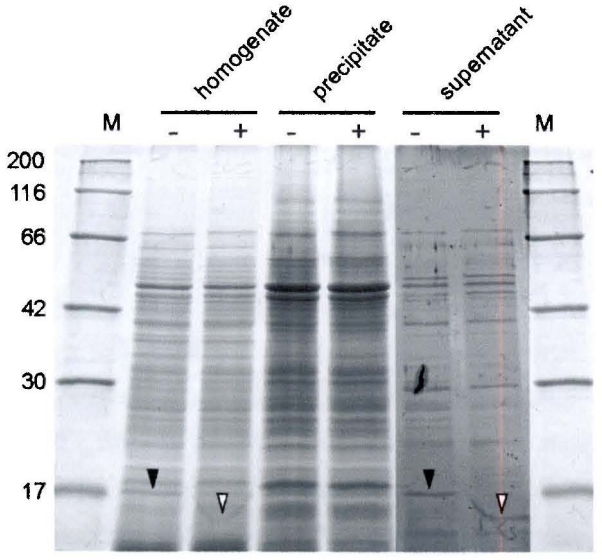

Fig. III.3. SDS-PAGE analysis showing the existence of a Ca^{2+}-sensitive protein in the cell homogenate. By addition of Ca^{2+}, a 17 kDa protein changed its electrophoretic mobility from 17 (filled arrows) to 15 kDa (open arrows) in apparent molecular weight. Note that the protein was detected in the supernatant after precipitate formation with Ca^{2+} (sup), but not in the precipitate (ppt). Molecular weights of the marker proteins (M) are indicated at the left of the figure. A part of the gel image (sup + and -) was artificially contrast-enhanced for demonstrating the existence of 17 kDa protein in this fraction.

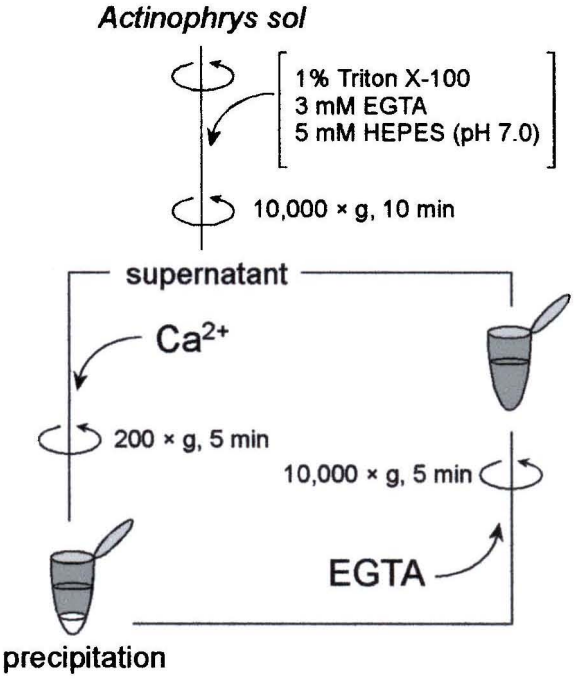

Fig. III.4. Schematic drawing of the procedure for preparing Ca^{2+}-induced precipitate. Cells were homogenized in a detergent-containing solution and a clear supernatant was obtained by centrifugation. After addition of Ca^{2+} to the supernatant, a white precipitate formed and was obtained as a pellet by low-speed centrifugation. The precipitate became dissolved by addition of EGTA, and reappeared by subsequent addition of Ca^{2+}.

proteins which had been present in the supernatant before addition of Ca^{2+}, respectively. The pellets which appeared after successive cycles of precipitate formation were subjected to SDS-PAGE and shown in Fig. III.5. The Coomassie brilliant blue-stained protein profiles remained constant, and there was no protein band with an increasing tendency after cycles of dis- and re-appearance of the precipitate. It was incidentally found that exogenous proteins added to the supernatant of the cell homogenate are incorporated to the Ca^{2+}-induced precipitate. For example, when BSA was added to the supernatant, a precipitate appeared as usual, but it contained BSA as one of the components of the precipitate (arrowhead in Fig. III.6). BSA was incorporated into the Ca^{2+}-induced precipitate in a concentration-dependent manner, and SDS-PAGE pattern of the intrinsic proteins was not affected by

the introduction of exogenous BSA protein. Many kinds of proteins seem to be incorporated to the precipitate, as all the marker proteins for SDS-PAGE were also incorporated (data not shown). This result suggests that the precipitate may include many proteins that are not essential for its Ca^{2+}-sensitivities but are just associated to the precipitate. The supernatant of the cell homogenate was fractionated by sucrose density gradient ultracentrifugation to identify essential components for the precipitate formation. Obtained fractions were subjected to SDS-PAGE and shown in Fig. III.7. Ca^{2+}-induced precipitates appeared only in fractions 2 to 5, in which a 50 kDa protein was particularly enriched. This fact raises a possibility that the 50 kDa protein is one of the necessary components for the formation of the precipitate.

When a Ca^{2+}-induced precipitate was slightly pressed with a glass needle from the top of a coverslip, the precipitate adhered to the surface of either the glass slide or the coverslip, in which the precipitate became clotted by adhesion of small granules close together. When EGTA solution was introduced from a side of the specimen, free granules were flashed away, and the clot of the precipitate became loosened and swollen to form a less refractive layer at the edge of the clotted precipitate (Fig. III.8a). By the addition of Ca^{2+}, contraction of the swollen layer occurred and the edges became tightened up (Fig. III.8b). When the precipitate was pressed hardly, it adhered to the glass surface like a viscous paste (Fig. III.9a). The adhered precipitate became contracted by the addition of Ca^{2+} (Fig. III.9b), and was relaxed by the following addition of EGTA (Fig. III.9c). Both contraction and relaxation of the adhered precipitate were not inhib-

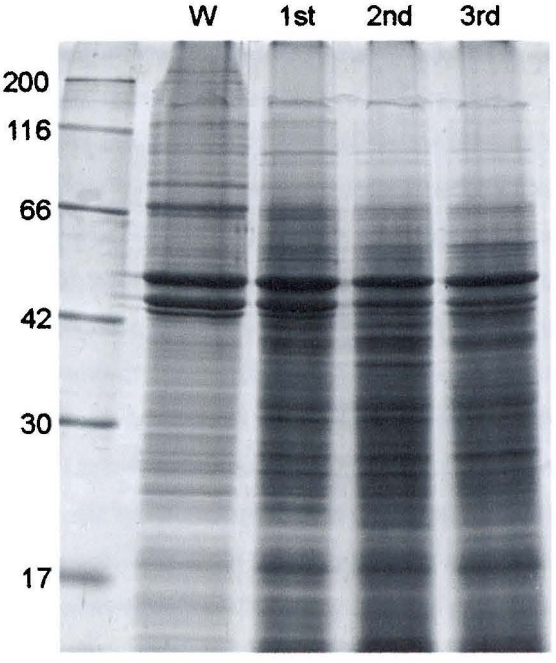

Fig. III.5. SDS-PAGE analysis of the precipitate after cycles of dis- and re-appearance. Samples represented as W, 1st, 2nd and 3rd show proteins in the whole-cell sample (W) and precipitates obtained after cycles of precipitation for one (1st), two (2nd) and three (3rd) times , respectively. A large number of proteins were present in the precipitate even after three cycles of precipitate formation, and no protein has been enriched.

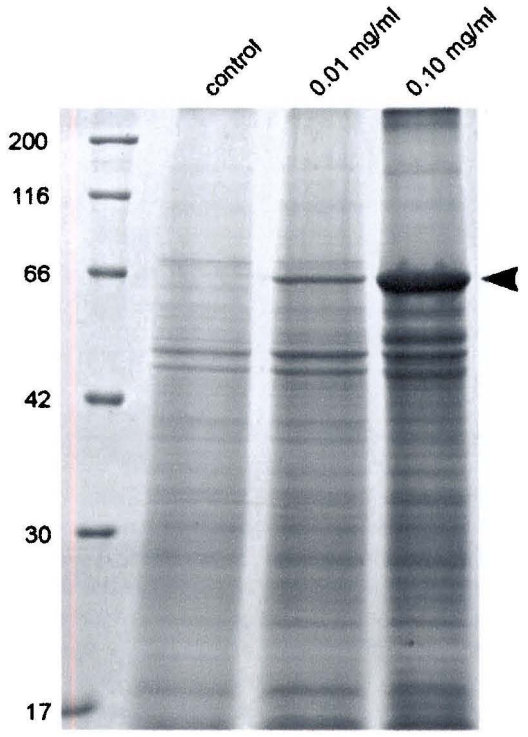

Fig. III.6. SDS-PAGE analysis of the Ca^{2+}-induced precipitate with bovine serum albumin (BSA). When BSA was added to the supernatant of the cell homogenate, it was recovered in the Ca^{2+}-induced precipitate in a concentration-dependent manner. BSA appeared as a predominant band when it was added at 0.1 mg/ml to the supernatant that contains 1 - 2 mg/ml of total intrinsic proteins.

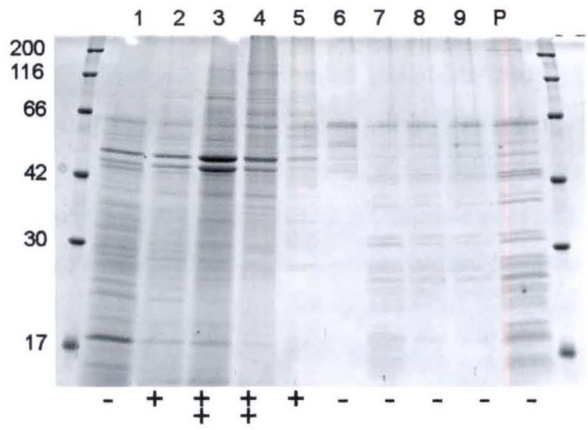

Fig. III.7. SDS-PAGE analysis of fractionated proteins of the supernatant of the cell homogenate by sucrose density gradient ultracentrifugation. Ca^{2+} was added to all the fractions after centrifugation, and precipitates appeared only in the fractions no. 2 to 5 (number of plus marks shows degree of precipitate formation, and minus marks represent no precipitate formation). In the fractions no. 3 and 4, most predominant proteins appear to have approximate molecular weights of about 50 kDa.

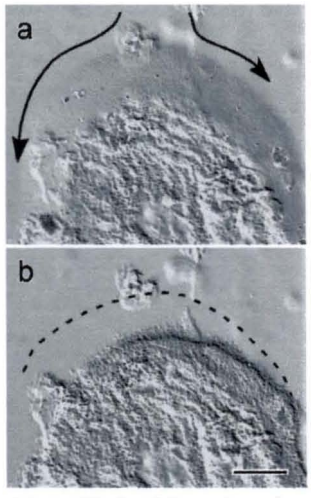

Fig. III.8. Sequential light micrographs of an adhered precipitate, showing its response to Ca^{2+}. When a precipitate was slightly compressed, it adhered to the surface of a glass slide. **a:** Free granules were flashed away from its edges by a stream of EGTA solution (arrows), and the precipitate remained on the glass surface with a transparent peripheral region. **b:** The peripheral region of the adhered precipitate suddenly tightened up by subsequent addition of Ca^{2+} ($[Ca^{2+}]_{free}$ = 2 mM). Broken line shows the periphery of the precipitate in EGTA solution (**a**). Solutions were applied from the top of the figures. Bar = 20 μm.

ited by treatment with colchicine (10 mM) or cytochalasin B (1 mM). As shown in Fig. III.10, contraction and relaxation of the adhered precipitate could be induced many times by alternate addition of Ca^{2+} (filled arrows) and EGTA (open arrows). Degree of contraction of the precipitate was dependent on free calcium concentration. As shown in Fig. III.11, the process of contraction and relaxation of the adhered precipitate was dependent

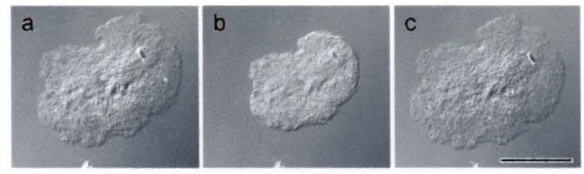

Fig. III.9. Sequential light micrographs of a precipitate strongly compressed on a glass surface, showing cyclic contraction and relaxation by successive addition of Ca^{2+} and EGTA. The precipitate that was attached to a glass surface had a paste-like appearance (**a**). Contraction (**b**) and relaxation (**c**) of the precipitate were induced repeatedly by successive additions of Ca^{2+} ($[Ca^{2+}]_{free}$ = 2 mM) and EGTA (3 mM). Bar = 20 μm.

on external free Ca^{2+} concentration, and was characterized by hysteresis. When free Ca^{2+} concentration was increased stepwise from 0 to 10^{-5} M, the adhered precipitate became contracted (filled circles) with its apparent Km value (or free Ca^{2+} concentration required for the half-maximum response) of 1.3×10^{-7} M. The following decrease in free Ca^{2+} concentration induced gradual relaxation of the contracted precipitate (open circles) with its apparent Km value of 1.3×10^{-8} M.

DISCUSSION

In the present study, Ca^{2+}-dependent contractility of the cytoplasm of the heliozoon *Actinophrys sol* was examined in vitro. A Ca^{2+}-induced precipitate was obtained from the cell homogenate, which retained its Ca^{2+}-dependent contractility. The clotted precipitate showed Ca^{2+}-dependent contraction that seems to share common contractile properties with the membrane-permeabilized cell models of *A. sol* (Arikawa et al., 2002b). In the actinophrid heliozoons *A. sol* and *Echinosphaerium akamae*, cytoplasmic contraction of permeabilized cell models repeatedly occurred by alternate addition of Ca^{2+} and EGTA, and it did not require ATP (Arikawa and Suzaki, 2002; Arikawa et al., 2002b). Similar contractility was found to exist inside isolated nuclei in *A. sol* and *E. akamae* (Arikawa and Suzaki, 2002; Arikawa et al., 2002a). However,

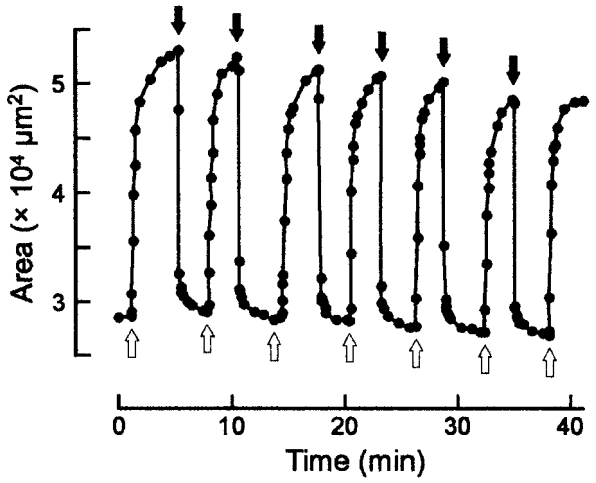

Fig. III.10. Continuous measurement of the projected area of the adhered precipitate measured on the video image. Cycles of contraction and relaxation of the adhered precipitate were repeatedly induced for 6 times within 40 minutes. Close and open arrows indicate the moments of additions of Ca^{2+} ($[Ca^{2+}]_{free}$ = 2 mM) and EGTA (3 mM), respectively.

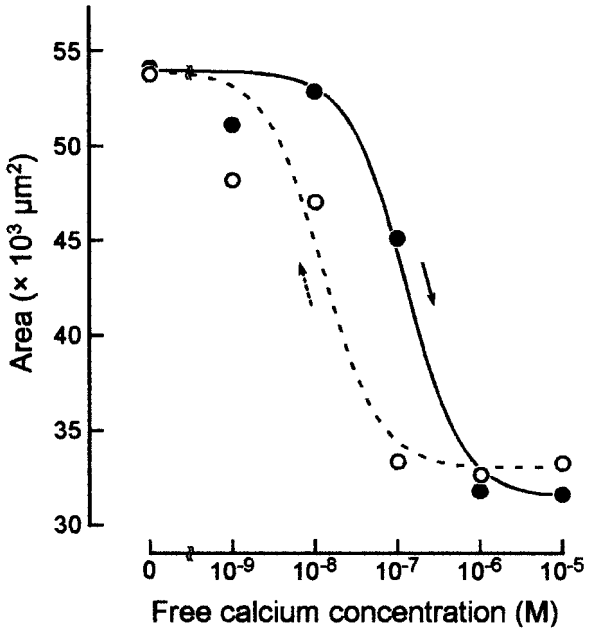

Fig. III.11. Relationship between projected area of the adhered precipitate and free calcium concentration in the surrounding medium, showing a hysteresis. Open circles represent processes of relaxation of the precipitate by applying decreasing concentrations of Ca^{2+} (Km = 1.3 × 10^{-8} M), and filled circles show a progressive change of the projected area of the precipitate induced by stepwise increase in Ca^{2+} concentration (Km = 1.3 × 10^{-7} M). The experiment started from $[Ca^{2+}]_{free}$ = 10^{-5} M, and the precipitate was subjected to a graded decreasing series of Ca^{2+} (the sequence of experiment is indicated by a broken arrow), and finally treated with EGTA. The same precipitate was then subjected to the increasing concentrations of Ca^{2+} in a sequence shown by a solid arrow.

neither formation nor contractility of the Ca^{2+}-induced precipitate have any relationship to the nuclear contraction, because nuclei were centrifugally removed in advance from the cell homogenate. The threshold level of free Ca^{2+} concentration for inducing cytoplasmic contraction in model cells was 2.4 × 10^{-8} M in *A. sol* (Arikawa et al., 2002b). Similarly, contraction of the clotted precipitate was also Ca^{2+}-dependent without any requirement of other energy supply, and its threshold level of free Ca^{2+} concentration was in the range of 10^{-7} - 10^{-8} M. These similarities strongly suggest that in vitro contraction of the clotted precipitate may reflect cytoplasmic contraction of the axopodia of *A. sol*, further strengthening the case for the involvement of Ca^{2+}-induced contraction of the CTS in the axopodial contraction. The CTS has been surmised to be responsible for the axopodial contraction (Suzaki et al., 1980a; Ando and Shigenaka, 1989; Suzaki et al., 1994). The CTS is morphologically distinct from other contractile organelles in other organisms, and shows a characteristic transformation when contraction occurs (Matsuoka et al., 1985; Kinoshita et al., 2001). SDS-PAGE analysis showed that a certain Ca^{2+}-sensitive protein exists in the cell homogenate (Fig. III.3). This protein has an apparent molecular weigh of 17 kDa with faster electrophoretic mobility in the presence of Ca^{2+}. Molecular weight and the Ca^{2+}-dependent mobility shift suggest that the protein may be related to Ca^{2+}-binding contractile proteins such as centrin (caltractin) and spasmin (Yamada and Asai, 1982; Salisbury et al., 1984; Coling and Salisbury, 1992) which are included in the calmodulin superfamily. However, after precipitate formation with Ca^{2+}, the 17 kDa protein was not detected in the precipitate but in the supernatant, indicating that the protein is not involved in the Ca^{2+}-induced precipitate.

It has been found that a contraction-

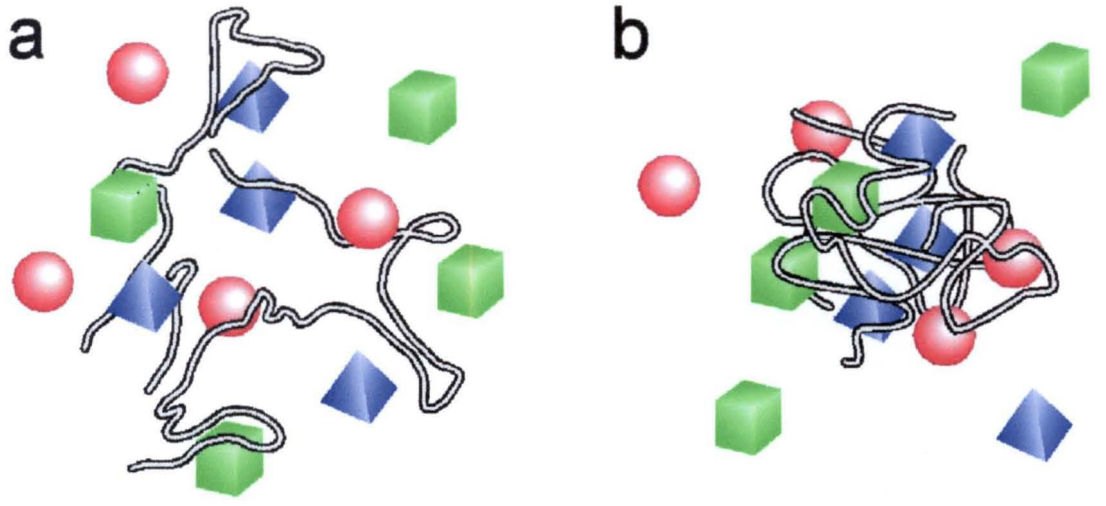

Fig. III.12. A schematic drawing illustrating possible involvement of the conformational change of CTS and other proteins in the process of contractile tubules aggregation. **a:** In the supernatant of the cell homogenate, individual CTSs are suspended in the medium with cytoplasmic proteins (colored objects). **b:** When Ca^{2+} is added to the cell homogenate, contraction of the CTS occurs. During this process, many, but not all, cytoplasmic proteins are incorporated in the contracted CTS, resulting in co-sedimentation of the proteins with CTS in the Ca^{2+}-induced precipitate.

extension cycle of the spasmoneme, a contractile organelle of the vorticellid ciliate, represented a kind of hysteresis (Ochiai et al., 1979). In this study, as shown in Fig. III.11, Ca^{2+}-dependent reactivation of the adhered precipitate also showed a hysteresis loop. Spasmin is a Ca^{2+}-binding protein with a molecular weight of about 17 kDa, and is a main component of the spasmoneme. Similarly, a 17 kDa protein was also detected in the cell homogenate of *A. sol.*, which showed a mobility shift on SDS-PADE gel in a Ca^{2+}-dependent manner. However, the protein remained in the supernatant after precipitate formation, and no proteins in the precipitate were affected by Ca^{2+} on SDS-PAGE mobility (Fig. III.3). These results suggest that the molecular mechanism of contraction and relaxation of the adhered precipitate may be different from that of spasmoneme contraction.

An SDS-PAGE gel in Fig. III.5 showed that a large number of proteins were present in the Ca^{2+}-induced precipitate. The protein profile remained unchanged even after repeated cycles of precipitate formation, indicating that the clotted precipitate is composed of many proteins. Moreover, when BSA was added to the supernatant of the cell homogenate, it was recovered in the Ca^{2+}-induced precipitate. From these results, it seems plausible that many of the component proteins of the Ca^{2+}-induced precipitate may be essential for neither formation nor contractility of the precipitate. Transformation of the CTS from tubular to granular forms occurs when axopodial contraction takes place (Suzaki et al., 1980a; Matsuoka et al., 1985; Ando and Shigenaka, 1989; Suzaki et al., 1994; Kinoshita et al., 2001). Furthermore, similar morphological change of the CTS has been observed in a cell homogenate of *Actinophrys* after addition of Ca^{2+} (Arikawa et al., 2002b). A possible mechanism for the precipitate formation is schematically shown in Fig. III.12. In the Ca^{2+}-free cell homogenate, the CTS is present in the elongated state with many kinds of cytoplasmic proteins (Fig. III.12a). By the addition of Ca^{2+}, the CTS transforms into a compact conglomerate of granular CTS (Fig. III.12b) as I have previously shown by negative-staining procedure (Arikawa et al., 2002b). These

reactions may involve some additional proteins, including even exogenous ones such as BSA, as well as formation of linkages between adjacent CTSs, and the precipitate formation may be based on resulting packing of the CTS and associated protein molecules. As an attempt to search for essential proteins for Ca^{2+}-sensitivity, further fractionation was carried out by sucrose density gradient ultracentrifugation (Fig. III.7). Although obtained fractions (numbers. 2-5 in Fig. III.7) still contained many proteins, a couple of proteins around 50 kDa in molecular weight were particularly enriched in these fractions. Immunoblotting analysis showed that these proteins were α- and β-tubulins, although there is no evidence that tubulins are essentially involved in either formation or contraction of the precipitate. Further purification and characterization of the proteins in the precipitate are now in progress to understand the molecular mechanism of this unique Ca^{2+}-dependent motility.

CHAPTER IV

High-Resolution Scanning Electron Microscopy of Chromatin Bodies and Replication Bands of Isolated Macronuclei in the Hypotrichous Ciliate *Euplotes aediculatus*

INTRODUCTION

Ciliated protozoans possess two different types of nuclei, micronucleus and macronucleus, within the cytoplasm (Raikov, 1996). Although the structure and the manner of nuclear replication are different from species to species, hypotrichous ciliates such as *Stylonychia*, *Oxytricha* and *Euplotes* possess the most complex macronuclear structures among the ciliates. During S-phase of the cell cycle, a specialized and light microscopically-visible structure, called the replication band (RB), appears in the macronucleus; the RB migrates through the macronucleus while replicating DNA (Raikov, 1969; Olins and Olins, 1981).

Using transmission electron microscopy, a large number of ultrastructural studies on chromatin and the RB have been carried out (Fauré-Fremiet et al., 1957; Kluss, 1962; Phegan and Moses, 1967; Ringertz et al., 1967; Evenson and Prescott, 1970). These studies have shown that chromatin bodies are composed of densely packed chromatin fibrils (Kluss, 1962; Ringertz et al., 1967; Olins et al., 1988), and that the chromatin bodies become disintegrated into their component fibrils in the RB for DNA replication. After DNA replication, these fibrils reassemble and organize themselves into new chromatin bodies (Kluss, 1962; Evenson and Prescott, 1970; Olins et al., 1988). In contrast to the abundant knowledge obtained by the transmission electron microscopy, very little information is available on the three-dimensional construction of the macronucleus and the RB. This might stem mainly from technical difficulties in demembranating the macronucleus. In this study, I employed an improved technique of isolation and demembranation of the macronucleus of the ciliate *Euplotes aediculatus*, and observed for the first time the surface structures of the chromatin bodies in the macronucleus by scanning electron microscopy. Combining both scanning and transmission electron microscopy, the three-dimensional construction of the macronucleus and the RB of *Euplotes* is discussed.

MATERIALS AND METHODS

Cell Culture

Euplotes aediculatus were collected from local drains in Fukuoka Prefecture, Japan, and maintained in a culture medium (44 μM KCl, 11 μM $CaCl_2$, 29 μM K_2HPO_4 and 11 μM $MgSO_4$, pH 7.0) at 20°C. The cells were fed 3 times a week with *Chilomonas paramecium* or *Chlorogonium elongatum*. For enrichment of the proportion of cells with RB in the macronucleus, cells were first starved for 3 - 4 days, fed with abundant prey, and finally harvested at 24 h after feeding (Olins et al., 1988).

Isolation of Macronuclei

Ciliates were washed with fresh culture me-

dium before they were used for experiments. They were then placed on a microscope slide with a little culture medium, and gently mixed with the same amount of 0.25 M sucrose solution (0.25 M sucrose and 2 mg/ml methyl green) by a glass needle. Methyl green dye was added to the sucrose solution for visualizing the macronuclei, without methyl green the nuclei became transparent and undetectable after isolation. The cells were placed on a coverslip with a small amount of the sucrose solution and frozen at -20°C in a conventional freezer. After thawing at room temperature, cells were gently disrupted by pipetting with a Pasteur pipette, whose tip had been pulled and cut into a diameter of approximately cell size (about 150 μm). Isolated macronuclei were washed with small air bubbles that were puffed out from the tip of a Pasteur pipette with a smaller tip (diameter of about 10 μm). This process was necessary for removing remnants of the nuclear membrane from the isolated macronucleus. The isolated nuclei were further cleaned with an excess amount of the sucrose solution, and drained on a coverslip till the nuclei became stuck to the glass surface. The coverslip was then immersed in 1% acetic acid solution for 5 min at room temperature for completely removing the nuclear membrane.

Scanning Electron Microscopy

Isolated macronuclei on the coverslip were washed with 10 mM phosphate buffer (pH 6.5) and fixed with a modified Shampy's fixative (2.7% OsO_4, 1% $K_2Cr_2O_7$, and 1% CrO_3) for 10 min at room temperature. The fixed samples were dehydrated with a graded ethanol series, and infiltrated in a mixture of ethanol and benzene (1:1), 100% benzene, and a mixture of benzene and p-dichlorobenzene (1:1) at room temperature (10 min for each step). Then the specimens were immersed in 100% p-dichlorobenzene at 60°C for 30 min, and gently placed on the surface of a SEM specimen stub that was pre-warmed at 60°C. Drying was carried out overnight at room temperature by simply leaving the specimen stub in a Petri dish with its lid slightly open for ventilation (Araki and Takahashi, 1978). The dried specimens were sputter coated with platinum/palladium (ca. 10 nm in thickness), and observed with a field emission scanning electron microscope (JEOL JSM-6401F).

Transmission Electron Microscopy

Living cells were prefixed with 2.5% glutaraldehyde in 25 mM cacodylate buffer (pH 7.0) for 3 min at room temperature, rinsed with the same buffer, and postfixed with buffered 1% OsO_4 for 30 min at room temperature. Isolated macronuclei were prepared as described above, washed in 10 mM phosphate buffer (pH 6.5), and fixed with the modified Shampy's fixative for 10 min at room temperature. Following preparations (rinse, dehydration, embedding, sectioning, staining, and obsavation) were carried out as described in Chapter I.

RESULTS

In this study, I observed the interior surface structures of isolated and demembranated macronuclei of *Euplotes aediculatus* at high resolution.

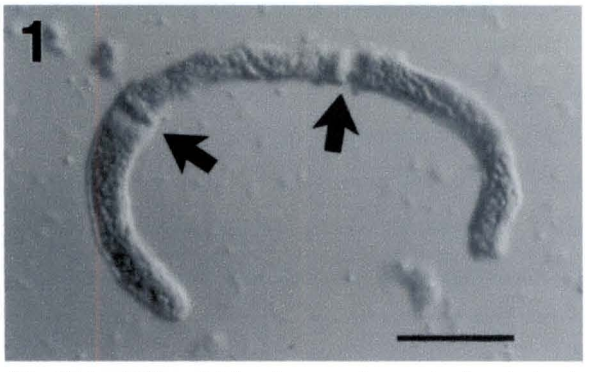

Fig. IV.1. Differential interference micrograph of an isolated macronucleus. Chromatin bodies and a set of replication bands (arrows) were well maintained even after isolation. Bar = 10 μm.

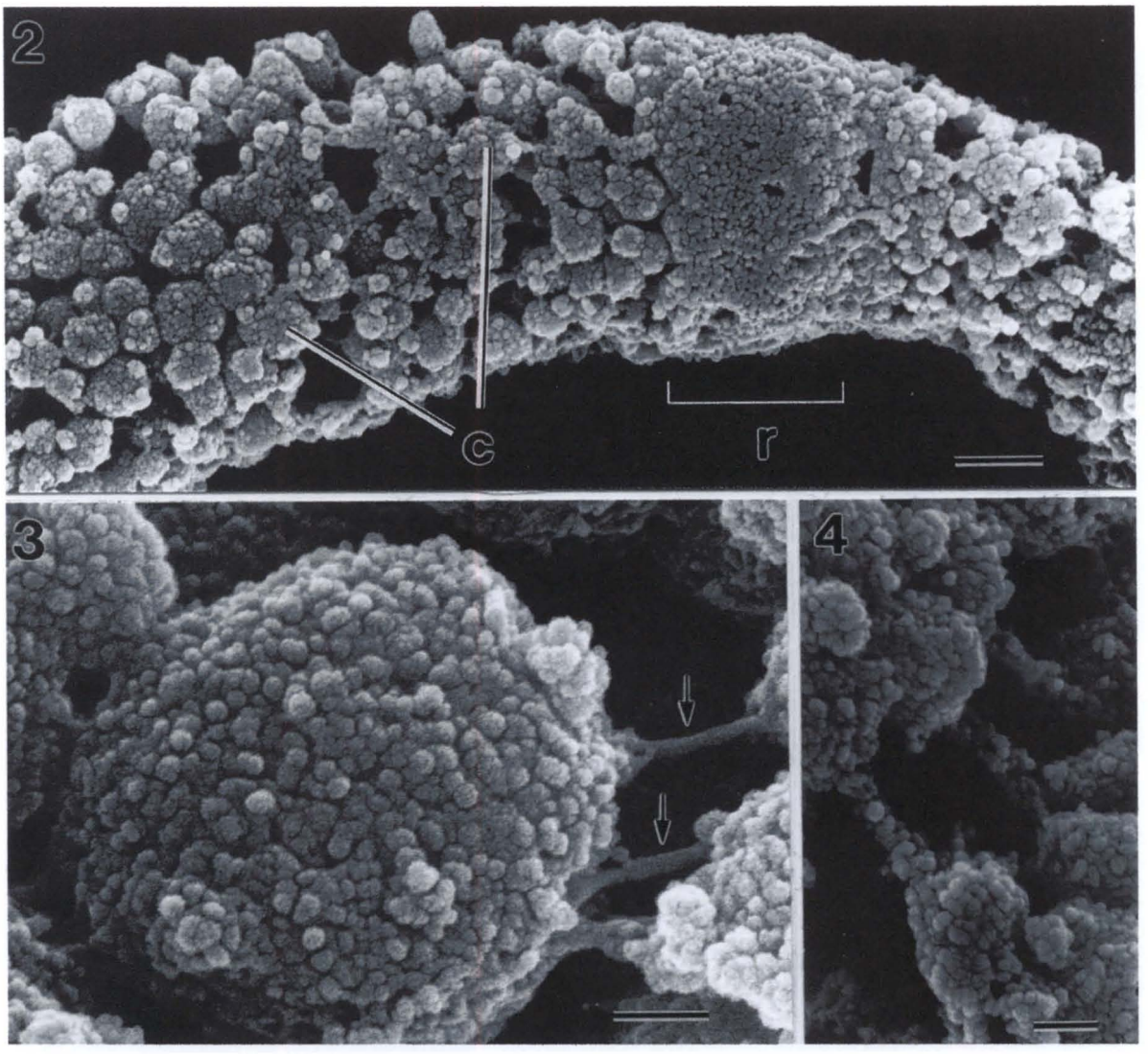

Fig. IV.2. Scanning electron micrograph of the replication band of an isolated and demembranated macronucleus. A large number of granular chromatin bodies (c) are packed in the macronucleus. The replication band (r) does not possess chromatin bodies, while consisted of 50 nm granules. In this micrograph, the replication band is migrating from left to right. Bar = 1 μm.

Fig. IV.3. Enlarged scanning electron micrograph of a chromatin body. Chromatin bodies varied in diameter, while their surfaces are consistently covered with 50 nm granules. Thin and smooth cross-bridge structures (about 40 nm in diameter) are present between chromatin bodies (arrows). Bar = 200 nm.

Fig. IV.4. Enlarged scanning electron micrograph showing another type of connecting bridges observed between chromatin bodies. This type of intra-chromatin bridge is covered by a series of 50 nm granules. Bar = 200 nm.

At the light microscopic level, the isolated macronuclei retained their original shape. As shown in Fig. IV.1, the characteristic C-shape, a set of RBs (arrows), and granular appearance of the chromatin bodies appeared unchanged. The nuclear matrix and nucleoli disappeared during the process of isolation and demembranation, but I could observe the surface of the chromatin body and the RB with high resolution (Figs. IV.2 - 4). A part of a macronucleus with an RB is shown in Fig. IV.2, in which the RB is under migration from left to right. The chromatin bodies located on the left of the RB (i.e. after DNA replication) were in the range of 0.3 - 1.0 μm in diameter, whereas those on the right of the RB (i. e. before replication) were smaller (0.2 - 0.4 μm in diameter). The surface of the chromatin body was

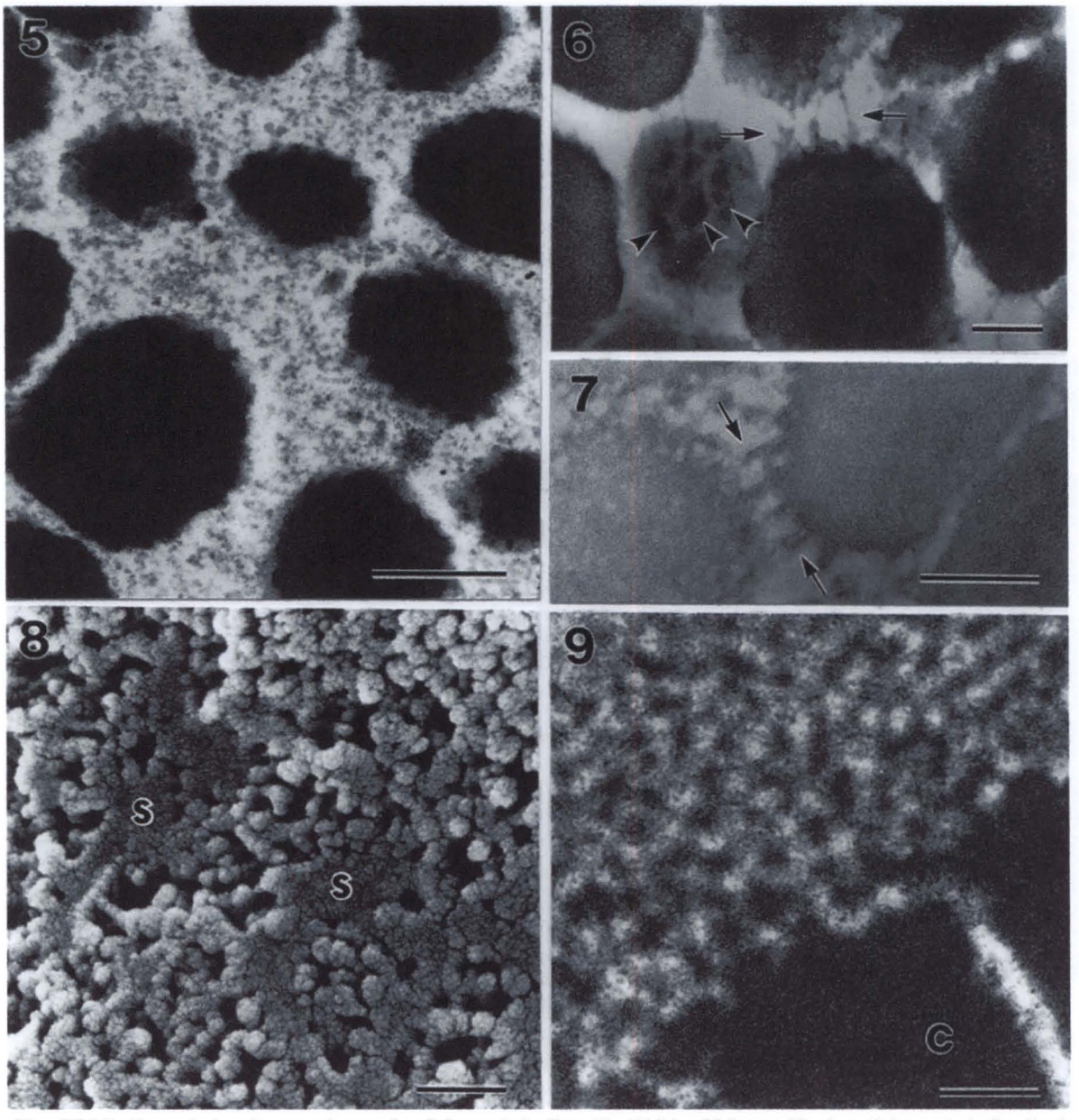

Figs. IV.5-7. Transmission electron micrographs of chromatin bodies. Fig. IV.5 is a high magnification of chromatin bodies fixed without macronuclear isolation. The chromatin bodies show rough contours and appear highly condensed. Filamentous bridges between chromatin granules are not clearly seen in this preparation, as the bridges might be embedded in the nuclear matrix. Bar = 500 nm. Fig. IV.6 and 7. Chromatin bodies in an isolated macronucleus. Bars = 200 nm. In Fig. IV.6, a tangential section of one chromatin body shows surface knobs of about 50 nm in size (arrowheads). As indicated by arrows, furthermore, chromatin bodies are connected with thin (Fig. IV.6) and thick (Fig. IV.7) bridges.

Fig. IV.8. Scanning electron micrograph of the surface of a replication band. The surface is mostly covered with 50 nm granules, in which patches of smooth areas (s) paved with 10 nm particles are present. Bar = 200 nm.

Fig. IV.9. High magnification transmission electron micrograph showing the periphery of a replication band. A network of 40 - 50 nm fibrils is continuously connected to the chromatin bodies (c). Upon closer look, the 40 - 50 nm fibrils seem to be composed of fine particles of ca. 10 nm in size. Bar = 200 nm.

found to be composed of small granules of 47 ± 12 nm (mean ± S.D., n = 135). The surface structure of the RB (the region marked "r" in Fig. IV.2) was different from other parts of the macronucleus; the region was completely bare of chromatin bodies, while it was evenly composed of granules. The diameter of these granules was 48.1 ± 11.5 nm (n = 66), which was not significantly different ($p < 0.01$)

from the diameter of the granules located on the chromatin bodies. Chromatin bodies were connected with each other by cross-bridges of two types. A thicker one about 100 nm in diameter was composed of a series of 50 nm granules (Fig. IV.4). A thinner one (about 30 - 40 nm in diameter) had a smooth surface (arrows in Fig. IV.3).

A transmission electron micrograph of an intact macronucleus (Fig. IV.5) shows that chromatin bodies have rough contours, and appear to be extremely condensed. The nuclear matrix is filled with small particles of various sizes. In contrast, isolated chromatin bodies showed lesser electron density, and the nuclear matrix was completely removed from the macronucleus (Fig. IV.6 and 7). The granular appearance of the surface of the chromatin body was apparent in a tangential grazing section of an isolated chromatin body (arrowheads in Fig. IV.6). The two different types of cross-bridge structures were also observed in thin sections (these structures are shown by arrows in Fig. IV.6 and 7). Thus, the characteristic surface appearances of the chromatin bodies observed by high-resolution SEM correspond well with those obtained by TEM observations, indicating that they are not artefacts produced during the process of nuclear isolation and preparation for scanning electron microscopy.

High-magnification SEM observations (Fig. 8) showed that the surface of the RB possesses patches of smooth regions in which the 50 nm granules appear to be disintegrated into their component sub-structures of fine granules (about 10 nm in diameter). A corresponding TEM picture is shown in Fig. 9, where chromatin bodies are continuously connected to the 50 nm granules at the edge of the RB. The 50 nm granules are embedded in fine granules of about 10 nm in diameter, which correspond well to the fine granules observed by SEM.

DISCUSSION

In the hypotrichous ciliates, including *Euplotes*, *Oxytricha* and *Stylonychia*, DNA replication in the macronucleus is carried out in the RB (Raikov, 1996; Olins and Olins, 1981). In *Euplotes*, a set of RBs appear at both ends of a C-shaped macronucleus, both move inward through the whole macronucleus, and finally disappear after they are fused (Prescott and Kimball, 1961; Kluss, 1962; Ringertz et al., 1967; Raikov, 1969). The RB is known to be composed of two morphologically distinct forward and rear zones (Prescott and Kimball, 1961; Stevens, 1963; Ringertz et al., 1967). In the forward zone, chromatin bodies become disintegrated into 40 - 50 nm fibrils and a complicated meshwork structure is formed (Olins and Olins, 1981; Olins et al., 1988). In the rear zone, the fibrils are further dissociated and thinner filaments of 2 - 10 nm in diameter appear (Olins et al., 1988). DNA replication is known to take place exclusively in the rear zone (Gall, 1959; Prescott and Kimball, 1961). After DNA replication, the filaments are reorganized into chromatin bodies which are usually bigger than those located at the pre-replication side of the RB (Ringertz et al., 1967). Chromatin bodies in the macronucleus are extremely condensed, without any indication of obvious substructures inside them (Olins et al., 1988, and Fig. IV.9 in this study). However, the chromatin body is considered to be composed of fine DNA-containing fibrils, since chromatin bodies are structurally continuous to the network of fine fibrils in the RB (Kluss, 1962; Ringertz et al., 1967; Olins et al., 1988).

In this study, I observed 3-dimensional surface structures of the RB in *Euplotes*. In the close proximity of the RB, the chromatin bodies were found to be disintegrated into small granules of

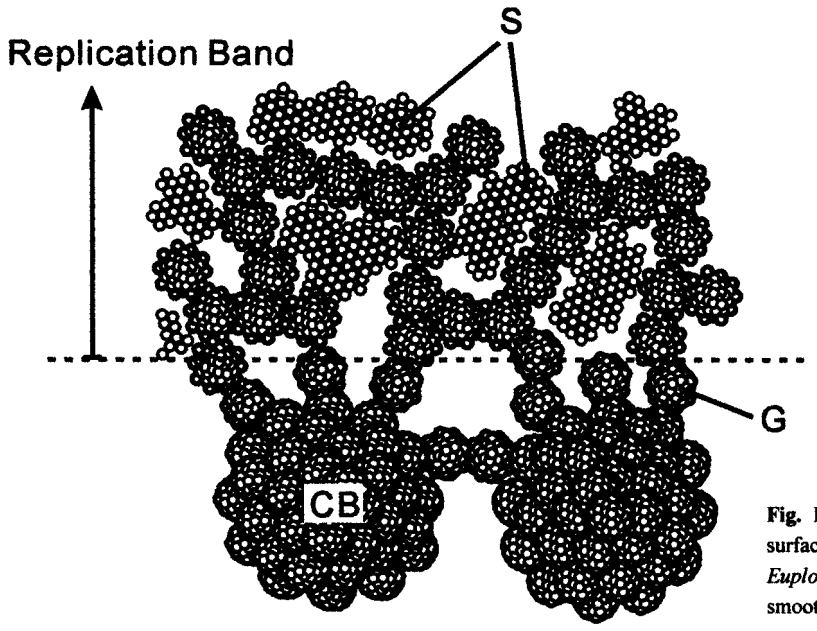

Fig. IV.10. Schematic representation of the surface structure in the macronucleus of *Euplotes aediculatus*. CB, chromatin body; S, smooth surface area; G, 50 nm granules.

about 50 nm in diameter. In the SEM observations, I could not distinguish the forward and rear zones of the RB. Small granules of ca. 50 nm in diameter were observed to be spread evenly all over the surface of the RB, in which patches of smooth areas of 10 nm granules were found. Transmission electron microscopy also failed to distinguish the two zones of the RB, but a network of 40 nm filaments was observed inside the RB. Judging from their sizes, the 50 nm surface granules on the RB might represent folded ends of the filaments which emerged on the surface of the RB. It is reported that the rear zone of the RB is an unstable structure, which easily disappears by various kinds of treatment (Evenson and Prescott, 1970; Olins et al., 1988; Allen et al., 1985). The rear zone was not clearly observed in the present study, probably because of the time-consuming isolation procedure applied to the macronucleus before it was chemically fixed. The smooth areas observed on the surface of the RB might be traces of the rear zone which had been distorted and reconstructed during the process of nuclear isolation.

Based on the present SEM and TEM observations, the morphological alteration of the chromatin structure during macronuclear replication is considered as follows (shown in Fig. IV.10): 1) The chromatin body is composed of aligned 40 - 50 nm granules, which are constructed with finer fibrils or linearly-connected small particles of about 10 nm in diameter. 2) The chromatin bodies become loosened prior to the DNA replication, and they become disintegrated into their component 40 - 50 nm granules, forming a meshwork structure in the RB. 3) The 40 - 50 nm granules become further disintegrated into 10 nm fine particles for DNA replication. 4) After the RB passes by, 40 - 50 nm fibrils are assembled again, from which bigger chromatin granules become reconstructed.

The unit genome of the hypotrichous ciliates (*Oxytricha*, *Stylonychia* and *Euplotes*) is known to be divided into 10,000 - 40,000 mini-chromosomes in the macronucleus (Klobutcher and Prescott, 1986). As the unit genome itself is also multiplied many times, the total number of mini-chromosomes within a single macronucleus is estimated at between 10^7 and 10^9 (Raikov, 1996). The volume of a single macronucleus of *Euplotes* is estimated to be

about 400 μm^3 from the light micrograph shown in Fig. IV.1. Assuming that about half of the macronuclear mass is occupied by the chromatin bodies as judged from the transmission electron micrograph in Fig. IV.5, one can estimate that total volume of the chromatin bodies in a macronucleus is about 200 μm^3. If we further assume that the chromatin bodies are tightly packed with 10 nm particles with a maximum volume density of 0.75 for solid spheres, a single 10 nm particle is calculated to be composed of 0.025 - 2.5 mini-chromosomes. Likewise, 3.16 - 316 mini-chromosomes correspond to a single 50 nm granule.

CHAPTER V

Ca^{2+}-dependent Contractility of Isolated and Demembranated Macronuclei in the Hypotrichous Ciliate *Euplotes aediculatus*

INTRODUCTION

Berezney and Coffey reported in 1974 that a stable structural framework in the nucleus, named "nuclear matrix", was detected in an isolated rat liver nucleus after chemical extractions (Berezney and Coffey, 1974). Many investigators explicitly speculated that the nuclear matrix may be a critical and facilitating element in nuclear functions. Although controversies still remain, numerous studies have led to the conclusion that the nuclear matrix is involved in gene expression, replication and transcription of DNA, and also processing and transportation of RNA (Pederson, 1998). Electron microscopic researches have revealed that the interior architecture of the nucleus is constructed by branched 10-nm filaments (Nickerson, 2001). In spite of the progress in characterization of nuclear proteins and ultrastructural properties of the nuclear matrix, dynamics and motility of the nucleus have received less attention.

A nuclear protein matrix was detected also in the macronucleus of the ciliate *Tetrahymena* (Herlan and Wunderlich, 1976). The nucleus of *Tetrahymena* has been extensively examined as a model system for studying basic structure and function of the eukaryotic nucleus (Gorovsky, 1973). In 1977, a reversibly contractile nuclear matrix was isolated from *Tetrahymena* macronuclei, and its mechanism of contraction was reported to be different from that of the actin-myosin interaction (Wunderlich and Herlan, 1977). Although ultrastructure and essential components of the nucleoskeleton have been well characterized, the biological significance of nuclear contractility remained unclear. Many protozoans possess nuclei unique in size and shape, which sometimes undergo vigorous shape changes (Raikov, 1996). The vegetative cells of hypotrichous ciliates such as *Stylonychia*, *Oxytricha*, and *Euplotes* have two types of nuclei, the micro- and the macronucleus, within the cytoplasm. In contrast to the micronucleus, the macronucleus changes both in shape and size during the cell cycle (Raikov, 1996). In spite of the large number of ultrastructural studies so far carried out (Fauré-Fremiet et al., 1957; Kluss, 1962; Phegan and Moses, 1967; Ringertz et al., 1967; Evenson and Prescott, 1970; Olins et al., 1988; Arikawa et al., 2000), there is no certain evidence that a contractile system exists in the macronucleus. In this study, I prepared an isolated and demembranated macronucleus of a hypotrichous ciliate *Euplotes aediculatus*, and found that it shows vigorous contraction and relaxation in a Ca^{2+}-dependent manner.

MATERIALS AND METHODS

Euplotes aediculatus cells were purchased from Carolina Biological Supply Company (Burlington, USA), and cultured in Volvic mineral water at 23 ± 1 °C. *Chlorogonium elongatum* was added twice a week as a food source. Subculturing was carried out at intervals of about 2 weeks.

Isolation of macronuclei was carried out according to Arikawa et al. (2000) with slight

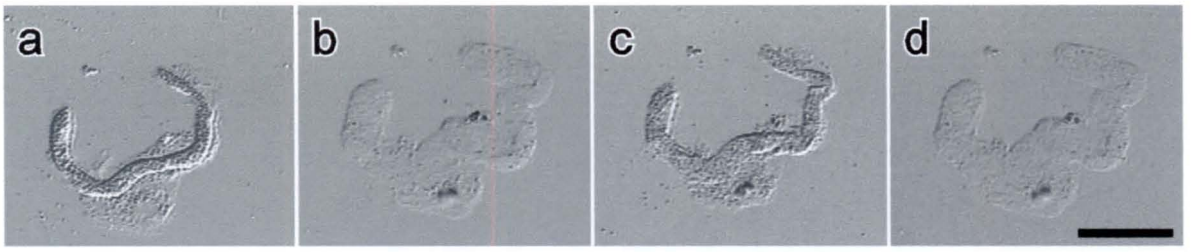

Fig. V.1. Sequential light micrographs showing repeated expansion and contraction of an isolated macronucleus of *Euplotes aediculatus*. **a:** A macronucleus just after isolation, showing the characteristic slender C-shape. **b:** The macronucleus expanded remarkably by the addition of 3 mM EGTA. **c:** After subsequent addition of Ca^{2+} at $[Ca^{2+}] = 2 \times 10^{-3}$ M, the relaxed macronucleus became contracted. **d:** After subsequent removal of Ca^{2+} by EGTA, the contracted macronucleus again expanded. Bar = 100 μm.

modifications. Washed cells were put on a hollow slide with a small amount of culture medium, and gently mixed with 250 mM sucrose. A little amount of methyl green dye was added to the sucrose solution for visualization of isolated macronuclei. After freezing at -20 °C and thawing at room temperature, macronuclei were isolated from the fragile cells by pipetting with a Pasteur pipette. By this procedure, remnants of the nuclear membrane became completely removed from the nuclear surface (Arikawa et al., 2000). After washing with fresh sucrose solution, isolated macronuclei were put on a glass slide coated with poly-L-lysine. To stick the isolated macronuclei on the surface of a glass slide, excess sucrose solution was removed by a thin-tipped Pasteur pipette. Light microscopic observation was curried out as described in Chapters I, II, and III.

RESULTS AND DISCUSSION

I have recently established a procedure for isolating *Euplotes* macronuclei and examined the three-dimensional surface structure of chromatin bodies and replication bands. By high-resolution scanning and transmission electron microscopy, I showed that the isolation procedure had no destructive effect on the ultrastructure of macronuclei (Arikawa et al., 2000). As shown in Fig. V.1a, the characteristic C-shaped appearance of a macronucleus in G1 phase remained unchanged after isolation and demembranation. When "EGTA solution" consisting of 3 mM EGTA and 5 mM HEPES (pH 7.0) was added, the macronucleus became swollen (Fig. V.1b). Then, "Ca^{2+} solution" consisting of 3 mM EGTA, 5 mM $CaCl_2$ and 5 mM HEPES (pH 7.0) was added, and the expanded macronucleus rapidly contracted and returned to its original shape (Fig. V.1c). The macronucleus expanded again on subsequent addition of EGTA solution (Fig. V.1d). Neither contraction nor relaxation of isolated macronuclei required ATP, and nuclear contraction was not induced by addition of Mg^{2+} or other cations even at concentrations higher than that required for Ca^{2+} (data not shown). The approximate area of an isolated macronucleus was continuously measured and is shown in Fig. V.2. Cycles of contraction and relaxation of the nucleus could be repeated several times by alternate addition of Ca^{2+} and EGTA (Fig. V.2a). One of the cycles is shown in detail in Fig. V.2b, which indicates that both contraction and relaxation responses took place within a few seconds. Although evidence for the presence of tubulin, actin and myosin in the nucleus of various kinds of cells has been shown (Douvas et al., 1975; Berrios and Fisher, 1986; Berrios et al., 1991; Nowak et al., 1997), there is no direct evidence to support possible involvement of these molecules in nuclear contractility. In this study, contraction and expan-

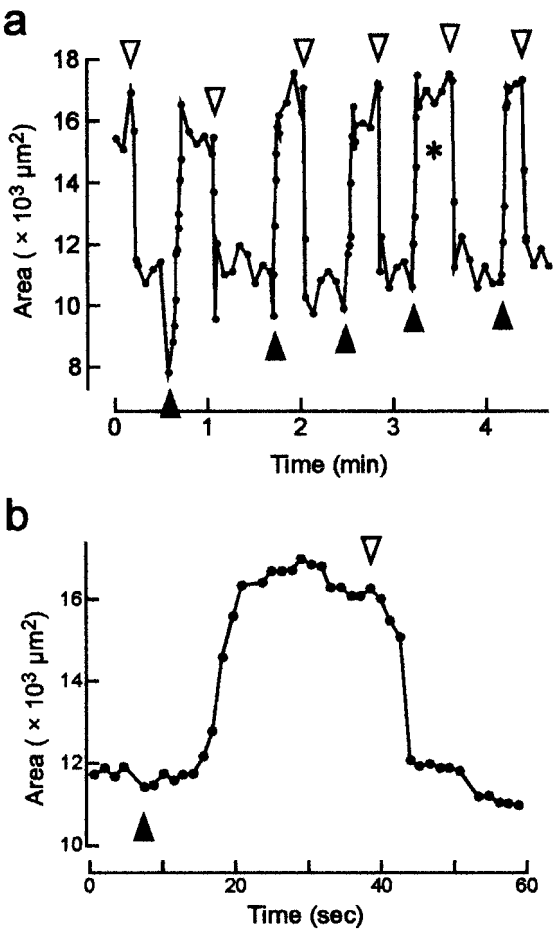

Fig. V.2. Trace of the approximate projected area of an isolated macronucleus. Open and filled arrowheads indicate the moments when Ca^{2+} ($[Ca^{2+}]$ = 2 mM) and EGTA (3 mM) were added, respectively. **a:** Cycles of contraction and expansion were observed several times by alternate addition of Ca^{2+} and EGTA. **b:** Enlargement of one of the cycles shown in panel **a** (marked with an asterisk). Both expansion and contraction occurred within a few seconds after removal and addition of Ca^{2+}, respectively.

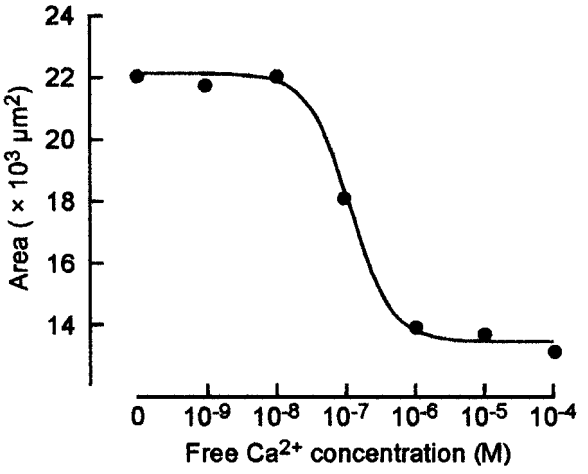

Fig. V.3. Relationship between approximate projected area of an isolated macronucleus and free Ca^{2+} concentration. The threshold level of free Ca^{2+} concentration for nuclear contraction was estimated as 1.1×10^{-7} M, by fitting a sigmoidal curve to the data.

sion of the isolated macronucleus were inhibited by neither colchicine (10 mM) nor cytochalasin B (1 mM), which suggests that the nuclear contractility in *Euplotes* is not mediated by tubulin- or actin-based machineries. The size of an isolated macronucleus at various concentrations of Ca^{2+} was measured and shown in Fig. V.3. The relationship between projected area of an isolated macronucleus and free Ca^{2+} concentration showed a sigmoidal dose-response with a threshold $[Ca^{2+}]$ level of 1.1×10^{-7} M.

Considerable evidence shows that cell nuclei in general vary in size and shape during the cell cycle and cell differentiation. In particular, nuclear enlargement precedes the onset of DNA synthesis (Arnold et al., 1972), while nuclear contraction appears to accompany cessation of DNA synthesis (Guttes and Guttes, 1969). The macronucleus of *Euplotes* also changes in size and shape in the cell cycle. To investigate whether contractility of the macronucleus persists throughout the cell cycle, I applied the same procedure at various phases in the cell cycle. Macronuclei in S phase and G2 or M phase were isolated and shown in Figs. V.4 and V.5, respectively. The presence of a set of replication bands (arrowheads in Fig. V.4) is a characteristic feature of the nucleus in S phase, where DNA replication is taking place (Gall, 1959; Prescott and Kimball, 1961; Raikov, 1969; Olins and Olins, 1981; Olins and Olins, 1987). When EGTA solution was added to a macronucleus in S phase, the nucleus became expanded within a few seconds (Fig. V.4b and c). The nuclear expansion was less evident around the replication bands as compared with other regions in the nucleus. With the subse-

Fig. V.4. Sequential light micrographs of an isolated macronucleus in S phase that possessed a pair of replication bands (arrowheads). The macronucleus adhered on a glass surface (**a**) became swollen on addition of EGTA (**b** and **c**). Micrographs in panels **b** and **c** were taken at 5 and 20 s after the addition of EGTA, respectively. The degree of nuclear expansion was restricted around the replication bands. The expanded macronucleus contracted after the addition of Ca^{2+} (**d**). Bar = 100 μm.

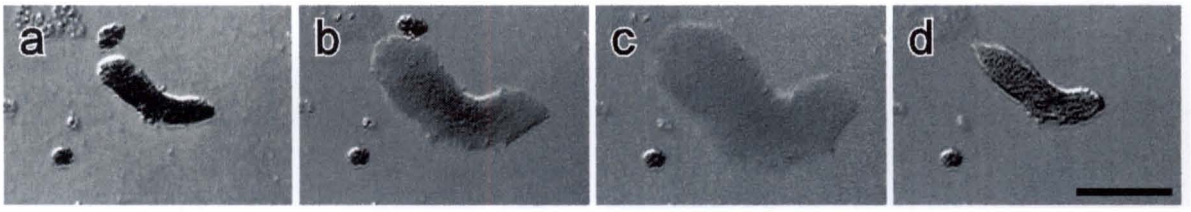

Fig. V.5. Light micrographs of an isolated macronucleus in G2 or M phase. Presence of a shorter and thicker macronucleus is characteristic of this phase of the cell cycle. The isolated macronucleus (**a**) became gradually expanded when EGTA solution was added (**b** and **c**), followed by contraction upon subsequent addition of Ca^{2+} solution (**d**). Micrographs in panels **b** and **c** were taken at 5 and 15 s after the addition of EGTA, respectively. Bar = 100 μm.

quent addition of Ca^{2+} solution, the swollen nucleus contracted to almost its original size (Fig. V.4d). Ca^{2+}-dependent contraction of the macronucleus was also observed in G2 or M phase (Fig. V.5) in which the macronucleus is shorter and thicker compared with those in S or G1 phases. An isolated macronucleus in G2 or M phase (Fig. V.5a) became expanded with the addition of EGTA solution (Fig. V.5b and c), then contracted on subsequent addition of Ca^{2+} solution (Fig. V.5d). These results indicate that a Ca^{2+}-dependent contractility of the macronucleus exists throughout the cell cycle, except for the region of the replication bands in S phase where contraction also took place but to a lesser degree. Electron microscopic studies on the replication bands which have been carried out by both transmission (Fauré-Fremiet et al., 1957; Kluss, 1962; Phegan and Moses, 1967, Ringertz et al., 1967; Olins and Olins, 1981; Allen et al, 1985; Olins and Olins, 1987; Olins et al., 1988) and scanning (Arikawa et al., 2000) electron microscopy, have shown that chromatin bodies are composed of densely-packed chromatin fibrils which become disintegrated into thin fibrils in the replication band. Such a morphological feature of the replication band may be related to its apparently lower Ca^{2+} contractility.

In order to examine if Ca^{2+}-dependent nuclear contractility as observed in *Euplotes* is shared with other cell types, other protozoan species and a mammalian culture cell were examined by employing the same procedure. As shown in Fig. V.6, contraction of isolated nuclei was observed in protozoans of different taxa (a heliozoon *A. sol* (Fig. V.6a and b) and a peniculine ciliate *P. bursaria* (Fig. V.6c and d)), and even in HeLa cells (Fig. V.6e and f). These results suggest the possibility that all eukaryotic cells possess a Ca^{2+}-dependent contractile machinery inside their nuclei.

Isolated macronuclei of *Tetrahymena pyriformis* were reported to show contraction by Ca^{2+} in an ATP-independent manner, with contraction of the nuclear membrane postulated as its mechanism (Wunderlich and Herlan, 1977; Wunderlich et al.,

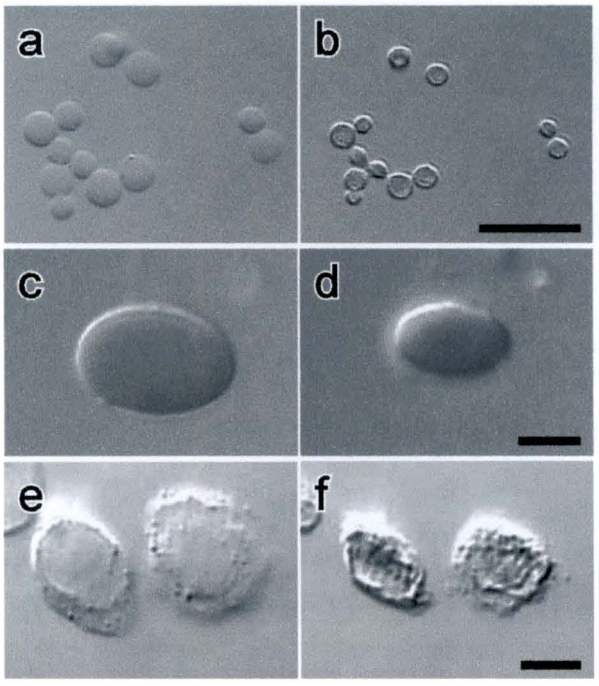

Fig. V.6. Light micrographs of isolated nuclei of various cell types. Nuclear contraction was induced by addition of Ca^{2+} ($[Ca^{2+}]$ = 2 mM) in the heliozoon *Actinophrys sol* (**a** and **b**), the ciliate *Paramecium bursaria* (**c** and **d**), and in HeLa cells (**e** and **f**). Nuclei in expanded and contracted states are shown in left (**a**, **c**, and **e**) and right (**b**, **d**, and **f**) panels, respectively. Bars = 50 μm (**b**) or 10 μm (**d** and **f**).

1978). Atomic force microscopic studies have shown that the conformational change of nuclear pore complex components may be responsible for the contraction of the nucleus (Rakowska et al., 1998; Oberleithner, 1999). However, in the present study, nuclear membranes were completely eliminated during preparation (Arikawa et al., 2000), which indicates that neither the nuclear membrane nor nuclear pore complexes are involved in the process of nuclear contraction in *Euplotes*. Berezney and Coffey have isolated a nucleoskeletal framework from rat liver nuclei which consists of a nuclear protein matrix (Berezney and Coffey, 1974; 1977). The nuclear matrices have also been identified in Chinese hamster cell nuclei (Hildebrand et al., 1975) and in nuclear ghosts prepared from HeLa cells (Riley et al., 1975), suggesting that these structures probably contain common components. However, less attention has been paid to their motile properties. In this study, the possibility was raised for the first time that a contractile system is present in many eukaryotic cell nuclei, although its biological significance is presently unclear. The fact that various kinds of cells including protozoans and cultured mammalian cells exhibited similar contraction suggests that this unique property of the nucleus has been conserved during the process of eukaryotic evolution.

CHAPTER VI

Ca^{2+}-dependent Nuclear Contraction in the Heliozoon *Actinophrys sol*

INTRODUCTION

A large number of investigations have been made on characteristic contractile systems in unicellular organisms. The spasmoneme of vorticellid ciliates (Asai et al., 1978; Ochiai et al., 1979; Yokoyama and Asai, 1987; Katoh and Naitoh, 1994; Katoh and Kikuyama, 1997; Moriyama et al., 1998), the myoneme of a heterotrichous ciliate (Ishida and Shigenaka, 1988; Ishida et al., 1996), and the flagellar root of green algae (Salisbury and Floyd, 1978; Salisbury et al., 1984; Coling and Salisbury, 1992; Salisbury, 1998) are well-known organelles which show Ca^{2+}-dependent contractility. Contraction of these organelles is considered to be generated by proteins such as centrin (caltractin) and spasmin (David and Vigues, 1994; Maciejewski et al., 1999), which belong to the calmodulin superfamily. Although much progress has been made on characterization of such Ca^{2+}-binding proteins and cytoplasmic contraction in a molecular level, less attention has been paid to the dynamics of the nucleus.

In 1974, a stable framework structure termed "nuclear matrix" has been found in an isolated rat liver nucleus by sequential chemical extractions (Berezney and Coffey, 1974; Berezney and Coffey, 1977). Since then, many investigations have been made to elucidate ultrastructure and possible functions of the nuclear matrix, and it is now clear that the nuclear matrix is involved in the processes of gene expression, replication and transcription of DNA, and also processing and transportation of RNA (Pederson, 1998). Ultrastructure of the nuclear matrix has also been well studied, and branched thin filaments with diameters of about 10 nm have been identified that construct the interior architecture of the nucleus (Nickerson, 2001). Despite considerable advances in physiological and morphological researches, evidence for the existence of contractility of the nuclear matrix has never been reported so far.

Recently, I have reported that Ca^{2+}-dependent contractility exists in an isolated and demembranated macronucleus of the hypotrichous ciliate *Euplotes aediculatus* (Arikawa et al., 2002a). Furthermore, similar nuclear contraction has been observed in several species of protozoan cells and even in cultured mammalian cells (HeLa cells). From these results, I have proposed the hypothesis for the first time that all eukaryotic cells possess a Ca^{2+}-dependent nuclear contractility which has been well preserved during the process of eukaryotic evolution. As one of the examples, isolated and detergent-extracted nuclei of the heliozoon *Actinophrys sol* have been demonstrated to express Ca^{2+}-dependent contractility. In the present study, physiological characterization of the contractility and ultrastructural observation of the isolated nucleus were carried out, and a possible mechanism of the Ca^{2+}-dependent nuclear contraction is presented.

MATERIALS AND METHODS

Organisms and Culture

Actinophryid heliozoon *Actinophrys sol* (protozoa) was axenically cultured in a co-culturing condition with *Chlorogonium elongatum* in 10% artificial sea water as described in Chapters II and

III. Subculturing was curried out at intervals of about 2 weeks. Centrifugally collected cells were gently washed with fresh 10% artificial seawater at room temperature before using for experiments.

Nuclear Isolation Procedures

Nuclei of *A. sol* were isolated by using a sucrose-Percoll separation technique. At first, a solution (solution A) consisting of 2.0 M sucrose, 10% Percoll, 3 mM EGTA and 5 mM HEPES (pH 7.0) was overlaid in a test tube with another solution (solution B) consisting of 2.0 M sucrose, 3 mM EGTA and 5 mM HEPES (pH 7.0). Washed cells were centrifugally collected and suspended in solution C consisting of 1.0 M sucrose, 3 mM EGTA and 5 mM HEPES (pH. 7.0), homogenized with a Teflon homogenizer, and placed on top of the layered solution in the test tube. After centrifugation at 750 g for 10 min, isolated nuclei were collected from the boundary between solutions A and B. Nuclei were again suspended in solution C, and were centrifuged at 750 g for 5 min. After removal of the supernatant, crude preparation of the nuclei was collected from the bottom of the test tube, and subjected to different concentrations of divalent cations or a fixative for electron microscopy.

Microscopy

Light and electron microscopy was carried out according to the procedures applied to the heliozoons and the ciliate as described in chapters I, II and V.

RESULTS

Reduction in Diameter of Isolated Nuclei

Actinophrys sol possesses a single nucleus within a cytoplasm. As shown in Fig. VI.1a, differential interference microscopy showed that a nucleus (marked "N") was located at the center of the cell body, and cortical nucleolar materials are present at the periphery of the nucleus. In this study, Ca^{2+}-dependent contractility was found to exist in isolated and detergent-extracted nuclei. Although nucleolar materials could no longer be observed after isolation, spherical shape of the nucleus was well preserved (Fig. VI.1b). When nuclear isolation was performed in the presence of calcium ions (2×10^{-3} M free Ca^{2+}), diameter of the nucleus decreased. The contour of the nucleus became prominent, and the nucleus showed a rigid appearance (Fig. VI.1c).

Diameter of isolated nuclei was measured under various conditions, and compared with that of the living cells (in Fig. VI.2). Nuclear diameter of the living cells was in the range of 10.9 - 19.9 μm, with the average value of 15.1 ± 1.7 μm (Fig. VI.2a). In the absence of Ca^{2+}, average diameters of the nucleus isolated without (Fig. VI.2b) and with detergent treatment (Fig. VI.2d) were slightly larger (15.9 ± 1.5 μm and 16.5 ± 1.7 μm, respectively) than that of the living cells (Fig. VI.2a). On the contrary, average diameters of nuclei which were isolated without (Fig. VI.2c) and with detergent (Fig. VI.2e) in a Ca^{2+}-containing solution (2×10^{-3} M free Ca^{2+}) were significantly smaller (12.4 ± 1.1 μm and 11.0 ± 1.3 μm, respectively). Compared with the nuclei in living cells, as shown in Fig. VI.2f, no diameter reduction was observed when nuclei were isolated in a solution containing 2 mM free Mg^{2+} (14.8 ± 1.4 μm on average). These results show that the diameters of isolated nuclei were decreased in a Ca^{2+}-dependent manner. The diameter reduction of the isolated nucleus was observed even in the presence of colchicine (10 mM) and cytochalasin B (1 mM), suggesting that the mechanism of the nuclear contraction is different from actin-myosin and tubulin-dynein interactions.

Diameters of isolated nucleus (n = 140) were

measured before and after contraction (Fig. VI.3a). By nuclear contraction, diameter of relaxed nuclei that ranged from 13.1 to 23.7 μm (17.8 ± 2.6 μm on average) decreased to 12.7 ± 1.9 μm with the ranged from 8.9 to 17.3 μm. The correlation coefficient between diameters of relaxed and contracted nucleus was calculated to be 0.74, which indicates that the degree of contraction is not significantly correlated with the nuclear size. Degree of nuclear contraction calculated from the average diameters measured before and after contraction was 63.7%. As shown in Fig. VI.3b, degree of contraction was estimated and plotted against the volume of relaxed nucleus. More than 80% of the nuclei showed contraction to the degree of 50 - 80%, although a few small nuclei (< 4,000 μm^3 in volume) showed less contractility (20 - 30% degree).

Ca^{2+}-dependency of the Nuclear Contraction

Isolated nuclei were attached to a glass surface and continuously observed under a light microscope. Contraction and relaxation cycle of an isolated and adhered nucleus could be repeated many times by alternate addition of Ca^{2+} and EGTA (Fig. VI.4), which indicates that such cycles were mediated by only Ca^{2+} without any other energy supply. The nuclei isolated in EGTA solution were in the state of expansion. They were contracted by addition of Ca^{2+} (2×10^{-3} M Ca^{2+}, white arrowheads), followed by re-expansion upon subsequent addition of EGTA (black arrowheads). Both contraction and expansion occurred within a few seconds after addition of Ca^{2+} and EGTA, respectively. Judging from the rapid responses of the nucleus, it may be difficult to explain the mechanism of the nuclear contraction and expansion by assembly and disassembly of certain filamentous structures existing inside the nucleus. The contraction-expansion cycle of the isolated nucleus was observed after treatment with 2 M NaCl for 30 min (data not shown), which suggests a possible involvement of the nucleoskeletal components in the Ca^{2+}-dependent nuclear contraction.

An isolated nucleus was attached to a glass surface and was treated with various concentrations of Ca^{2+}. Fractional volume of a responded nucleus was measured during both contraction and expansion processes and shown in Fig. VI.5. In the contraction process (open circles), the nucleus isolated in an EGTA solution became slightly contracted when 1×10^{-7} M Ca^{2+} was added, and it contracted completely when Ca^{2+} concentration was increased (> 10^{-6} M). Degree of contraction of the contracted nucleus reached around 60%. During the expansion

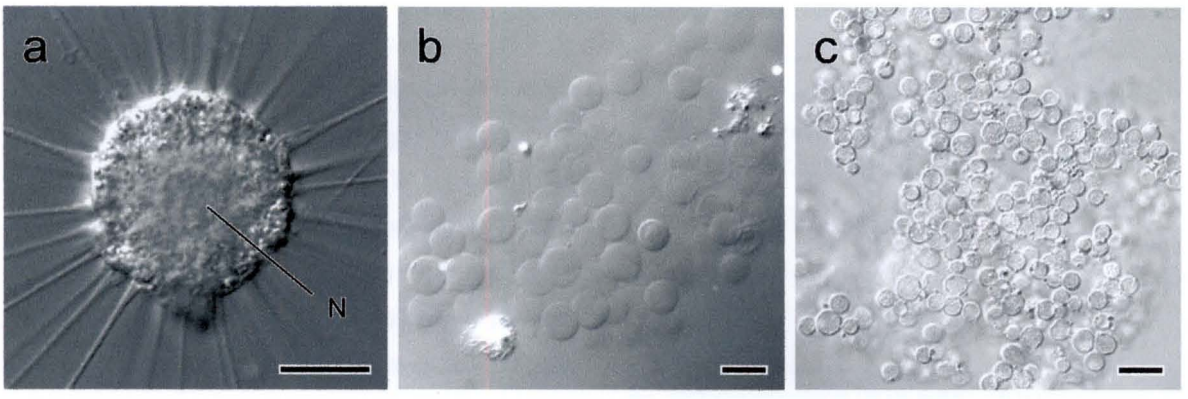

Fig. VI.1. Light micrographs of *Actinophrys sol.* **a:** A living cell showing a spherical nucleus (N) at the center of the cell body. **b:** Isolated nuclei in a Ca^{2+}-free solution. The spherical shape of the nucleus was well preserved after isolation and detergent-extraction with 1% Triton X-100. **c:** When nuclei were isolated in a Ca^{2+}-containing solution (2 mM free Ca^{2+}), diameters of the nuclei became reduced and the periphery of the nuclei showed sharp profiles. Bars = 20 μm.

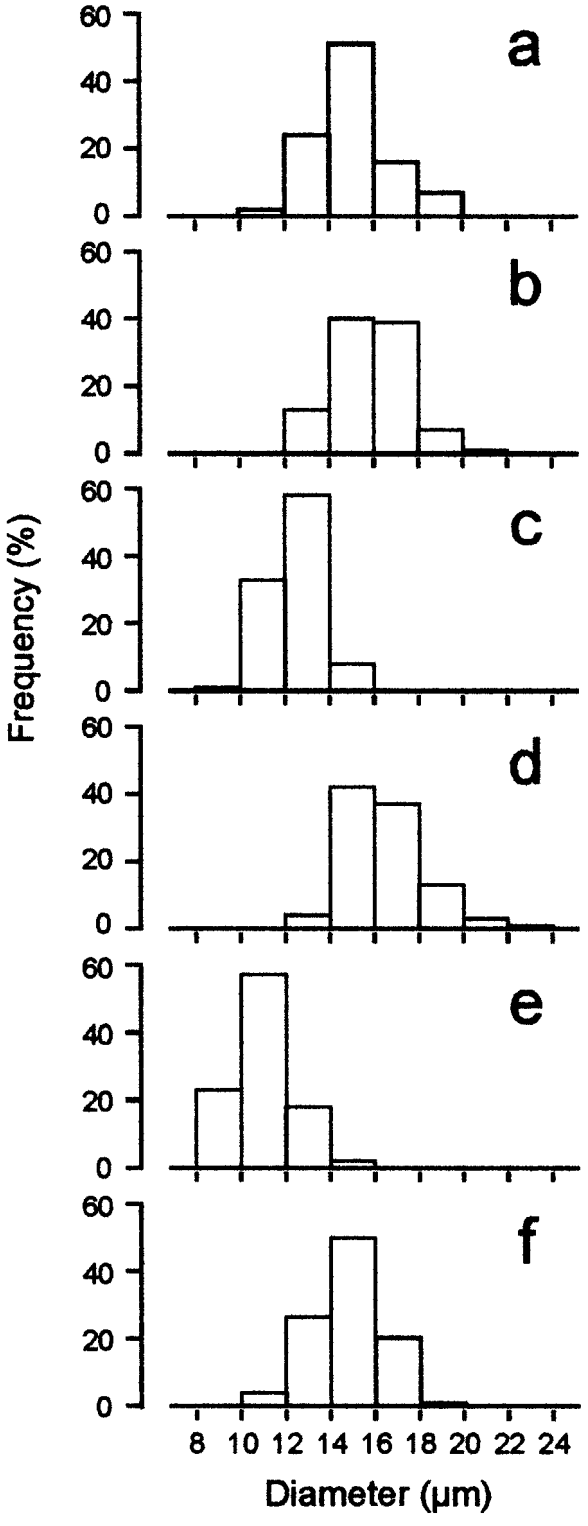

Fig. VI.2. Ca^{2+}-dependent diameter reduction of nuclei. **a:** nuclei observed in living cells. **d-f:** isolated nuclei. Compared with the living cells (**a**), no diameter reduction was observed in nuclei isolated in Ca^{2+}-free solutions by either homogenization (**b**) or detergent treatment (**d**). When nuclei were isolated in Ca^{2+} containing solutions (2 mM free Ca^{2+}) by homogenization (**c**) or by detergent treatment (**e**), diameter reduction was significantly observed. Mg^{2+} (2 mM) could not induce nuclear reduction in diameter (**f**).

process (filled circles), the contracted nucleus recovered almost to its initial shape when Ca^{2+} concentration became lowered (< 10^{-7} M). After full expansion, although the reason remains unknown, volume of the nucleus tended to become larger than that of the nucleus before contraction. Ca^{2+} thresholds, or half-maximum concentrations of Ca^{2+}, for contraction and expansion of the nucleus were estimated by fitting the data with sigmoidal curves to be 2.9×10^{-7} M and 1.0×10^{-7} M, respectively.

Change of the Image Profile at Nuclear Contraction

To obtain high-contrasted images, I used a light microscope (Olympus BX-50) equipped with Nomarski differential interference contrast (DIC) optics and a high resolution digital camera (Olympus DP11). As shown in an inserted light micrograph in Fig. VI.6a, surface of an isolated nucleus appeared to be smooth, and no structural components were observed inside the nucleus. By the effect of DIC optics, left-side of the nuclear edge appeared as a bright crescent, while the opposite side appeared as a dark crescent. The DIC effect on the nucleus was also represented as image intensity profiles shown in Fig. VI.6a and b, in which image intensities in rectangles were analyzed. In an expanded nucleus in EGTA solution, a peak of brightness (filled arrow) is present that represents the location of the left-side edge of the nucleus. The brightness profile has a depression at the right edge of the nucleus as shown by a filled arrow. The intensity profile inside the nucleus shows a smooth curve. These characteristics indicate that the optical density in the nucleus is different from the surrounding medium, and that the nucleus is composed of an optically uniform material. When the isolated nucleus became contracted by the addition of Ca^{2+}, appearance of the nucleus and

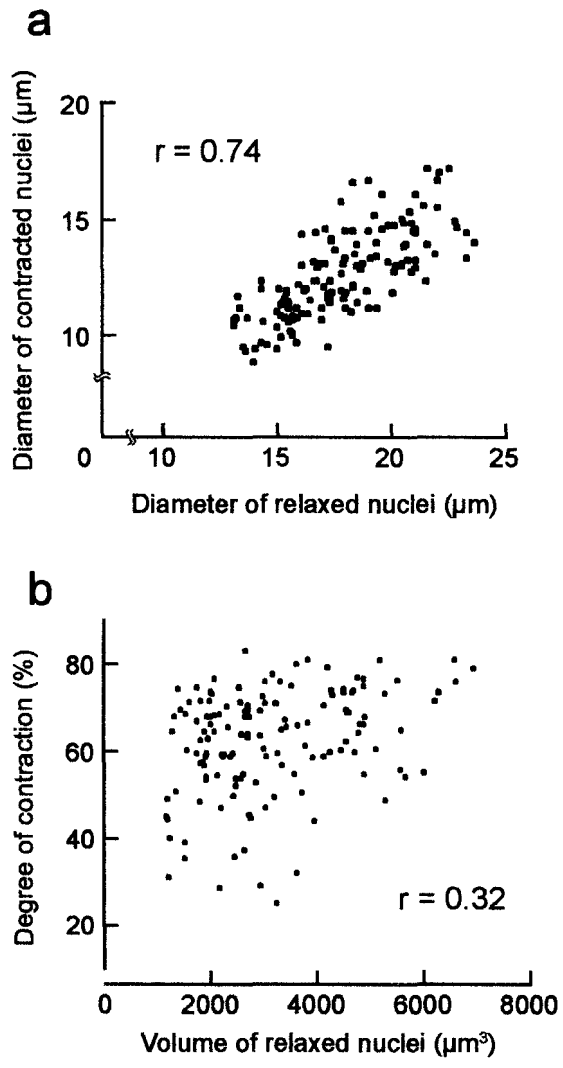

Fig. VI.3. **a:** Relationship between diameters of isolated nuclei (n = 140) measured before and after contraction. Diameters of relaxed nuclei ranged from 13.1 to 23.7 μm, which decreased to the range between 8.9 and 17.3 μm. The correlation coefficient between diameters of relaxed and contracted nucleus was calculated to be 0.74. **b:** Relationship between the degree of nuclear contraction and the volume of relaxed nuclei. The degree of contraction (D) was calculated as: D = 100 - 100 × (Vco / Vre), where Vre and Vco are the volume of relaxed and contracted nucleus, respectively. More than 80% of nuclei showed contraction of which degree was in the range from 50 to 80%.

its brightness profile changed as shown in Fig. VI.6b. Nuclear diameter reduced from 20 to 13 μm. Brightness increased at the left edge of the nuclear edge (white arrow), while it decreased at the right edge (black arrow). The change was accompanied by decrease and increase of the brightness at regions just beneath the left and right edges as shown by black and white arrowheads, respectively. Furthermore, brightness inside the nucleus became rough and irregular. Such changes in brightness pattern suggest that optical density inside the nucleus increased, especially in the periphery of the nucleus, when contraction occurred.

Ultrastructural Observations

In this study, electron microscopy was carried out to examine ultrastructural changes inside a nucleus that have happened during nuclear contraction in responses to addition of Ca^{2+}. As shown in Fig. VI.7a, in a living cell nucleus, a large number of electron dense nucleolar materials were located just beneath the inner surface of the nuclear envelope, and thin filaments were scattered to form a meshwork inside the nucleus. Although the nucleolar materials disappeared during nuclear isolation, the spread meshwork of thin filaments was well preserved (Fig. VI.7b). When Ca^{2+} (2 mM) was added to the isolated and extracted nucleus, the thin filaments became aggregated and changed their appearances to a mass of thicker filaments (Fig. VI.7c). After the Ca^{2+}-induced aggregation of the thin filaments occurred, the nucleolplasm other than the filaments appeared sparse, while the inner layer of the nuclear membrane became dense in appearance. By subsequent addition of EGTA to the nucleus, the thicker filaments became disintegrated and loose, resulting in re-distribution of the thin filament spread around inside of the nucleus (Fig. VI.7d).

DISCUSSION

In this study, I investigated Ca^{2+}-dependent contractility of an isolated and detergent-extracted nucleus of the heliozoon *Actinophrys sol.* In actinophryid heliozoons such as *Actinophrys* and *Echinosphaerium*, cytoplasmic contraction is commonly

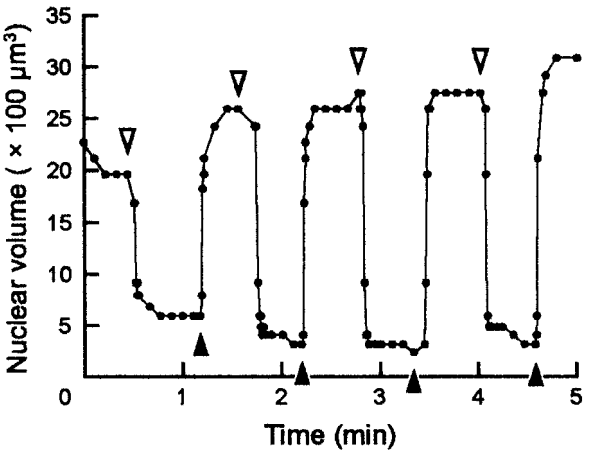

Fig. VI.4. Sequential measurement of the nuclear volume during cyclic contraction and relaxation. An isolated nucleus was contracted by addition of 2 mM Ca^{2+} (open arrowheads), followed by relaxation upon subsequent addition of EGTA (filled arrowheads). Such cycles could be repeated many times by alternate addition of Ca^{2+} and EGTA.

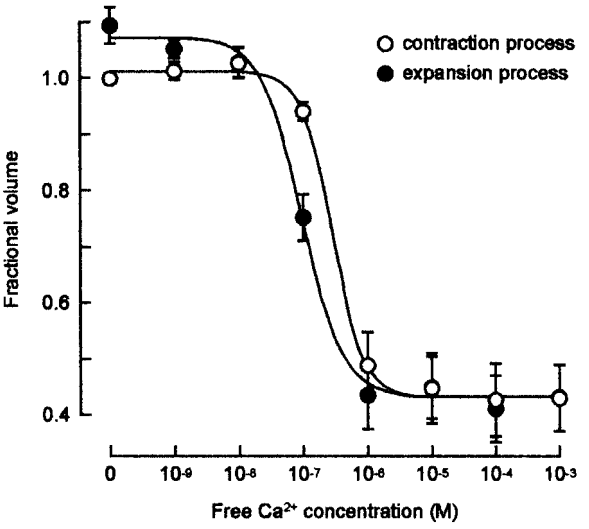

Fig. VI.5. Ca^{2+}-dependent contraction and expansion of isolated nuclei. When Ca^{2+} concentration was raised stepwise, isolated nucleus contracted with the threshold Ca^{2+} level of 2.9×10^{-7} M, and reached up to around 60% degree of contraction. The contracted nucleus expanded gradually when Ca^{2+} concentration became lowered, and the threshold level of Ca^{2+} for the nuclear expansion was 1.0×10^{-7} M. Open and filled circles represent the processes of contraction and expansion, respectively.

observed during the process of food uptake. Heliozoon cells possess a large number of needle-like axopodia that radiate from their spherical cell bodies. When a small organism becomes a close contact with the surface of an axopodium, rapid shortening of the axopodium occurs, and an attached prey organism is conveyed toward the cell body (Ockleford and Tucker, 1973; Suzaki et al., 1980a; Sakaguchi et al., 1998). Inside the axopodium, a bundle of microtubules was located throughout the length of an axopodium as cytoskeletal elements (Tilney and Porter, 1965; Tilney et al., 1966; Ockleford, 1974, Shigenaka and Kaneda, 1979). A bundle of contractile filamentous structures termed "contractile tubules structure (CTS)" also runs parallel with the axopodial microtubules (Suzaki et al., 1980a; Shigenaka et al., 1982). Electron microscopy has shown that the CTS changes its appearance from tubular to granular forms inside a contracted cytoplasm when the axopodial contraction occurs (Matsuoka et al., 1985; Ando and Shigenaka, 1989; Sugiyama et al., 1992; Suzaki et al., 1994; Kinoshita et al., 2001). By using permeabilized cell models, it has been found that the driving force for the axopodial contraction is not generated by disassembly of the axonemal microtubules but Ca^{2+}-dependent transformation of the CTS is responsible to the motile for it (Suzaki et al. 1992; Arikawa and Suzaki, 2002; Arikawa et al., 2002b). In this study, an isolated and detergent-extracted nucleus showed Ca^{2+}-dependent contractility which is similar to that of the cytoplasm of permeabilized cell models. When cytoplasmic contraction of the permeabilized cell model was induced by an addition of Ca^{2+}, simultaneous contraction of the nuclei was also observed (Arikawa and Suzaki, 2002). Detailed ultrastructural observations of the nucleus throughout the stages of the vegetative life cycle *A. sol* have shown that CTS is not present in the nucleus (Mignot, 1980; Mignot, 1984). Therefore, it may not be possible to explain the mechanism of the nuclear contraction by the transformation of the CTS. Although the CTS is present near the periphery of the nucleus where axonemal microtubules are termi-

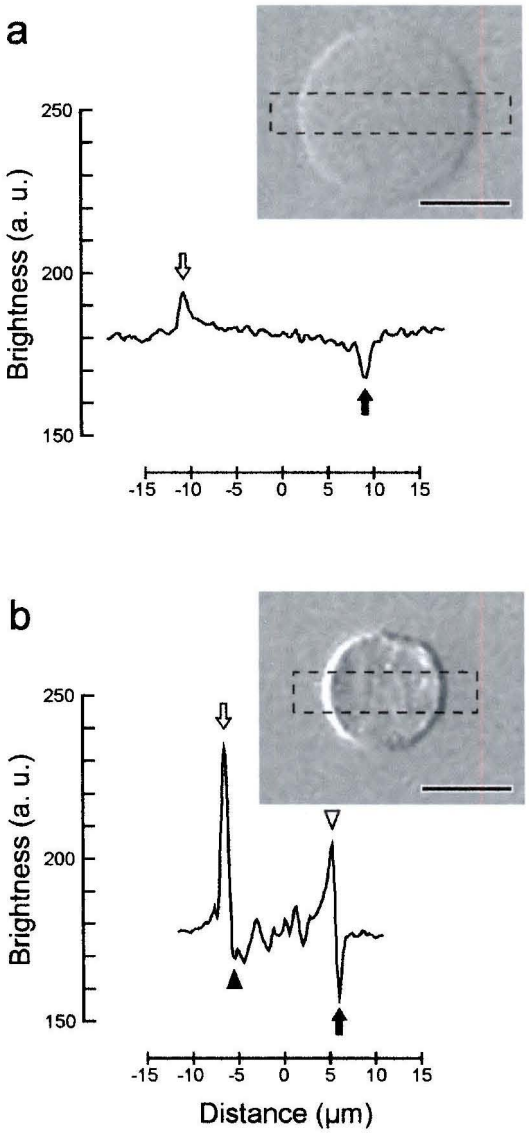

Fig. VI.6. Changes in brightness profiles of an isolated nucleus during contraction. Vertical and lateral axes of the graphs represent averaged brightness in delimited area (rectangles with broken lines) shown in arbitrary unit and distance from the center of an isolated nucleus, respectively. Compared with a relaxed nucleus (**a**), brightness at both sides of the contracted nucleus (**b**) show sharper profiles (white and black arrows). Furthermore, dark and bright areas appeared just inside both edges (black and white arrowheads), and brightness inside the nucleus showed a rough and disordered profile. Bar = 10 μm.

nated (Suzaki et al., 1980a), it seems unlikely to speculate that CTS is also associated with the outer surface of the nucleus and regulates nuclear contraction.

Isolated *Tetrahymena* macronuclei have been reported in 1977 to show Ca^{2+}-dependent reversible contraction of which mechanism may be different from the actin-myosin contraction system (Wunderlich and Herlan, 1977). By counting the frequency of nuclear pore complexes per unit area in both contracted and expanded macronuclei, the macronuclear contraction has been attributed to contraction of the nuclear membrane (Wunderlich et al., 1978). Moreover, atomic force microscopy has revealed that the nuclear contraction can be explained by a calcium-sensitive shape change of individual nuclear pore complexes (Rakowska et al., 1998; Oberleithner et al., 1999; Danker and Oberleithner, 2000). However, in this study, isolated nuclei of *A. sol* did not preserve their nuclear membranes and nuclear pore complexes any longer. In the isolated macronucleus of *Euplotes*, Ca^{2+}-dependent contraction was also observed even after the nucleus had been completely demembranated (Arikawa et al., 2000; Arikawa et al., 2002a). These facts indicate that neither nuclear membranes nor nuclear pore complexes may be involved in the nuclear contraction.

As shown in Fig. VI.4, contraction and expansion of an adhered nucleus were completed within a few seconds. Thus, it may be difficult to explain the dynamics of isolated nucleus by the mechanism of de- and re-polymerization of certain filamentous structures such as F-actin and microtubules. Although actin, myosin, and tubulin molecules have been detected in various kinds of cell nuclei (Douvas et al., 1975; Berrios and Fisher, 1986; Berrios et al., 1991; Nowak et al., 1997), no direct evidence has been reported so far that these molecules are involved in nuclear contraction. In this study, contraction and expansion of the adhered nuclei were observed even in the presence of colchicine (10 mM) and cytochalasin B (1 mM), indicating that the mechanism of the nuclear contraction in *A. sol* may be different from microtubules-

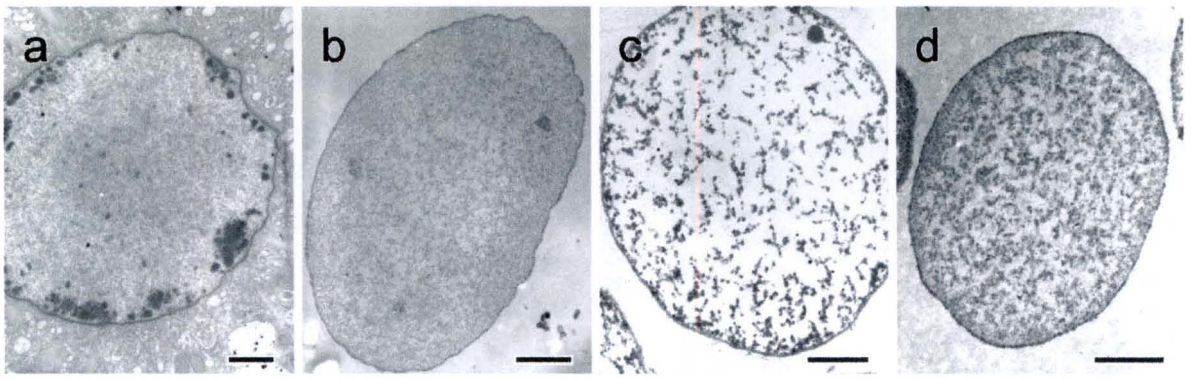

Fig. VI.7. Electron micrographs showing ultrastructural changes of isolated nuclei during contraction and relaxation. **a:** Electron dense nucleolar materials were located just beneath the nuclear membrane. A meshwork of thin filaments was evenly distributed inside the nucleus of a living cell. **b:** Isolated and detergent-extracted nucleus. The nucleolar materials disappeared during isolation procedures, but the meshwork structure was well preserved even after isolation. **c:** By addition of Ca^{2+} (2 mM free Ca^{2+}), thin filaments became aggregated to form thicker filaments. **d:** The thicker filaments were disintegrated and became loose by subsequent addition of EGTA (3 mM). Bars = 2 μm.

or actomyosin-based machineries.

The nuclear matrix is defined as a residual nuclear framework after sequential extraction procedures, and consists of two components: the nuclear lamina and an internal nuclear network (Nickerson, 2001; Martelli et al., 2002). The inner nuclear architecture is connected to the nuclear lamina and built on an underlying network of branched 10 nm filaments (He et al., 1990; Nickerson et al., 1997). It is widely understood that the nuclear lamins are major components of the nuclear lamina which construct a mesh-like network of intermediate filaments underlying the inner periphery of the nuclear membrane (Aebi et al., 1986; Nigg, 1992; Moir and Goldman, 1993). Recent studies have revealed that lamins are present not only at the periphery of the nucleus but also within the nucleoplasm, and form an internal nucleoskeleton as well as a peripheral lamina (Belmont et al., 1993; Bridger et al., 1993; Moir et al., 1994; Hozák et al., 1995; Neri et al., 1999). It may be natural to consider that the network structure inside the nucleus in *A. sol* may also be constructed by 10 nm intermediate filaments or lamina. Furthermore, it is widely regarded that the nuclear matrix is a ubiquitous nuclear structure in all eukaryotic cells. Although, unfortunately, I could not detect nuclear lamin proteins by using a commercially-available anti-lamin antibody. However, the fact that the nuclear matrix has been detected in nuclei of various unicellular organisms such as *Tetrahymena* (Herlan and Wunderlich, 1976; Wunderlich and Herlan, 1977), *Amphidinium* (Minguez et al., 1994) and *Euglena* (Wen, 2000) strongly suggests that the meshwork structure observed inside the isolated and detergent-extracted nucleus of *A. sol* is a nuclear matrix that is constructed by the nuclear lamina. Thus, my observations also support an idea that the nuclear matrix structure has been highly conserved during the eukaryotic evolution. However, there are no molecular clues to explain the Ca^{2+}-dependent contractility of the nuclear matrix at all. My findings in this study only suggest a possibility for the first time that the nucleus possesses contractility which is regulated by Ca^{2+}-dependent dis- and re-aggregation of the nuclear lamina filaments.

An alternative possibility for the nuclear contraction arises that the nuclear contraction is directly or indirectly mediated by a certain Ca^{2+}-binding protein. A large number of studies have revealed that Ca^{2+}-binding proteins exist within

various kinds of nucleus, and play important roles in many nuclear events (Gilchrist and Pierce, 1993; Gilchrist et al., 1994; Czubryt et al., 1996; Badminton et al., 1998; Gilchrist et al., 2002). However, Ca^{2+}-dependent functions of these proteins have not entirely been made clear. In spite of an attempt to detect Ca^{2+}-binding proteins in this study by using "Stains-all" and "ruthenium red" staining method or a Ca^{2+}-dependent mobility shift assay on separated nuclear proteins by SDS-PAGE, I could not obtain any positive results. Further studies are required to elucidate the molecular mechanism of the Ca^{2+}-dependent nuclear contraction.

GENERAL DISCUSSION

Axopodial Contraction

In this study, I attempted to elucidate the mechanism of axopodial contraction of the heliozoons *Echinosphaerium akamae* and *Actinophrys sol* by using permeabilized cell models, and showed a direct evidence that the CTS is a contractile structure which responds to Ca^{2+}. A Ca^{2+}-dependent transformation of the CTS from tubular to granular forms was observed to occur in the axopodial cytoplasm without accompanying disassembly of the microtubules. This result indicates that the CTS is responsible for contraction of the axopodial cytoplasm in a Ca^{2+}-dependent manner, resulting in rapid shortening of the axopodium (Chapters I and II). To further identify the molecular basis for CTS contractility, possible involvement of a Ca^{2+}-sensitive protein was examined. As described in Chapters II and III, a Ca^{2+}-induced precipitate was obtained from the cell homogenate of *Actinophrys sol*. Although no Ca^{2+}-sensitive protein was detected in the precipitate, a precipitate adhered to the glass surface showed Ca^{2+}-dependent contractility which was similar to that of the cell models. These results indicate that the CTS must have been successfully isolated, in which Ca^{2+}-dependent contractility was maintained. The crucial problem to be solved in the future is how the CTS contracts. By electron microscopy, the CTS has been observed to have an appearance of a small tubule, but it sometimes show lamellar or granular appearances, and frequently surrounded by membrane-like structures. Judging from these ultrastructural observations, the process of transformation of the CTS has been speculated to involve not only granulation but also twisting and/or coiling of the tubules (Shigenaka et al., 1982; Matsuoka et al., 1985; Kinoshita et al., 2001). In this study, the isolated CTS in vitro was observed to change its appearance from tubules to granules by addition of Ca^{2+} (Fig. 6 in Chapter II). If the process of Ca^{2+}-induced transformation of the CTS could be examined in details by modulating Ca^{2+} concentration at around the threshold level, one might be able to find out by electron microscopy intermediate structures of the CTS between tubular and granular stages, which may allow us to understand the precise mechanism of transformation of the CTS.

In this study, when Ca^{2+} was added at micromolar level to the membrane-permeabilized cell models of *E. akamae* and *A. sol*, granulation of the CTS was induced without affecting to the axonemal microtubules, resulted in formation of many cyoplasmic swellings along the length of an axopodium (Fig. 1 in Chapter I and Fig. 1 in Chapter II). This phenomenon is similar to the "beading phenomenon" that is frequently observed in living cells (Suzaki et al., 1980a). These results suggest that the threshold level of Ca^{2+} for contraction of the CTS is lower than that for disassembly of microtubules, and that the contraction of the CTS does not always accompany breakdown of the axonemal microtubules. To induce axopodial shortening, contraction of the CTS and disassembly of the axonemal microtubules must occur simultaneously. Although the CTS is located in the vicinity of the microtubules throughout the length of axopodia (Shigenaka and Kaneda, 1979, Suzaki et al., 1980a; Shigenaka et al., 1982), no structural connection between the CTS and the axonemal microtubules

has been observed so far. If the CTS is closely associated with the axonemal microtubules and contraction of the CTS generates mechanical force which is sufficient to disintegrate microtubules, it is difficult to explain the phenomenon of cytoplasmic beading, because it is formed by contraction of the CTS inside the axopodial cytoplasm without disassembly of the microtubules. Consequently, in the case of axopodial contraction, concentration of cytoplasmic Ca^{2+} is supposed to be high enough to induce not only granulation of the CTS but also disassembly of axonemal microtubules. In contrast, when cytoplasmic beadings appear, cytoplasmic Ca^{2+} concentration may not be sufficient for inducing microtubule disassembly. Further cytochemical investigations are required to elucidate difference in Ca^{2+}-sensitibity between the CTS and the axonemal microtubules. Moreover, for complete contraction of an axopodium, the distal end of a bundle of CTS must be connected to the inner surface of the axopodial membrane, and the proximal end must be anchored deep inside the cell body. So far, no structural relationship between the CTS and the plasma membrane has been described. Furthermore, even length of a unit structure of the CTS remains to be examined. Further electron microscopic observation is required to determine the ultrastructure of the intact CTS in the axopodium.

As described in INTRODUCTORY REVIEW, Ca^{2+} has been regarded to play an important role in the axopodial contraction. From the results obtained in this study, in conjunction with former experimental conclusions, a possible process of axopodial contraction may be summarized as follows. Although the mechanism of signal transduction on the axopodial surface is unclear, attachment of a prey to the surface of an axopodium is perceived by the axopodial membrane as a signal for triggering influx of extracellular Ca^{2+} into the axopodial cytoplasm and/or release of Ca^{2+} from Ca^{2+}-sequestering vesicles located beneath the axopodial membrane. The increase of Ca^{2+} concentration inside the axopodium may induce transformation of the CTS and degradation of the axonemal microtubules, resulting in contraction of the axopodium. After contraction, Ca^{2+} concentration recovers to its resting level, probably by using Ca^{2+} pumps in the plasma membrane. Re-elongation of the contracted CTS and polymerization of microtubules then occur, and finally a fully extended axopodium is reconstructed. The mechanism of Ca^{2+}-induced transformation of the CTS is still unknown. Purification of the CTS and identification of Ca^{2+}-sensitive proteins are to be carried out to further understanding the mechanism of molecular interaction between the CTS and Ca^{2+}. Furthermore, existence of Ca^{2+} pump on the axopodial membrane or surrounding vesicles is still uncertain. Cytochemical localization and biochemical characterization of Ca^{2+}-ATPase are required to investigate the possible involvement of Ca^{2+} ions in axopodial contraction.

Nuclear Contraction

In 1974, Berezney and Coffey have introduced the term "nuclear matrix" for the first time to indicate the nuclear framework which resists against removal from the nucleus by a series of chemical extractions (Berezney and Coffey, 1974). Although some controversy remains, nuclear matrix is currently regarded as a nucleoskeletal structure facilitating various nuclear activities (Martelli et al., 1996; Pederson, 1998; Hancock, 2000; Pederson, 2000; Martelli et al., 2002). However contractile properties of the nuclear matrix have never been reported so far. Evidences obtained in this study suggest for the first time that the nuclear matrix possesses a Ca^{2+}-dependent contractility which

might have been retained by all the eukaryotic organisms as a common property, and is conserved in spite of a long history of eukaryotic evolution. However, the biological significance of the nuclear contraction remained unclear. Judging from the evidence that Ca^{2+} concentration in a nucleus may be regulated independently from cytosolic Ca^{2+} (Badminton et al., 1998), the nuclear contraction may be closely related to some original functions of the nucleus. For example, particularly in ciliates, transformation of the nucleus is sometimes observed during the process of nuclear division in mitosis, and characteristic elongation and contraction of the micronucleus are frequently observed in meiosis. It is worthwhile monitoring Ca^{2+} concentration inside a nucleus during such nuclear events.

REFERENCES

Aebi U., Cohn J., Buhle L., and GeraceL. 1986. The nuclear lamina is a meshwork of intermediate-type filaments. *Nature*. 323: 560-564.

Allen R. L., Olins A. L., Harp J. M., and Olins D. E. 1985. Isolation and characterization of chromatin replication bands and macronuclei from *Euplotes eurystomus*. *Eur. J. Cell Biol.* 39: 217-223.

Amos W. B. 1975. Contraction and calcium binding in the vorticellid ciliates. *In*: Molecules and Cell Movement. Inoué S. and Stephens R. E. editors. Raven Press/ New York. 411-436.

Ando M. and Shigenaka Y. 1989. Structure and function of the cytoskeleton in heliozoa. I. Mechanism of rapid axopodial contraction in *Echinosphaerium*. *Cell Motil. Cytoskel.* 14: 288-301.

Araki J. and Takahashi I. 1978. p-Dichlorobenzene drying method-for minute parasites. *J. Electr. Microsc.* 27: 362 (abstr.).

Arikawa M. and Suzaki T. 2002. Reactivation of Ca^{2+}-dependent cytoplasmic contraction in permeabilized cell models of the heliozoon *Echinosphaerium akamae*. *Cell Motil. Cytoskel.* 53: 267-272.

Arikawa M., Momokawa N., Saito A., Omura G., Khan S. M. M. K., Suetomo Y., Kakuta S., and Suzaki T. 2002b. Ca^{2+}-dependent contractility of isolated and demembranated macronuclei in the hypotrichous ciliate *Euplotes aediculatus*. *Cell Calcium*. In press.

Arikawa M., Saito A., Omura G., Khan S. M. M. K., Kinoshita E., and Suzaki T. 2002a. Ca^{2+}-dependent cytoplasmic contractility of the heliozoon *Actinophrys sol*. *Eur. J. Protistol.* 38: 365-372.

Arikawa M., Watanabe A., Watanabe K., and Suzaki T. 2000. High-resolution scanning electron microscopy of chromatin bodies and replication bands of isolated macronuclei in the hypotrichous ciliate *Euplotes aediculatus*. *Eur. J. Protistol.* 36: 40-45.

Arnold E. A., Yawn D. H., Brown D.G., Wyllie R.C., and Coffey D.S. 1972. Structural alteration in isolated rat liver nuclei after removal of template restriction by polyanions. *J. Cell Biol.* 53: 737-757.

Asai H., Ochiai T., Fukui K., Watanabe M., and Kano F. 1978. Improved preparation and cooperative calcium contraction of glycerinated *Vorticella*. *J. Biochem.* 83: 795-798.

Badminton M. N., Kendall J. M., Rembold C. M., and Campbell A. K. 1998. Current evidence suggests independent regulation of nuclear calcium. *Cell Calcium*. 23: 79-86.

Belmont A. S., Zhai Y., and Thilenius A. 1993. Lamin B distribution and association with peripheral chromatin revealed by optical sectioning and electron microscopy tomography. *J. Cell Biol.* 123: 1671-1685.

Berezney R. and Coffey D. S. 1974. Identification of a nuclear protein matrix. *Biochem. Biophys. Res. Commun.* 60: 1410-1417.

Berezney R. and Coffey D. S. 1977. Nuclear matrix. Isolation and characterization of a framework structure from rat liver nuclei. *J. Cell Biol.* 73: 616-637.

Berrios M. and Fisher P. A. 1986. A myosin heavy chain-like polypeptide is associated with the nuclear envelope in higher eukaryotic cells. *J. Cell Biol.* 103: 711-724.

Berrios M., Fisher P. A., and Matz E. C. 1991. Localization of a myosin heavy chain-like polypeptide to *Drosophila* nuclear pore complexes. *Proc. Natl. Acad. Sci. USA*. 88: 219-223.

Bridger J. M., Kill I. R., O'Farrell M., and Hutchison C. J. 1993. Internal lamin structures within G_1 nuclei of human dermal fibroblasts. *J. Cell Sci.* 104: 297-306.

Coling D. E. and Salisbury J. L. 1992. Characterization of the calcium-binding contractile protein centrin from *Tetraselmis striata* (Pleurastrophyceae). *J. Protozool.* 39: 385-391.

Czubryt M. P., Ramjiawan B., Gilchrist J. S. C., Massaeli H., and Pierce G. N. 1996. The presence and partitioning of calcium binding proteins in hepatic and cardiac nuclei. *J. Mol. Cell. Cardiol.* 28: 455-465.

Danker T. and Oberleithner H. 2000. Nuclear pore function viewed with atomic force microscopy. *Eur. J. Physiol.* 439: 671-681. First published on February 11, 2000; 10.1007/s004240000249

David C. and Viguès B. 1994. Calmyonemin: A 23 kDa analogue of algal centrin occurring in contractile myonemes of *Eudiplodinium maggii* (Ciliate). *Cell Motil. Cytoskel.* 27: 169-179.

Douvas A. S., Harrington C. A., and Bonner J. 1975. Major nonhistone proteins of rat liver chromatin: preliminary identification of myosin, actin, tubulin, and tropomyosin (contractile proteins/ endogenous protease digestion of chromatin). *Proc. Natl. Acad. Sci. USA*. 72: 3902-3906.

Edds K. T. 1975. Motility in *Echinosphaerium nucleofilum*. 1. An analysis of particle motions in the axopodia and a direct test of the involvement of the axoneme. *J. Cell Biol.* 66: 680-685.

Evenson D. P. and Prescott D. M. 1970. Disruption of DNA synthesis in *Euplotes* by heat shock. *Exp. Cell Res.* 63: 245-252.

Fauré-Fremiet E., Rouiller C., and Gauchery M. 1957. La réorganization macronucléaire chez les *Euplotes*. *Exp. Cell Res.* 12: 135-144.

Gall J. G. 1959. Macronuclear duplication in the ciliated protozoan *Euplotes*. *J. Biophys. Biochem. Cytol.* 5: 295-308.

Gilchrist J. S. C., Abrenica B., DiMario P. J., Czubryt M. P., and Pierce G. N. 2002. Nucleolin is a calcium-binding protein. *J. Cell. Biochem.* 85: 268-278.

Gilchrist J. S. C. and Pierce G. N. 1993. Identification and purification of a calcium-binding protein in hepatic nuclear membranes. *J. Biol. Chem.* 268: 4291-4299.

Gorovsky M. A. 1973. Macro- and micronuclei of *Tetrahymena pyriformis*: A model system for studying the structure and function of eukaryotic nuclei. *J Protozool.* 20: 19-25.

Gilchrist J. S. C., Czubryt M. P., and Pierce G. N. 1994. Calcium and calcium-binding proteins in the nucleus. *Mol. Cell. Biochem.* 135: 79-88.

Guttes E. and Guttes S. 1969. Initiation of mitosis in interphase plasmodia of *Physarum polycephalum* by coalescence with premitotic plasmodia. *Experientia* 25: 1168-1170.

He D., Nickerson J. A., and Penman S. 1990. Core filaments of the nuclear matrix. *J. Cell Biol.* 110: 569-580.

Herlan G. and Wunderlich F. 1976. Isolation of a nuclear protein matrix from Tetrahymena macronuclei. Cytobiologie. 13: 291-296.

Hildebrand C. E., Okinaka R. T., and Gurley L. R. 1975. Existence of a residual nuclear protein matrix in cultured Chinese hamster cells. *J. Cell Biol.* 67: 169a.

Hozák P., Sasseville A. M., Raymond Y., and Cook P. R. 1995. Lamin proteins form an internal nucleoskeleton as well as a peripheral lamina in human cells. *J. Cell Sci.* 108: 635-644.

Huang B. and Pitelka D. R. 1973. The contractile process in the ciliate, *Stentor coeruleus*. I. The role of microtubules and filaments. *J. Cell Biol.* 57: 704-728.

Ishida H. and Shigenaka Y. 1988. Cell model contraction in the ciliate *Spirostomum*. *Cell Motil. Cytoskel.* 9: 278-282.

Ishida H., Suzaki T, and Shigenaka Y. 1996. Effect of Mg^{2+} on Ca^{2+}-dependent contraction of a *Spirostomum* cell model. *Eur. J. Protistol.* 32: 316-319.

Katoh K. and Kikuyama M. 1997. An all-or-nothing rise in cytosolic [Ca^{2+}] in *Vorticella* sp. *J. Exp. Biol.* 200: 35-40.

Katoh K. and Naitoh Y. 1994. Control of cellular contraction by calcium in *Vorticella*. *J. Exp. Biol.* 189: 163-177.

Kinoshita E., Shigenaka Y., and Suzaki T. 2001. The ultrastructure of contractile tubules in the heliozoon *Actinophrys sol* and their possible involvement in rapid axopodial contraction. *J. Eukaryot. Microbiol.* 48: 519-526.

Klobutcher L. A. and Prescott D. M. 1986. The special case of the hypotrichs. *In* The molecular biology of ciliated protozoa. Gall J. G. editor. Academic Press/ Orlando. 111-154.

Kluss B. C. 1962. Electron microscopy of the macronucleus of *Euplotes eurystomus*. *J. Cell Biol.* 13: 462-465.

Laemmli U. K. 1970. Cleavage of structural proteins during the assembly of the head of bacteriophage T4. *Nature*. 277: 680-685.

Maciejewski J. J., Vacchiano E. J., Mccutcheon S. M., and Buhse H. E. Jr. 1999. Cloning and expression of a cDNA encoding a *Vorticella convallaria* spasmin: an EF-hand calcium-binding protein. *J. Eukaryot. Microbiol.* 46: 165-173.

Martelli A. M., Falcieri E., Zweyer M., Bortul R., Tabellini G., Cappellini A., Cocco L., and Manzoli L. 2002. The controversial nuclear matrix: a balanced point of view. *Histol. Histopathol.* 17: 1193-1205.

Matsuoka T. and Shigenaka Y. 1984. Localization of calcium during axopodial contraction in heliozoan, *Echinosphaerium akamae*. *Biomed. Res.* 5: 425-432.

Matsuoka T. and Shigenaka Y. 1985. Calcium localization during microtubular disassembly in heliozoan cells. *J. Electron Microsc.* 34: 33-37.

Matsuoka T., Shigenaka Y., and Naitoh Y. 1985. A model of contractile tubules showing how they contract in the heliozoan *Echinosphaerium*. *Cell Struct. Funct.* 10: 63-70.

Mignot J. P. 1980. Étude ultrastructurale de la pédogamie chez *Actinophrys sol* (heliozoaire). II. Les divisions de maturation. *Protistologica*. T. XVI: 205-225.

Mignot J. P. 1984. Étude ultrastructurale de la mitose végétative chez l'héliozoaire *Actinophrys sol*. *Protistologica*. T. XX: 247-263.

Mínguez A., Franca S., and Moreno Díaz de la Espina S. 1994. Dinoflagellates have a eukaryotic nuclear matrix with lamin-like proteins and topoisomerase II. *J. Cell Sci.* 107: 2861-2873.

Moir R. D. and Gorldman R. D. 1993. Lamin dynamics. *Curr. Opin. Cell Biol.* 5: 408-411.

Moir R. D., Michelle-Lowy M., and Goldman R. D. 1994. Dynamic properties of nuclear lamins: Lamin B is associated with sites of DNA replication. *J. Cell Biol.* 125: 1201-1212.

Moriyama Y., Hiyama S., and Asai H. 1998. High-speed video cinematographic demonstration of stalk and zooid contraction of *Vorticella convallaria*. *Biophys. J.* 74: 487-491.

Neri L. M., Raymond Y., Giordano A., Capitani S., and Martelli A. M. 1999. Lamin A is part of the internal nucleoskeleton of human erythroleukemia cells. *J. Cell Physiol.* 178: 284-295.

Nickerson J. A. 2001. Experimental observations of a nuclear matrix. *J. Cell Sci.* 114: 463-474.

Nickerson J. A., Krockmalnic G., Wan K. M., and Penman S. 1997. The nuclear matrix revealed by eluting chromatin from a cross-linked nucleus. *Proc. Natl. Acad. Sci. USA.* 94: 4446-4450.

Nigg E. A. 1992. Assembly-disassembly of the nuclear lamina. *Curr. Opin. Cell Biol.* 4: 105-109.

Nowak G., Pestic-Dragovich L., Hozák P., Philimonenko A., Simerly C., Schatten G., and de Lanerolle P. 1997. Evidence for the presence of myosin I in the nucleus. *J. Biol. Chem.* 272: 17176-17181.

Oberleithner H. 1999. Aldosterone and nuclear signaling in kidney. *Steroids*. 64: 42-50.

Ochiai T., Asai H., and Fukui K. 1979. Hysteresis of contraction-extension cycle of glycerinated *Vorticella*. *J. Protozool.* 26: 420-425.

Ockleford C. D. 1974. Cytokinesis in the heliozoan *Actinophrys sol*. *J. Cell Sci.* 16: 499-517.

Ockleford C. D. and Tucker J. B. 1973. Growth, breakdown, repair, and rapid contraction of microtubular axopodia in the heliozoan *Actinophrys sol*. *J. Ultrastruct. Res.* 44: 369-387.

Olins A. L. and Olins D. E. 1981. Stereo-electron microscopy of nuclear structure and replication in ciliated protozoa (hypotricha). *Eur. J. Cell Biol.* 25: 120-130.

Olins A. L., Olins D. E., Derenzini M., Hernandez-Verdun, Gounon P., Robert-Nicoud M., and Jovin T. M. 1988. Replication bands and nucleoli in the macronucleus of *Euplotes eurystomus*: an ultrastructural and cytochemical study. *Biol. Cell.* 62: 83-93.

Olins D. E. and Olins A. L. 1987. In vitro DNA synthesis in the

macronuclear replication band of *Euplotes eurystomus*. *J. Cell Biol.* 104: 1125-1132.

Patterson D. J. and Hausmann K. 1982. Morulate bodies in Actinophryid heliozoa: a fixation artefact derived from microtubules? *Cell Struct. Funct.* 7: 341-348.

Pederson T. 1998. Thinking about a nuclear matrix. *J. Mol. Biol.* 277: 147-159.

Phegan W. D. and Moses M. J. 1967. Transitions in chromatin fine structure during replication in *Euplotes*. *J. Cell Biol.* 35: 103A (abstr.).

Prescott D. M. and Kimball R. F. 1961. Relation between RNA, DNA and protein synthesis in the replicating nucleus of *Euplotes*. *Proc. Natl. Acad. Sci. USA.* 47: 686-693.

Raikov I. B. 1996. Nuclei of ciliates. *In* Ciliates: cells as organisms. Hausmann K. and Bradbury P. C. editors. Gustav Fischer Verlag/ Stuttgart, Jena, New York. 221-242.

Raikov I. B. 1969. The macronucleus of ciliates. *In* Research in protozoology. Vol. 3. Chen T. -T. editor. Pergamon Press/ New York. 1-128.

Rakowska A., Danker T., Schneider S. W., and Oberleithner H. 1998. ATP-induced shape change of nuclear pores visualized with the atomic force microscope. *J. Membr. Biol.* 163: 129-136.

Reynolds E. S. 1963. The use of lead citrate at high pH as an electron-opaque stain in electron microscopy. *J. Cell Biol.* 17: 208-211.

Riley D. E., Keller J. M., and Byers B. 1975. The isolation and characterization of nuclear ghosts from cultured HeLa cells. *Biochem.* 14: 3005-3013.

Ringertz N. R., Ericsson J. L. E., and Nilsson O. 1967. Macronuclear chromatin structure in *Euplotes*. *Exp. Cell Res.* 48: 97-117.

Sakaguchi M. and Suzaki T. 1999. Monoxenic culture of the heliozoon *Actinophrys sol*. *Eur. J. Protistol.* 35: 411-415.

Sakaguchi M., Hausmann K., and Suzaki T. 1998. Food capture and adhesion by the heliozoon *Actinophrys sol*. *Protoplasma.* 203: 130-137.

Salisbury J. L. 1998. Roots. *J. Eukaryot. Microbiol.* 45: 28-32.

Salisbury J. L. and Floyd G. L. 1978. Calcium-induced contraction of the rhizoplast of a quadriflagellate green alga. *Science.* 202: 975-977.

Salisbury J. L., Baron A., Surek B., and Melkonian M. 1984. Striated flagellar roots: isolation and partial characterization of a calcium-modulated contractile organelle. *J. Cell Biol.* 99: 962-970.

Schliwa M. 1976. The role of divalent cations in the regulation of microtubule assembly. In vivo studies on microtubules of heliozoan axopodium using the ionophore A23187. *J. Cell Biol.* 70: 527-540.

Shigenaka Y. and Kaneda M. 1979. Studies on the cell fusion of heliozoans. IV. An electron microscopical study on the fusion process accompanied with axopodial degradation. *Annot. Zool. Japon.* 52: 28-39.

Shigenaka Y., Watanabe K., and Kaneda M. 1974. Degrading and stabilizing effects of Mg^{2+} ions on microtubule-containing axopodia. *Exp. Cell Res.* 85: 391-398.

Shigenaka Y., Watanabe K., Suzaki T. 1980. Taxonomic studies on two heliozoans, *Echinosphaerium akamae* sp. nov. and *Echinosphaerium ikachiensis* sp. nov. *Annot. Zool. Japon.* 53: 103-119.

Shigenaka Y., Yano K., Yogosawa R., and Suzaki T. 1982. Rapid contraction of the microtubules-containing axopodia in a large heliozoan *Echinosphaerium*. *In* Biological functions of microtubules and related structures. H. Sakai, H. Mohri, and G.G. Borisy, editors. Academic Press/ Tokyo, Japan. 105-114.

Smith P. K., Krohn R. I., Hermanson G. T., Mallia A. K., Gartner F. H., Provenzano M. D., Fujimoto E. K., Goeke N. M., Olson B. J., and Klenk D. C. 1985. Measurement of protein using bicinchoninic acid. *Anal. Biochem.* 150: 76-85.

Spurr A. R. 1969. A low-viscosity epoxy resin embedding medium for electron microscopy. *J. Ultrastruct. Res.* 26: 31-43.

Stevens A. R. 1963. Electron microscope autoradiography of DNA and RNA synthesis in *Euplotes eury*stomus. *J. Cell Biol.* 19: 67A (abstr.).

Sugiyama M., Ikegawa S., Masuyama E., Suzaki T., Ishida M., and Shigenaka Y. 1992. Isolation and properties of the axopodial cytoskeleton of a heliozoan, *Echinosphaerium akamae*. *Eur. J. Protistol.* 28: 214-219.

Suzaki T., Ando M., Inai Y., and Shigenaka Y. 1994. Structure and function of the cytoskeleton in heliozoa. III. Rapid microtubule disorganization during axopodial contraction in *Echinosphaerium*. *Eur. J. Protistol.* 30: 404-413.

Suzaki T., Ando M., Ishigame K., Shigenaka Y., and Sugiyama M. 1992. Structure and function of the cytoskeleton in heliozoa. II. Measurement of the force of rapid axopodial contraction in *Echinosphaerium*. *Eur. J. Protistol.* 28: 430-433.

Suzaki T. and Shigenaka Y. 1982. Intra-axopodial particle movement and axopodial surface motility in *Echinosphaerium akamae*. *In*: Biological functions of microtubules and related structures. Sakai H., Mohri H., Borisy G. G., editors. Academic Press/ Tokyo, Japan. 91-103.

Suzaki T. and Williamson R. E. 1986. Reactivation of euglenoid movement and flagellar beating in detergent-extracted cells of *Astasia longa*. Different mechanisms of force generation are involved. *J. Cell Sci.* 80: 75-89.

Suzaki T., Shigenaka Y., and Takeda Y. 1978. Studies on the cell division of heliozoans. II. Active role of axopodia on division process and transformation of remnants of cytoplasmic connecting bridge to new axopodia. *Cell Struct. and Funct.* 3: 209-218.

Suzaki T., Shigenaka Y, Watanabe S., and Toyohara A. 1980a. Food capture and ingestion in the large heliozoan, *Echinosphaerium nucleofilum*. *J. Cell Sci.* 42: 61-79.

Suzaki T., Toyohara A., Watanabe S., Shigenaka Y., and Sakai H. 1980b. Microtubules in protozoan cells. Continuous transition between microtubules and macrotubules revealed by a newly devised isolation technique. *Biochem. Res.* 1: 207-215.

Tilney L. G. and Porter K. R. 1965. Studies on Microtubules in heliozoa. I. The fine structure of *Actinosphaerium nucleofilum* (Barrett), with particular reference to the axial rod structure. *Protoplasma.* 60: 317-344.

Tilney L. G., Hiramoto Y., and Marsland D. 1966. Studies on the microtubules in heliozoa. III. A pressure analysis of the role of these structures in the formation and maintenance

of the axopodia of *Actinosphaerium nucleofilum* (Barrett). *J. Cell Biol.* 29: 77-95.

Watters C. 1968. Studies on the motility of the heliozoa. I. The locomotion of *Actinosphaerium eichhorni* and *Actinophrys* sp. *J. Cell Sci.* 3: 231-244.

Wen J. 2000. The nuclear matrix of *Euglena gracilis* (Euglenophyta): A stage of nuclear matrix evolution? *Biol. Cell.* 92: 125-131.

Wunderlich F. and Herlan G. 1977. A reversibly contractile nuclear matrix. Its isolation, structure, and composition. *J. Cell Biol.* 73: 271-278.

Wunderlich F., Giese G., and Bucherer C. 1978. Expansion and apparent fluidity decrease of nuclear membranes induced by low Ca/Mg. Modulation of nuclear membrane lipid fluidity by the membrane-associated nuclear matrix proteins? *J. Cell Biol.* 79: 479-490.

Yamada K. and Asai H. 1982. Extraction and some properties of the proteins, spastin B, from the spasmoneme of *Carchesium polypinum*. *J. Biochem.* 91: 1187-1195.

Yogosawa-Ohara R. and Shigenaka Y. 1985. Twisting contraction mechanism of a heterotrichous ciliate, *Spirostomum ambiguum*. I. Role of the myoneme. *Cytobios* 44: 7-17.

Yogosawa-Ohara R., Suzaki T., and Shigenaka Y. 1985. Twisting contraction mechanism of a heterotrichous ciliate, *Spirostomum ambiguum*. 2. Role of longitudinal microtubular sheet. *Cytobios* 44: 215-230.

Yokoyama Y. and Asai H. 1987. Contractility of the spasmoneme in glycerinated *Vorticella* stalk induced by various divalent metal and lanthanide ions. *Cell Motil. Cytoskel.* 7: 39-45.